PHYSICAL REVIEW D **87,** 093006 (2013)

Dark matter, baryogenesis and neutrino oscillations from right-handed neutrinos

Laurent Canetti,[1] Marco Drewes,[2,3] Tibor Frossard,[4] and Mikhail Shaposhnikov[1]

[1]*ITP, EPFL, CH-1015 Lausanne, Switzerland*

[2]*Institut für Theoretische Teilchenphysik und Kosmologie, RWTH Aachen, D-52056 Aachen, Germany*

[3]*Physik Department T31, Technische Universität München, James Franck Straße 1, D-85748 Garching, Germany*

[4]*Max-Planck-Institut für Kernphysik, Saupfercheckweg 1, 69117 Heidelberg, Germany*

(Received 8 October 2012; published 10 May 2013)

We show that, leaving aside accelerated cosmic expansion, all experimental data in high energy physics that are commonly agreed to require physics beyond the Standard Model can be explained when completing the model by three right-handed neutrinos that can be searched for using present-day experimental techniques. The model that realizes this scenario is known as the Neutrino Minimal Standard Model (νMSM). In this article we give a comprehensive summary of all known constraints in the νMSM, along with a pedagogical introduction to the model. We present the first complete quantitative study of the parameter space of the model where no physics beyond the νMSM is needed to simultaneously explain neutrino oscillations, dark matter, and the baryon asymmetry of the Universe. The key new point of our analysis is leptogenesis after sphaleron freeze-out, which leads to resonant dark matter production, thus evading the constraints on sterile neutrino dark matter from structure formation and x-ray searches. This requires one to track the time evolution of left- and right-handed neutrino abundances from hot big bang initial conditions down to temperatures below the QCD scale. We find that the interplay of resonant amplifications, *CP*-violating flavor oscillations, scatterings, and decays leads to a number of previously unknown constraints on the sterile neutrino properties. We furthermore reanalyze bounds from past collider experiments and big bang nucleosynthesis in the face of recent evidence for a nonzero neutrino mixing angle θ_{13}. We combine all our results with existing constraints on dark matter properties from astrophysics and cosmology. Our results provide a guideline for future experimental searches for sterile neutrinos. A summary of the constraints on sterile neutrino masses and mixings has appeared in Canetti *et al.* [Phys. Rev. Lett. **110**, 061801 (2013)]. In this article we provide all details of our calculations and give constraints on other model parameters.

DOI: 10.1103/PhysRevD.87.093006 PACS numbers: 14.60.St, 98.80.Cq, 11.30.Fs, 11.30.Er

I. INTRODUCTION

The Standard Model of particle physics (SM), together with the theory of general relativity (GR), allows one to explain almost all phenomena observed in nature in terms of a small number of underlying principles—Poincaré invariance, gauge invariance, and quantum mechanics—and a handful of numbers. In the SM these are 19 free parameters that can be chosen as three masses for the charged leptons; six masses, three mixing angles, and one *CP*-violating phase for the quarks; three gauge couplings and two parameters in the scalar potential and the QCD vacuum angle. Three leptons, the neutrinos, remain massless in the SM and appear only with left-handed chirality. GR adds another two parameters to the barcode of nature, the Planck mass and the cosmological constant.

Despite its enormous success, we know for sure that the above is not a complete theory of nature for two reasons.[1] On one hand, it treats gravity as a classical background for the SM, which is a quantum field theory. Such a description necessarily breaks down at energies near the Planck scale M_P and has to be replaced by a theory of quantum gravity. We do not address this problem here, which is of little relevance for current and near-future experiments. On the other hand, the SM fails to explain a number of experimental facts. These are neutrino oscillations, the observed baryon asymmetry of the Universe (BAU), the observed dark matter (DM), and the accelerated expansion of the Universe today. In addition, there are a number of cosmological problems (e.g., the flatness and horizon problems). These can be explained by cosmic inflation, another phase of accelerated expansion in the Universe's very early history, for which the SM cannot provide a mechanism either. To date, these are the only confirmed empirical proofs of physics beyond the SM.[2] In this article we argue that, leaving aside accelerated cosmic expansion, all of them

[1]We do not address theoretical issues of "aesthetic" nature such as fine-tuning in the context of the hierarchy problem, the strong *CP* problem, and the flavor structure. They may be interpreted as hints for new physics, but could also simply represent nature's choice of parameters.

[2]We leave aside all experimental and observational anomalies that do not lead to a claim of detection of new physics, i.e., that may be explained within the SM or by systematic errors. This includes the long-standing problem of the muon magnetic moment, the inconclusive results of different direct DM searches, as well as various anomalies of limited statistical significance.

may be explained by adding three right-handed (sterile) neutrinos to the SM that can be found in experiments.

The model in which this possibility can be realized is known as the Neutrino Minimal Standard Model (νMSM) [1–3]. The νMSM is an extension of the SM that aims to explain all experimental data with only minimal modifications. This, in particular, means that there is no modification of the gauge group, the number of fermion families remains unchanged, and no new energy scale above the Fermi scale is introduced.[3] The matter content is, in comparison to the SM, complemented by three right-handed counterparts to the observed neutrinos. These are singlet under all gauge interactions. Over the past years, different aspects of the νMSM have been explored using cosmological, astrophysical, and experimental constraints [1–3,6–31]. Moreover, it was suggested that cosmic inflation [32–34] and the current accelerated expansion [35–38] may also be accommodated in this framework by nonminimal coupling of the Higgs field to gravitational Ricci scalars and by introducing yet another particle—the dilaton—realizing exact, but spontaneously broken scale invariance.[4] However, though the abundances of dark and baryonic matter have been estimated individually in the framework of the νMSM, to date it has not been verified that there is a range of right-handed neutrino parameters for which they can be explained *simultaneously* without any new physics between the Fermi and Planck scales, and, in particular, for experimentally accessible sterile neutrinos. Claims made in Ref. [3] were based on estimates and turn out to be somewhat premature from today's point of view due to constraints on the properties of DM sterile neutrinos from Ly_α and x-ray observations, which were not known at that time. These constraints can be resolved if DM production is enhanced by a lepton asymmetry generated after sphaleron freeze-out. In this article we present detailed results of the first complete quantitative study to identify the range of parameters that allows one to simultaneously explain neutrino oscillations, the observed DM density Ω_{DM}, and the observed BAU, responsible for today's remnant baryonic density Ω_B. In the following we refer to this situation, in which no physics beyond the νMSM is required to explain these phenomena, as scenario I. In this scenario DM is made of one of the right-handed neutrinos, while the other two are responsible for baryogenesis and the generation of active neutrino masses. We also study systematically how the constraints relax if one allows the sterile neutrinos that compose DM to be produced by some mechanism beyond the νMSM (scenario II). Finally, we briefly comment on a scenario III, in which the νMSM is a theory of baryogenesis and neutrino oscillations only, with no relation to DM. A more precise definition of these scenarios is given in Sec. II B. Only scenarios I and II are studied in this article, which is devoted to the νMSM as the common origin of DM, neutrino masses, and the BAU. While scenario II has previously been studied in Ref. [22], the constraints coming from the requirement to thermally produce the observed Ω_{DM} in scenario I are calculated for the first time in this work. We combine our results with bounds coming from big bang nucleosynthesis (BBN) and direct searches for sterile neutrinos, which we rederive in the face of recent data from neutrino experiments (in particular, $\theta_{13} \neq 0$).

The centerpiece of our analysis is the study of all lepton numbers throughout the evolution of the early Universe. As will be explained below, in the νMSM, lepton asymmetries are crucial for both baryogenesis and DM production. We determine the time evolution of left- and right-handed neutrino abundances for a wide range of sterile neutrino parameters from hot big bang initial conditions at temperatures $T \gg T_{\mathrm{EW}} \sim 200$ GeV down to temperatures below the QCD scale by means of effective kinetic equations. They incorporate various effects, including thermal production of sterile neutrinos from the primordial plasma, coherent oscillations, backreaction, washouts, resonant amplifications, decoherence, finite temperature corrections to the neutrino properties, and the change in the effective number of degrees of freedom in the SM background. Many of these were only roughly estimated or completely neglected in previous studies. The various different time scales appearing in the problem make an analytic treatment or the use of a single *CP*-violating parameter impossible in most of the parameter space. Most of our results are obtained numerically. However, the parametric dependence on the experimentally relevant parameters (sterile neutrino masses and mixings) can be understood in a simple way. Furthermore, we discover a number of tuning conditions that can be understood analytically and that allow one to reduce the dimensionality of the parameter space.

We find that there exists a considerable fraction of the νMSM parameter space in which the model can simultaneously explain neutrino oscillations, dark matter, and the baryon asymmetry of the Universe. This includes a range of masses and couplings for which the right-handed neutrinos can be found in laboratory experiments [16]. The main results of our study, constraints on sterile neutrino masses and mixings, have previously been presented in Ref. [1]. In this article we give details of our calculation and constraints on other model parameters, which are not discussed in Ref. [1].

The remainder of this article is organized as follows. In Sec. II we overview the νMSM and its parametrization and describe the Universe history in this framework, including

[3]Because of this, the technical hierarchy problem may be absent in the νMSM because no new states with energies between the electroweak and the Planck scale are required [4,5].

[4]Inflation can be realized without introducing the nonminimal coupling by adding an extra scalar to the νMSM [15]. This inflaton can be light enough to be detected in direct searches [39]. It also provides a new mechanism for sterile neutrino dark matter production [15] (see also Refs. [40,41]).

baryogenesis and dark matter production. In Sec. III we discuss different experimental and cosmological bounds on the properties of right-handed neutrinos in the νMSM. In Sec. IV we formulate the kinetic equations which are used to follow the time evolution of sterile neutrinos and active neutrino flavors in the early Universe. In Sec. V we present our results on baryogenesis in scenario II. In Sec. VI we study the generation of lepton asymmetries at late times, essential for thermal dark matter production in the νMSM. In Sec. VII we combine the constraints of the two previous sections and define the region of parameters where scenario I can be realized; i.e., the νMSM explains simultaneously neutrino masses and oscillations, dark matter, and baryon asymmetry of the Universe. In Sec. VIII we present our conclusions. In a number of appendixes we give technical details on kinetic equations (Appendix A), on the parametrization of the νMSM Lagrangian (Appendix B), on different notations to describe lepton asymmetries (Appendix C), and on the decay rates of sterile neutrinos (Appendix D).

II. THE νMSM

The νMSM is described by the Lagrangian

$$\mathcal{L}_{\nu\text{MSM}} = \mathcal{L}_{\text{SM}} + i\overline{\nu_R}\partial\!\!\!/\nu_R - \overline{L_L}F\nu_R\tilde{\Phi} - \overline{\nu_R}F^\dagger L_L\tilde{\Phi}^\dagger - \frac{1}{2}(\overline{\nu_R^c}M_M\nu_R + \overline{\nu_R}M_M^\dagger\nu_R^c). \quad (1)$$

Here we have suppressed flavor and isospin indices. $\mathcal{L}_{\text{SM}}$ is the Lagrangian of the SM. F is a matrix of Yukawa couplings and M_M a Majorana mass term for the right-handed neutrinos ν_R. $L_L = (\nu_L, e_L)^T$ are the left-handed lepton doublets in the SM and Φ is the Higgs doublet. We chose a basis where the charged lepton Yukawa couplings and M_M are diagonal. The Lagrangian (1) is well known in the context of the seesaw mechanism for neutrino masses [43–46] and leptogenesis [47]. While the eigenvalues of M_M in most models are related to an energy scale far above the electroweak scale, it is a defining assumption of the νMSM that the observational data can be explained without involvement of any new scale above the Fermi one.

A. Mass and flavor eigenstates

For temperatures $T < M_W$ below the mass of the W boson we can, to a good approximation, replace the Higgs field Φ by its vacuum expectation value $v = 174$ GeV. Then (1) can be written as

$$\mathcal{L} = \mathcal{L}_{\text{SM}} + i\overline{\nu_{R,I}}\partial\!\!\!/\nu_{R,I} - (m_D)_{\alpha I}\overline{\nu_{L,\alpha}}\nu_{R,I} - (m_D^*)_{\alpha I}\overline{\nu_{R,I}}\nu_{L,\alpha} - \frac{1}{2}((M_M)_{IJ}\overline{\nu_R^c}\nu_{R,J} + (M_M)_{IJ}^*\overline{\nu_{R,I}}\nu_{R,J}^c) \quad (2)$$

with the Dirac mass matrix $m_D = Fv$. When the eigenvalues of M_M are much larger than those of m_D, the seesaw mechanism naturally leads to light active and heavy sterile neutrinos. This hierarchy is realized in the νMSM.

In the seesaw limit $m_D \ll M_M$ (in terms of eigenvalues), the complete 6×6 neutrino mass matrix has two sets of eigenvalues in vacuum. Three of them are of the same order as the eigenvalues of M_M; the other three are suppressed by two powers of the active-sterile mixing matrix $\theta_{\alpha I} = (m_D M_M^{-1})_{\alpha I}$. Expansion in θ allows us to block-diagonalize the mass matrix. At leading order one obtains the 3×3 mass matrices

$$m_\nu = -\theta M_M \theta^T, \quad (3)$$

$$M_N = M_M + \frac{1}{2}(\theta^\dagger\theta M_M + M_M^T\theta^T\theta^*). \quad (4)$$

The mass matrices m_ν and M_N are not diagonal and lead to neutrino oscillations. Diagonalizing them yields the mass eigenstates in vacuum. Due to the seesaw hierarchy $\theta \ll 1$ there are two distinct sets of them: on one hand, active neutrinos ν_i with masses m_i, which are mainly mixings of the SU(2) charged fields ν_L,

$$P_L\nu_i = \left(U_\nu^\dagger\left(\left(\mathbb{1} - \frac{1}{2}\theta\theta^\dagger\right)\nu_L - \theta\nu_R^c\right)\right)_i, \quad (5)$$

and on the other hand, sterile neutrinos[5] N_I with masses M_I, which are mainly mixings of the singlet fields ν_R,

$$P_R N_I = \left(U_N^\dagger\left(\left(\mathbb{1} - \frac{1}{2}\theta^T\theta^*\right)\nu_R + \theta^T\nu_L^c\right)\right)_I. \quad (6)$$

Here $P_{R,L}$ are chiral projectors and N_I (ν_i) are Majorana spinors, the left chiral (right chiral) part of which is fixed by the Majorana relations $N_I^c = N_I$ and $\nu_i = \nu_i^c$. The matrix U_N diagonalizes the sterile neutrino mass matrix M_N defined in (4). The entries of the matrix θ determine the active-sterile mixing angles. While there is very little mixing between active and sterile flavors at all temperatures of interest, the oscillations between sterile neutrinos can be essential for the generation of a lepton asymmetry.

m_ν can be parametrized in the usual way by active neutrino masses, mixing angles and phases, $m_\nu = U_\nu\text{diag}(m_1, m_2, m_3)U_\nu^T$. In the basis where the charged lepton Yukawas are diagonal, U_ν is identical to the Pontecorvo-Maki-Nakagawa-Sakata lepton mixing matrix. The physical sterile neutrino masses M_I are given by the eigenvalues of $M_N^\dagger M_N$. In the seesaw limit the diagonal elements of M_N are much bigger than the off-diagonals and are very close to the entries of M_M. We nevertheless need to keep terms $\mathcal{O}(\theta^2)$ because the masses M_2 and M_3 are degenerate in the νMSM (see Sec. II F), and the mixing of the sterile neutrinos $N_{2,3}$ amongst each other may be large despite the seesaw hierarchy.[6] This mixing is given by the matrix U_N, which can be seen as an analogue to U_ν. We

[5] In Ref. [6] the notation is slightly different and the letter "N_I" does not denote mass eigenstates.

[6] It turns out that in scenario I the region where U_N is close to the identity phenomenologically is the most interesting: see Sec. II F.

chose the phase convention in U_N such that $M_N = U_N \mathrm{diag}(M_1, M_2, M_3) U_N^T$, with M_I real and positive. Note, however, that U_N cannot be tested in realistic low energy experiments at this stage. The experimentally measurable combination is defined in Eq. (7).[7] It is worth noting that due to (4) the matrix U_N is real at this order in F.

The experimentally relevant coupling between active and sterile species is given by the matrix Θ with[8]

$$\Theta_{\alpha I} \equiv (\theta U_N^*)_{\alpha I} = (m_D M_M^{-1} U_N^*)_{\alpha I}. \tag{7}$$

In practice, experiments to date cannot distinguish the sterile flavors and are only sensitive to the quantities

$$U_\alpha^2 \equiv \sum_I \Theta_{\alpha I} \Theta_{\alpha I}^* = \sum_I \theta_{\alpha I} \theta_{\alpha I}^*. \tag{8}$$

B. Benchmark scenarios

The notation introduced above allows us to define scenarios I–III, introduced in Sec. I, more precisely.

(I) In scenario I no physics beyond the νMSM is needed to explain the observed Ω_{DM}, neutrino masses and Ω_B. DM is composed of thermally produced sterile neutrinos N_1. N_2 and N_3 generate active neutrino masses via the seesaw mechanism, and their CP-violating oscillations produce lepton asymmetries in the early Universe. The effect of N_1 on neutrino masses and lepton asymmetry generation is negligible. This is because its Yukawa couplings $F_{\alpha 1}$ must be tiny by the known constraints on DM, cf. Sec. III A 2. The lepton asymmetries produced by $N_{2,3}$ are crucial on two occasions in the history of the Universe: On one hand, the asymmetries generated at early times ($T \gtrsim 140$ GeV) are responsible for the generation of a BAU via flavored leptogenesis; on the other hand, the late-time asymmetries ($T \sim 100$ MeV) strongly affect the rate of thermal N_1 production. Due to the latter the requirement to produce the observed Ω_{DM} imposes indirect constraints on the particles $N_{2,3}$. There are determined in Secs. VI and VII and form the main result of our study.

(II) In scenario II the roles of $N_{2,3}$ and N_1 are the same as in scenario I, but we assume that DM was produced by some unknown mechanism beyond the νMSM. The astrophysical constraints on the N_1 mass and coupling equal those in scenario I. $N_{2,3}$ are again required to generate the active neutrino masses via the seesaw mechanism and to produce sufficient flavored lepton asymmetries at $T \sim 140$ MeV to explain the BAU. However, there is no need for a large late-time asymmetry. This considerably relaxes the bounds on $N_{2,3}$. Scenario II is studied in detail in Sec. V.

(III) In scenario III the νMSM is not required to explain DM; i.e., it is considered to be a theory of neutrino masses and low energy leptogenesis only. Then, all three N_I can participate in the generation of lepton asymmetries. This makes the parameter space for baryogenesis considerably bigger than in scenarios I and II, including new sources of CP violation. We do not study scenario III in this work; some aspects are discussed in Ref. [30].

C. Effective theory of lepton number generation

In scenarios I and II the lightest sterile neutrino N_1 is a DM candidate. In this article we focus on these two scenarios. If N_1 is required to compose all observed DM, its mass M_1 and mixing are constrained by observational data; see Sec. III. Its mixing is so small that its effect on the active neutrino masses is negligible. Note that this implies that one active neutrino is much lighter than the others [with mass smaller than $\mathcal{O}(10^{-5})$ eV [2]]. If experiments find three massive active neutrinos, this finding would exclude the νMSM with three sterile neutrinos as common and only origin of active neutrino oscillations, dark matter and baryogenesis. N_1 does not contribute significantly to the production of lepton asymmetry at any time either. This process can therefore be described in an effective theory with only two sterile flavors $N_{2,3}$. In the following we will almost exclusively work in this framework. To simplify the notation, we will use the symbols M_N and U_N for both the full (3×3) mass matrix and mixing matrices defined above and the $(2 \times 2$ and $3 \times 2)$ submatrices that only involve the sterile flavors $I = 2, 3$, which appear in the effective theory. The mixing between N_1 and $N_{2,3}$ is negligible due to the smallness of $F_{\alpha 1}$, which is enforced by the seesaw relation (3) and the observational bounds on M_1 summarized in Sec. III A 2. The effective $N_{2,3}$ mass matrix can be written as

$$M_N = M \mathbb{1}_{2\times 2} + \Delta M \sigma_3 + M^{-1} \mathrm{Re}(m_D^\dagger m_D), \tag{9}$$

where σ_3 is the third Pauli matrix and we choose the parametrization $M_M = \mathrm{diag}(M - \Delta M, M + \Delta M)$. This equality holds because we choose M_M real and diagonal. The physical masses M_2 and M_3 are given by the eigenvalues of M_N. They read

$$M_{2,3} = \bar{M} \pm \delta M, \tag{10}$$

[7] This does not mean that U_N is not physical. After diagonalization of M_N, it appears in the coupling of the sterile mass eigenstates N_I to the electroweak current (in contrast to ν_R, N_I couples to the weak current via its ν_L^c component). Six of the 18 νMSM parameters are contained in U_N. Experimentally these are, however, only accessible in processes of higher order in F and with ideal detectors, which have a mass resolution that is high enough to distinguish different sterile neutrino mass eigenstates.

[8] In Eq. (6) the matrix $U_N^\dagger \theta^T = \Theta^T$ appears (rather than Θ) because the N_I couple to $\nu_{L,\alpha}$, but overlap with $\nu_{L,\alpha}^c$.

$$\bar{M} = M + \frac{1}{2M}\,\mathrm{Re}(\mathrm{tr}(m_D^\dagger m_D)), \tag{11}$$

$$(\delta M)^2 = \left(\frac{1}{2M}(\mathrm{Re}(m_D^\dagger m_D)_{33} - \mathrm{Re}(m_D^\dagger m_D)_{22}) + \Delta M\right)^2 + \frac{1}{M^2}\,\mathrm{Re}(m_D^\dagger m_D)_{23}^2. \tag{12}$$

For all parameter choices we are interested in, $\bar{M} \simeq M$ holds to a very good approximation. The masses $M_{2,3}$ are too big to be sensitive to loop corrections. In contrast, the splitting δM can be considerably smaller than the size of radiative corrections to $M_{2,3}$ [48]. The above expressions have a different shape than those given in Ref. [6] because we use a different base in flavor space; see Appendix B.

These above formulas hold for the (zero temperature) masses in the microscopic theory. At finite temperature the system is described by a thermodynamical ensemble, the properties of which can usually be described in terms of quasiparticles with temperature-dependent dispersion relations. We approximate these by temperature-dependent "thermal masses."

D. Thermal history of the Universe in the νMSM

Apart from the very weakly coupled sterile neutrinos, the matter content of the νMSM is the same as that of the SM. Therefore, the thermal history of the Universe during the radiation dominated era is similar in both models. Here we only point out the differences that arise due to the presence of the fields ν_R; see Fig. 1. They couple to the SM only via the Yukawa matrices F, which are constrained by the seesaw relation. For sterile neutrino masses below the electroweak scale, the abundances are too small to affect the entropy during the radiation dominated era significantly. However, the additional sources of CP violation contained in them have a huge effect on the lepton chemical potentials in the plasma.

1. Baryogenesis

The νMSM adds no new degrees of freedom to the SM above the electroweak scale. As a consequence of the smallness of the Yukawa couplings F, the N_I are produced only in negligible amounts during reheating [33]. Therefore, the thermal history for $T \gg T_{\mathrm{EW}}$ closely resembles that in the SM.[9] The sterile neutrinos have to be produced thermally from the primordial plasma in the radiation dominated epoch. During this nonequilibrium process, all Sakharov conditions [49] are fulfilled:

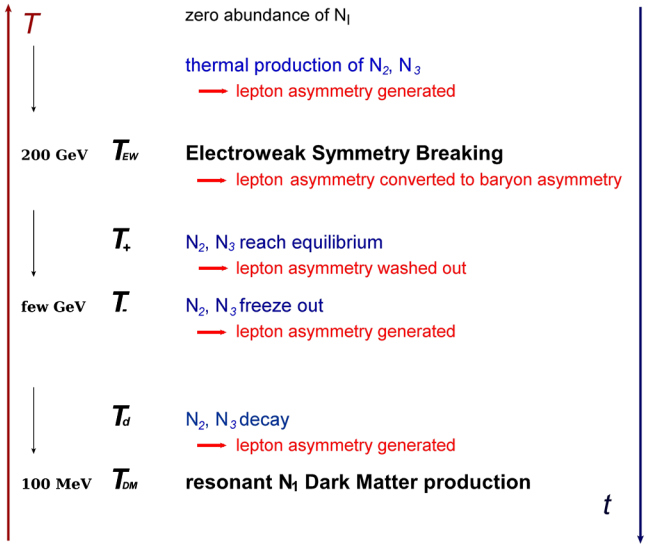

FIG. 1 (color online). The thermal history of the Universe in the νMSM.

Baryon number is violated by SM sphalerons [50], and the oscillations amongst the sterile neutrinos violate CP [51]. Sources of this CP violation are the complex phases in the Yukawa couplings $F_{\alpha I}$. Due to the Majorana mass M_M neither the individual (active) leptonic currents, defined in (A45) and (A46), nor the total lepton number are strictly conserved. However, for $T \gg M$ the effect of the Majorana masses is negligible. Though the neutrinos are Majorana particles, one can define *neutrinos* and *antineutrinos* as the two helicity states, transitions between which are suppressed at $T \gg M$. We will, in the following, always use the terms "neutrinos" and "antineutrinos" in this sense.

In scenarios I and II the abundance of N_1 remains negligible until $T \sim 100$ MeV because of the smallness of its coupling that is required to be in accordance with astrophysical bounds on DM; see Sec. III A 2. $N_{2,3}$, on the other hand, are produced efficiently in the early Universe. During this process flavored "lepton asymmetries" can be generated [51]. $N_{2,3}$ reach equilibrium at a temperature T_+ [6]. Though the total lepton number (A45) at $T_+ \gg M$ is very small, there are asymmetries in the above helicity sense in the individual active and sterile flavors. Sphalerons, which only couple to the left chiral fields, can convert them into a baryon asymmetry. The washout of lepton asymmetries becomes efficient at $T \lesssim T_+$. It is a necessary condition for baryogenesis that this washout has not erased all asymmetries at T_{EW}, which is always fulfilled for $T_+ \lesssim T_{\mathrm{EW}}$. The BAU at $T \sim T_{\mathrm{EW}}$ can be estimated by today's baryon to photon ratio; see Ref. [42] for a recent review. A precise value can be obtained by combining data from the cosmic microwave background and large scale structure [52],

$$\eta_B = (6.160 \pm 0.148) \times 10^{-10}. \tag{13}$$

[9] If a nonminimal coupling of the Higgs field Φ to gravity is introduced in the νMSM, Φ can play the role of the inflaton. Though in this way no fields are added, the thermal history at very early times (during reheating) changes due to a nonminimal coupling to curvature; see Ref. [33]. Here we assume an initial state without N_I at $T \gg T_{\mathrm{EW}}$.

The parameter η_B is related to the remnant density of baryons Ω_B, in units of the critical density, by $\Omega_B \simeq \eta_B/(2.739 \times 10^{-8} h^2)$, where h parametrizes today's Hubble rate $H_0 = 100h$ (km/s)/Mpc. In order to generate this asymmetry, the effective (thermal) masses $M_2(T)$ and $M_3(T)$ of the sterile neutrinos in the plasma need to be quasidegenerate at $T \gtrsim T_{\rm EW}$; see Sec. II F.

After N_2 and N_3 reach equilibrium, the lepton asymmetries are washed out. This washout takes longer than the kinetic equilibration, but it has been estimated in Ref. [6] that no asymmetries survive until $N_{2,3}$-freeze-out at $T = T_-$. In Ref. [53] it has been suggested that some asymmetries may be protected from this washout by the chiral anomaly, which transfers them into magnetic fields. Here we take the most conservative approach and assume that no asymmetry survives between T_+ and T_-. Around $T = T_-$, the interactions that keep $N_{2,3}$ in equilibrium become inefficient. During the resulting freeze-out the Sakharov conditions are again fulfilled and new asymmetries are generated. Even later, a final contribution to the lepton asymmetries is added when the unstable particles $N_{2,3}$ decay at a temperature T_d.

2. DM production

The abundance of the third sterile neutrino N_1 in scenario I remains below equilibrium at all times due to its small Yukawa coupling. In the absence of chemical potentials, the thermal production of these particles (Dodelson-Widrow mechanism [54]) is not sufficient to explain all dark matter as relic N_1 abundance if the observational bounds summarized in Sec. III are taken into consideration. However, in the presence of a lepton asymmetry in the primordial plasma, the dispersion relations of active and sterile neutrinos are modified by the Mikheyev-Smirnov-Wolfenstein effect (MSW effect) [55,56]. The thermal mass of the active neutrinos can be large enough to cause a level crossing between the dispersion relation for active and sterile flavors at $T_{\rm DM}$, resulting in a resonantly enhanced production of N_1 [19] (resonant or Shi-Fuller mechanism [57]). This mechanism requires a lepton asymmetry $|\mu_\alpha| \gtrsim 8 \times 10^{-6}$ to be efficient enough to explain the entire observed dark matter density $\Omega_{\rm DM}$ in terms of N_1 relic neutrinos [19]. Here we have characterized the asymmetry by[10]

$$\mu_\alpha = \frac{n_\alpha}{s}, \tag{14}$$

where s is the entropy density of the Universe and n_α the total number density (particles minus antiparticles) of active (SM) leptons of flavor α. The relations between μ_α defined in (14) and other ways to characterize the asymmetry (e.g., the chemical potential) are given in Appendix C.

3. Cosmological constraints

Thus, in scenario I there are two cosmological requirements related to the lepton asymmetry that have to be fulfilled to produce the correct Ω_B and $\Omega_{\rm DM}$ within the νMSM:

(i) $\mu_\alpha \sim 10^{-10}$ at $T_{\rm EW} \sim 200$ GeV for successful baryogenesis and

(ii) $|\mu_\alpha| > 8 \times 10^{-6}$ at $T_{\rm DM}$ for dark matter production.

In scenarios I and II the asymmetry generation in both cases relies on a resonant amplification and quasidegeneracy of M_2 and M_3, which we discuss in Sec. II F. This may be considered as fine-tuning. On the other hand, the fact that the BAU (and thus the baryonic matter density Ω_B) and DM production in the SM both rely on essentially the same mechanism may be considered as a hint for an explanation for the apparent coincidence $\Omega_B \sim \Omega_{\rm DM}$, though the connection is not obvious as Ω_B and $\Omega_{\rm DM}$ also depend on other parameters.

In scenario II only the condition (i) applies. The resulting constraints on the $N_{2,3}$ properties have been studied in detail in Ref. [22]. In Sec. V we update this analysis in the face of recent data from neutrino experiments, in particular, evidence for an active neutrino mixing angle $\theta_{13} \neq 0$ [58–60]. In Sec. VI we include the second condition and study which additional constraints come from the requirement $|\mu_\alpha| > 8 \times 10^{-6}$ at $T_{\rm DM}$. Previous estimates suggest $T_{\rm DM} \sim 100$ MeV $\lesssim T_{\rm QCD}$ [19] and $T_- < M_W$ [6,21], where M_W is the mass of the W boson and $T_{\rm QCD}$ the temperature at which quarks form hadrons.

Though we are concerned with the conditions under which N_1 can explain all observed dark matter, the N_1 will not directly enter our analysis because the lepton asymmetry that is necessary for resonant N_1 production in scenario I is created by $N_{2,3}$. Instead, we derive constraints on the properties of $N_{2,3}$, which can be searched for in particle colliders. N_1, in contrast, cannot be detected directly in the laboratory due to its small coupling. However, the N_1 parameter space is constrained from all sides by indirect observations, including structure formation, Ly_α forest, x rays, and phase space analysis; see Sec. III.

E. Parametrization

Adding k flavors of right-handed neutrinos to the SM with three active neutrinos extends the parameter space of the model by $7k - 3$ parameters. In the νMSM $k = 3$; thus, there are 18 parameters in addition to those of the SM. These can be chosen as the masses m_i and M_I of the three active and three sterile neutrinos, respectively, and three mixing angles as well as three phases in each of the

[10]Note that μ_α is not a chemical potential, but an abundance (or yield). We chose the symbol μ for notational consistency with Ref. [6]. The relation of μ_α to the lepton chemical potential μ_α is given in Appendix C.

mixing matrices U_ν and U_N that diagonalize m_ν and M_N, respectively.

In the following we consider an effective theory with only two right-handed neutrinos, which is appropriate to describe the generation of lepton asymmetries in scenarios I and II. After dropping N_1 from the Lagrangian (2), the effective Lagrangian contains 11 new parameters in addition to the SM. Seven of them are related to the active neutrinos. In the standard parametrization these are two masses m_i (one active neutrino has a negligible mass), three mixing angles θ_{ij}, a Dirac phase δ, and a Majorana phase ϕ. They can, at least in principle, be measured in active neutrino experiments. The remaining four are related to sterile neutrino properties. In the common Casas-Ibarra parametrization [61] two of them are chosen as M_2, M_3. The last two are the real and imaginary parts of a complex angle ω.[11] The Yukawa coupling is written as

$$F = U_\nu \sqrt{m_\nu^{\rm diag}}\,\mathcal{R}\,\sqrt{M_M}, \tag{15}$$

where $m_\nu^{\rm diag} = {\rm diag}(m_1, m_2, m_3)$. For normal hierarchy of active neutrino masses ($m_1 \simeq 0$), $\mathcal{R}$ is given by

$$\mathcal{R} = \begin{pmatrix} 0 & 0 \\ \cos(\omega) & \sin(\omega) \\ -\xi\sin(\omega) & \xi\cos(\omega) \end{pmatrix} \text{normal hierarchy}, \tag{16}$$

while for inverted hierarchy ($m_3 \simeq 0$), it reads

$$\mathcal{R} = \begin{pmatrix} \cos(\omega) & \sin(\omega) \\ -\xi\sin(\omega) & \xi\cos(\omega) \\ 0 & 0 \end{pmatrix} \text{inverted hierarchy}, \tag{17}$$

where $\xi = \pm 1$. The matrix U_ν can be parametrized as

$$U_\nu = V_{23} U_\delta V_{13} U_{-\delta} V_{12} {\rm diag}(e^{i\alpha_1/2}, e^{i\alpha_2/2}, 1) \tag{18}$$

with $U_{\pm\delta} = {\rm diag}(e^{\mp i\delta/2}, 1, e^{\pm i\delta/2})$ and

$$V_{23} = \begin{pmatrix} 1 & 0 & 0 \\ 0 & c_{23} & s_{23} \\ 0 & -s_{23} & c_{23} \end{pmatrix},$$
$$V_{13} = \begin{pmatrix} c_{13} & 0 & s_{13} \\ 0 & 1 & 0 \\ -s_{13} & 0 & c_{13} \end{pmatrix}, \tag{19}$$
$$V_{12} = \begin{pmatrix} c_{12} & s_{12} & 0 \\ -s_{12} & c_{12} & 0 \\ 0 & 0 & 1 \end{pmatrix},$$

where c_{ij} and s_{ij} stand for $\cos(\theta_{ij})$ and $\sin(\theta_{ij})$, respectively, and α_1, α_2 and δ are the CP-violating phases. For normal hierarchy the Yukawa matrix F only depends on the phases α_2 and δ; for the inverted hierarchy, it depends on δ and the difference $\alpha_1 - \alpha_2$. This is because N_1 has no measurable effect on neutrino masses due to $M_1 \ll M_{2,3}$. In practice, we will use the following parameters: two active neutrino masses m_i, five parameters in the active mixing matrix (three angles, one Dirac phase, one Majorana phase), the average physical sterile neutrino mass $\bar{M} = (M_1 + M_2)/2 \simeq M$, and the mass splitting ΔM.

[11] Note that F as a polynomial in $z = e^{i\omega}$ only contains terms of the powers z and $1/z$.

TABLE I. Neutrino masses and mixings as found in Ref. [62]. We parametrize the masses m_i according to $m_1 = 0$, $m_2^2 = m_{\rm sol}^2$, $m_3^2 = m_{\rm atm}^2 + m_{\rm sol}^2/2$ for normal hierarchy and $m_1^2 = m_{\rm atm}^2 - m_{\rm sol}^2/2$, $m_2^2 = m_{\rm atm}^2 + m_{\rm sol}^2/2$, $m_3 = 0$ for inverted hierarchy. Using the values for θ_{13} found more recently in Refs. [60,63] has no visible effect on our results.

$m_{\rm sol}^2[{\rm eV}^2]$	$m_{\rm atm}^2[{\rm eV}^2]$	$\sin^2\theta_{12}$	$\sin^2\theta_{13}$	$\sin^2\theta_{23}$
7.58×10^{-5}	2.35×10^{-3}	0.306	0.021	0.42

The masses and mixing angles of active neutrinos have been measured (the absolute mass scale is fixed, as the lightest active neutrino is almost massless in scenarios I and II). We use the experimental values obtained from the global fit published in Ref. [62] in all calculations, which are summarized in Table I. Shortly after we finished our numerical studies, the mixing angle θ_{13} was measured by the Daya Bay [60] and RENO [63] collaborations. The values found there slightly differ from the one given in Ref. [62]; see also Ref. [64]. We checked that the effect of using one or the other value on the generated asymmetries is negligible, which justifies using the self-consistent set of parameters given in Table I. The remaining parameters can be constrained in decays of sterile neutrinos in the laboratory.

It is one of the main goals of this article to impose bounds on the parameters to provide a guideline for experimental searches. In order to identify the interesting regions in parameter space, we proceed as follows. We neglect ΔM in (15), but of course keep it in the effective Hamiltonian introduced in Sec. IV. This is allowed in the region $\Delta M \ll M$, which we consider in this work. Unless stated differently, we always allow the CP-violating Majorana and Dirac phases to vary. We then numerically determine the values that maximize the asymmetry and fix them to those. In Sec. V, where we study condition (i) for baryogenesis, we apply the same procedure to ω. On the other hand, requirement (ii), necessary to explain $\Omega_{\rm DM}$ in scenario I, almost fixes the parameter ${\rm Re}\,\omega$ to a multiple of $\pi/2$.[12] In Sec. VI we therefore fix ${\rm Re}\,\omega = \pi/2$.

The remaining parameters ξ, M, ΔM and ${\rm Im}\,\omega$ contain a redundancy. For $\Delta M \ll M$ changing simultaneously the signs of ξ, ΔM and ${\rm Im}\,\omega$, along with the transformation ${\rm Re}\,\omega \leftrightarrow \pi - {\rm Re}\,\omega$, corresponds to swapping the names of N_2 and N_3. To be definite, we always choose $\xi = 1$ and

[12] This is explained in Sec. II F.

consider both signs of $\mathrm{Im}\omega$. Our main results consist of bounds on the parameters M, $\mathrm{Im}\omega$ and ΔM.

For experimental searches the most relevant properties of the sterile neutrinos are the masses $\bar{M} \simeq M$ and their mixing with active neutrinos. We therefore also present our results in terms of M, the physical mass splitting δM and

$$U^2 \equiv \mathrm{tr}(\Theta^\dagger \Theta) = \mathrm{tr}(\theta^\dagger \theta) = \sum_\alpha U_\alpha^2, \tag{20}$$

where Θ and U_α^2 are given by (7) and (8), respectively. U^2 measures the mixing between active and sterile species. δM and U^2 can, however, not be mapped on parameters in the Lagrangian in a unique way; there exists more than one choice of ω leading to the same U^2.

F. "Fine-tunings" and the constrained νMSM

In most models that incorporate the seesaw mechanism the eigenvalues of M_M are much larger than the electroweak scale. It is a defining feature of the νMSM that all experimental data can be explained without the introduction of such a new scale. In order to keep the sterile neutrino masses below the electroweak scale and the active neutrino masses in agreement with experimental constraints, the Yukawa couplings F have to be very small. As a consequence of this, the thermal production rates for lepton asymmetries are also very small unless they are resonantly amplified. In scenarios I and II this requires a small mass splitting between M_2 and M_3. This can either be viewed as fine-tuning or be related to a new symmetry [6,10]. In the following we focus on these two scenarios, I and II. We do not discuss the origin of the small mass splitting here, but only list the implications.[13]

Fermionic dispersion relations in a medium can have a complicated momentum dependence. In the following we make the simplifying assumption that all neutrinos have hard spatial momenta $\bar{p} \sim T$ and parametrize the effect of the medium by a temperature-dependent quasiparticle mass matrix $M_N(T)$,[14] which we define as $M_N(T)^2 = H^2 - \bar{p}^2$ at $|\mathbf{p}| = \bar{p} \sim T$. Here H is the dispersive part of the temperature-dependent effective Hamiltonian given in Appendix A, cf. (A32). The general structure of $M_N(T)$ is rather complicated, but we are only interested in the regimes $T \lesssim M$ (DM production) and $T > T_{\mathrm{EW}}$ (baryogenesis). Analogous to the vacuum notation in (10)–(12), we refer to the temperature-dependent eigenvalues of $M_N(T)$ as $M_1(T)$ and $M_2(T)$, their average as $\bar{M}(T)$ and their splitting as $\delta M(T)$. Though N_I are the fields whose excitations correspond to mass eigenstates in the microscopic theory, the mass matrix $M_N(T)$ in the effective quasiparticle description is not necessarily diagonal in the N_I basis for $T \neq 0$. The effective physical mass splitting $\delta M(T)$ depends on T in a nontrivial way. This dependence is essential in the regime $\bar{M}(T) \gg \delta M(T)$, which we are mainly interested in. In principle, $\bar{M}(T)$ also depends on temperature. This dependence is practically irrelevant at $T \lesssim T_-$ and replacing $\bar{M}(T)$ by M during late time leptogenesis does not cause a significant error.

There are three contributions to the temperature-dependent physical mass splitting: the splitting ΔM that appears in the Lagrangian, the Dirac mass $m_D(T) = F v(T)$ that is generated by the coupling to the Higgs condensate, and thermal masses due to forward scattering in the plasma, including Higgs particle exchange.[15] The interplay between the different contributions leads to nontrivial effects as the temperature changes.

1. Baryogenesis

For successful baryogenesis it is necessary to produce a lepton asymmetry of $\mu_\alpha \sim 10^{-10}$ at $T \gtrsim T_+$ that survives until T_{EW} and is partly converted into a baryon asymmetry by sphalerons; see condition (i). In this work we focus on scenarios I and II, in which only two sterile neutrinos $N_{2,3}$ are involved in baryogenesis. In these scenarios baryogenesis is only possible if the physical mass splitting is sufficiently small [$\delta M(T) \ll M$] and leads to a resonant amplification. On the other hand, it should be large enough for the sterile neutrinos to perform at least one oscillation. Thus, baryogenesis is most efficient if it is of the same order of magnitude as the relaxation rate (or thermal damping rate) at $T \gtrsim T_+$,

$$\delta M(T) \sim (\Gamma_N)(T)_{IJ}. \tag{21}$$

Here Γ_N is the temperature-dependent dissipative part of the effective Hamiltonian that appears in the kinetic equations given in Sec. IV; it is defined in Appendix A 3 b and calculated in Sec. IV B. It is essentially given by the sterile neutrino thermal width. However, (21) only provides a rule of thumb to identify the region where baryogenesis is most efficient. Numerical studies in Sec. V show that the observed BAU can be explained even far away from this point, for $M \gg \delta M(T) \gg \Gamma_N(T)$. Thus, the mass degeneracy $\delta M(T) \ll M$ is the only serious tuning required in scenario II. In Ref. [30] it has been found that no such mass degeneracy is required in scenario III.

[13]As far as this work is concerned the sterile neutrino mass spectrum in the νMSM follows from the requirement to simultaneously explain Ω_B and Ω_{DM}. It is in accordance with the principle of minimality and the idea to explain new physics without the introduction of a new scale (above the electroweak scale). In this work we do not discuss a possible origin of the mass spectrum and flavor structure in the SM and νMSM, which to date is purely speculative. Ideas on the origin of a low seesaw scale can be found in Refs. [65,66] and references therein, cf. also Refs. [67–83]. Some speculations on the small mass splitting have been made in Refs. [6,10,48,84]. A similar spectrum has been considered in a supersymmetric theory in Ref. [85].

[14]See, e.g., Refs. [86–89] for a discussion of the quasiparticle description.

[15]We ignore the running of the mass parameters, which has been studied in Ref. [48].

2. Dark matter production

In scenario I N_1 dark matter has to be produced thermally from the primordial plasma [54]. In the absence of chemical potentials, the resulting spectrum of N_1 momenta has been determined in Ref. [24]. State of the art x-ray observations, structure formations and Ly_α forest observations suggest that this production mechanism is not sufficient to explain Ω_{DM} because the required N_1 mass and mixing are astrophysically excluded [21,90]. However, in the presence of a lepton chemical potential, the dispersion relation for active neutrinos is modified due to the MSW effect. If the chemical potential is large enough, this can lead to a level crossing between active and sterile neutrinos, resulting in a resonant amplification of the N_1 production rate [57]. The full dark matter spectrum is a superposition of a smooth distribution from the nonresonant production and a nonthermal spectrum with distinct peaks at low momenta from a resonant mechanism. In order to explain all observed dark matter by N_1 neutrinos, lepton asymmetries $|\mu_\alpha| \sim 8 \times 10^{-6}$ are required at $T_{\mathrm{DM}} \sim 100$ MeV [19]. This is the origin of condition (ii) already formulated in Sec. II D. Again, the resonance condition (21) indicates the region where the asymmetry production is most efficient. For $T_d, T_- \ll T_{\mathrm{EW}}$ it imposes a much stronger constraint on the mass splitting than during baryogenesis because the thermal rates Γ_N are much smaller.

The asymmetries μ_α can be created in two different ways, either during the freeze-out of $N_{2,3}$ around $T \sim T_-$ or in their decay at $T \sim T_d$. During these processes we can use the vacuum value for v. As discussed in Appendix A 3 a, the temperature dependence of $\delta M(T)$ is weak for $T < T_-$. The rates, on the other hand, still depend rather strongly on temperature; thus, it is usually not possible to fulfill the requirement (21) at $T = T_-$ and $T = T_d$ simultaneously. Therefore, one can distinguish two scenarios: The asymmetry generation is efficient either during freeze-out (freeze-out scenario) or during decay (decay scenario). On the other hand, (21) can be fulfilled simultaneously at $T = T_+$ and $T = T_d$ or at $T = T_+$ and $T = T_-$ because at $T = T_+$ the mass splitting also depends on temperature. The strongest fine-tuning requirement in the νMSM is therefore[16]

$$\begin{aligned} &\delta M(T_+) \sim (\Gamma_N)_{IJ}(T_+) \quad \text{and} \quad \delta M(T_-) \sim (\Gamma_N)_{IJ}(T_-) \\ \text{or} \quad &\delta M(T_+) \sim (\Gamma_N)_{IJ}(T_+) \quad \text{and} \quad \delta M(T_d) \sim (\Gamma_N)_{IJ}(T_d). \end{aligned} \tag{22}$$

From (12) it is clear that during the decay $\delta M(T_d) \approx \delta M(T = 0)$ and

$$\delta M \geq \frac{1}{2M}(\mathrm{Re}(m_D^\dagger m_D)_{33} - \mathrm{Re}(m_D^\dagger m_D)_{22}) + \Delta M, \tag{23}$$

$$|\delta M| \geq \frac{1}{M}\,\mathrm{Re}(m_D^\dagger m_D)_{23}. \tag{24}$$

Fulfilling the resonance condition (21) at low temperatures requires a precise cancellation of the parameters in (23) and (24), both of which have to be fulfilled individually. The condition (24) imposes a strong constraint on the active neutrino mass matrix (3). It can be fulfilled when the real part of the off-diagonal elements is small. Note that this, due to (9), implies that U_N is close to unity. This is certainly the case when the real part of complex angle ω in $\mathcal{R}$ is a multiple of $\pi/2$. In Secs. VI and VII we will focus on this region and always choose $\mathrm{Re}\omega = \pi/2$. It should be clear that this is a conservative approach, since the production of lepton asymmetries can also be efficient away from the maximally resonant regions defined by (22). The lower bound (23) can always be made consistent with (21) by adjusting the otherwise unconstrained parameter ΔM. At tree level this parameter is effectively fixed by

$$\Delta M = -\frac{1}{2M}(\mathrm{Re}(m_D^\dagger m_D)_{33} - \mathrm{Re}(m_D^\dagger m_D)_{22}) \pm \delta M, \tag{25}$$

where the dependence of the right-hand side on ΔM is weak. The range of values for ΔM dictated by this condition is extremely narrow; it is fixed to values around $\Delta M/M \sim 10^{-11}$ at a relative precision of roughly 10^{-13}. This is imposed by the required tuning $\delta M/M \lesssim 10^{-13}$ we find numerically. Quantum corrections are of order $\sim m_i$ [48], i.e., much bigger than $\delta M(T_-)$. The high degree of tuning, necessary to explain the observed Ω_{DM}, is not understood theoretically. Some speculations can be found in Refs. [6,10,48,84]. However, the origin of this fine-tuning plays no role in the present work.

In the following we will refer to the νMSM with the condition $\mathrm{Re}\omega = \frac{1}{2}$ and the fixing of ΔM as constrained νMSM. Since the first term in the square root in (12) also depends on $\mathrm{Re}\omega$, fixing this parameter exactly to a multiple of $\pi/2$ usually does not exactly give the minimal δM. However, it considerably simplifies the analysis, and deviations from such a value can, in any case, only be small due to the above considerations.

III. EXPERIMENTAL SEARCHES AND ASTROPHYSICAL BOUNDS

The experimental, astrophysical and BBN bounds presented in this section and in the figures in Secs. V, VI, and VII are derived under the premise that the mass and mixing of N_1 qualify it as a DM candidate, while $N_{2,3}$ are responsible for baryogenesis (scenarios I and II). Some of them loosen if one drops the DM requirement and considers the νMSM as a theory of baryogenesis and neutrino oscillations only in scenario III.

[16] It is in fact sufficient for baryogenesis if $\delta M(T) \sim (\Gamma_N)_{IJ}(T)$ at some temperature $T > T_+$ as long as some flavor asymmetries survive until T_{EW}. The washout of the μ_α typically becomes efficient around T_+, but chemical equilibration can take a long time if active neutrinos of one flavour couple to the sterile neutrinos much weaker than those of the other two.

A. Existing bounds

A detailed discussion of the existing experimental and observational bounds on the νMSM can be found in Ref. [21]. Some updates that incorporate the effect of recent measurements of the active neutrino mixing matrix U_ν, in particular, $\theta_{13} \neq 0$, have been published in Refs. [26,27,29]. In the following we reanalyze all relevant constraints on the seesaw partners $N_{2,3}$ from direct search experiments and BBN in the face of these experimental results. We also briefly review existing constraints on the dark matter candidate N_1.

As far as the known (active) neutrinos are concerned, the main prediction of the νMSM is that one of them is (almost) massless. This fixes the absolute mass scale of the remaining two neutrinos [2]. Currently, there is neither a clear prediction for the phases in U_ν in the νMSM nor an experimental determination, though the experimental value for θ_{13} [60,63] suggests that a measurement, in principle, might be possible. Regarding the sterile neutrinos, one has to distinguish between $N_{2,3}$ and N_1.

1. Seesaw partners N_2 and N_3

LHC.—The small values of $M_I \ll v$, in principle, make it possible to produce them in the laboratory. However, the smallness of the Yukawa couplings F implies that the branching ratios are very small. Therefore, the number of collisions (rather than the required collision energy) is the main obstacle in direct searches for the sterile neutrinos. This number is too small in high energy experiments such as ATLAS or CMS [91].[17] It is therefore a prediction of the νMSM that the LHC finds no new particles except the Higgs boson. Vice versa, the lack of findings of new physics beyond the SM at the LHC can be viewed as indirect support for the model (though this prediction is of course relaxed if nature happens to be described by the νMSM plus something else).

Direct searches.—The sterile neutrinos participate in all processes that involve active neutrinos, but with a probability that is suppressed by the small mixings U_α^2. The mixing of $N_{2,3}$ to the SM is large enough that they can be found experimentally [16]. A number of experiments that allow us to constrain the sterile neutrino properties have been carried out in the past [92,93], in particular, CERN PS191 [94,95], NuTeV [96], CHARM [97], NOMAD [98] and BEBC [99] (see Ref. [100] for a review). These can be grouped into beam dump experiments and peak searches.

Peak search experiments look for the decay of charged mesons into charged leptons ($e^\pm$ or $\mu^\pm$) and neutrinos. Due to the mixing of the active neutrino flavor eigenstates with the sterile neutrinos, the final state in a fraction of decays suppressed by U_e^2 (or U_μ^2) is $e^\pm + N_I$ (or $\mu^\pm + N_I$). The kinematics of the two-body decay can be reconstructed from the detected charged lepton, but the sterile flavor cannot be determined because of the N_I mass degeneracy. Therefore, these experiments are only sensitive to the inclusive mixing U_α^2 defined in (8), where α is the flavor of the charged lepton.

In beam dump experiments, sterile neutrinos are also created in the decay of mesons, which have been produced by sending a proton beam onto a fixed target. A second detector is placed near the beamline to detect the decay of the sterile neutrinos into charged particles. Also in beam dump experiments, the sterile flavors cannot be distinguished. In this case, the expected signal is of the order $U_\alpha^2 U_\beta^2$ because creation and decay of the N_I each involve one active-sterile mixing. For instance, the CERN PS191 experiment constrains the combinations $(U_e^2)^2$, $(U_\mu^2)^2$, $U_e^2 U_\mu^2$ and[18]

$$\sum_\beta U_\alpha^2 (c_\beta U_\beta^2), \tag{26}$$

where

$$c_e = \frac{1 + 4\sin^2\theta_W + 8\sin^2\theta_W}{4}, \qquad c_\mu = c_\tau = \frac{1 - 4\sin^2\theta_W + 8\sin^2\theta_W}{4}. \tag{27}$$

This set differs from the quantities considered by the experimental group [94,95]. It has been pointed out in Ref. [27] that the original interpretation of the PS191 (and also CHARM) data cannot be directly applied to the seesaw Lagrangian (1). The authors of Ref. [27] translate the bounds on active-sterile neutrino mixing published by the PS191 and CHARM collaborations into bounds that apply to the νMSM and kindly provided us with their data. We use these bounds, along with the NuTeV constraints, as an input to constrain the region in the νMSM parameter space that is compatible with experiments.

Our results are displayed as green lines of different shades in the summary plots in Figs. 7, 13, and 14 in Secs. V and VII. The different lines have to be interpreted as follows. Each shade of green corresponds to one experiment. For each experiment, there is a solid and a dashed line. The solid line is an exclusion bound. This means that there exists no choice of νMSM parameters that leads to a combination of U^2 and M above this line, which is consistent with Table I and the experiment in question. In order to obtain the exclusion bound from an experiment for a particular choice of M, we varied the CP-violating phases and Imω.[19] We checked, for each choice, whether the

[17]The authors of Ref. [91] claim that this conclusion may be avoided for M near the electroweak scale if there is a strong cancellation between the contributions from different right-handed neutrinos to the light neutrino masses.

[18]There are also constraints on U_τ^2 which are, however, too weak to be of practical relevance.

[19]The mixings U_α^2 do not depend on Reω, and the dependence on ΔM is negligible.

resulting U_α^2 are compatible with the experiment in question. The exclusion bound in the M-U^2 plane is obtained from the set of parameters that leads to the maximal U^2 for a given M amongst all choices that are in accordance with experiment. The exclusion plots are independent of the other lines in the summary plots. The dashed lines (in the same shade as the exclusion plots) represent the bounds imposed by each experiment if the CP-violating phases are self-consistently fixed to the values that we used to produce the red and blue lines in the summary plots, which encircle the regions in which enough asymmetry is created to explain the BAU and DM. The NuTeV experiment puts bounds only on the mixing angle U_μ^2. This induces a much weaker constraint in the M-U^2 plane for inverted mass hierarchy than the other experiments. Our results differ from those of Ref. [22]. In this reference, the experimental constraints on the individual U_α^2 were directly reported in the M-U^2 plane plotted in Fig. 3 of Ref. [22]. Moreover, only the PS191 exclusion bound was computed by distinguishing between mass hierarchies.

Active neutrino oscillation experiments.—The region below the seesaw line in Figs. 7, 11, 13, and 14 is excluded because, for the experimental values listed in Table I, there exists no choice of νMSM parameters that would lead to this combination of M and U^2.

Big bang nucleosynthesis.—It is a necessary requirement that $N_{2,3}$ have decayed sufficiently long before BBN that their decay products do not affect the predicted abundances of light elements, which are in good agreement with observation. The total increase of entropy due to the $N_{2,3}$ decay is small, but the decay products have energies in the GeV range and even a small number of them can dissociate enough nuclei to modify the light element abundances. Since the sterile neutrinos are created as flavor eigenstates, they oscillate rapidly around the time of BBN. On average, they spend roughly half the time in each flavor state, and it is not the individual lifetimes of each flavor that determine the relaxation time, but rather their average. This allows us to estimate the inverse $N_{2,3}$ lifetime τ by $\tau^{-1} \simeq \frac{1}{2}\,\mathrm{tr}\Gamma_N$ at $T = 1$ MeV. For $\tau < 0.1$ s the decay products and all secondary particles have lost their excess energy to the plasma in collisions and reached equilibrium by the time of BBN.[20] We impose the condition $\tau < 0.1$ s and vary all free parameters to identify the region in the M-U^2 plane consistent with this condition. The BBN exclusion bounds in Figs. 7, 13, and 14 represent the region in which no choice of νMSM parameters exists that is consistent with Table I and the above condition. Note that $\tau^{-1} \simeq \frac{1}{2}\,\mathrm{tr}\Gamma_N$ and the condition $\tau < 0.1$ s are both rough estimates; the BBN bound we plot may change by a factor of order 1 when a detailed computation is performed.

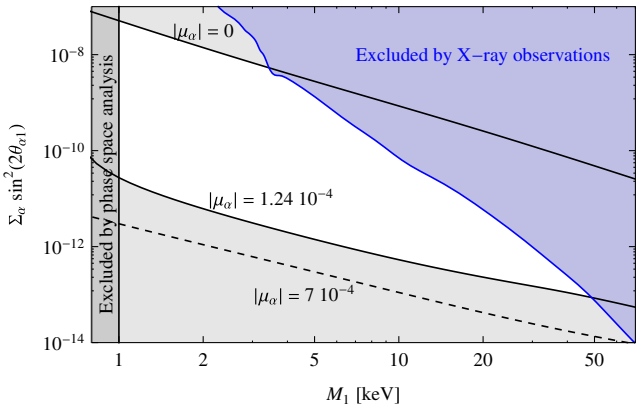

FIG. 2 (color online). Different constraints on N_1 mass and mixing. The blue region is excluded by x-ray observations, and the dark gray region $M_1 < 1$ keV by the Tremaine-Gunn bound [114,115,137]. The points on the upper solid black line correspond to observed Ω_{DM} produced in scenario I in the absence of lepton asymmetries (for $\mu_\alpha = 0$) [19]; points on the lower solid black line give the correct Ω_{DM} for $|\mu_\alpha| = 1.24 \times 10^{-4}$, the maximal asymmetry we found. The region between these lines is accessible for $0 \leq |\mu_\alpha| \leq 1.24 \times 10^{-4}$. We do not display bounds derived from Ly_α forest observations because they depends on μ_α in a complicated way, and the calculation currently includes considerable uncertainties [90].

2. Dark matter candidate N_1

The possibility of sterile neutrino DM has been studied by many authors; see, e.g., Refs. [7,13,21,90,101–131]. The coupling of the DM candidate N_1 is too weak to be constrained by any past laboratory experiment. However, there are various different requirements that constrain the allowed region in the $\theta_{\alpha 1}^2$-M_1 plane. N_1 has to have a lifetime comparable to the age of the Universe and be consistent with bounds from indirect DM searches; it is subject to phase space density restrictions (because it is a fermion) and its gravitational clustering must reproduce the observed structure in the Universe.[21] In scenario I, it is, in addition, crucial that the right amount of Ω_{DM} can be produced within the νMSM.

As a decaying dark matter candidate, N_1 particles produce a distinct x-ray line in the sky that can be searched for (see, e.g., Refs. [7,12,13,109,122–125,127,128,134–136]). These pose an *upper bound* on M_1 in the keV range [109,110,124] that depends on the mixing, cf. Fig. 2. A lower limit $M_1 \sim 1$ keV can be obtained when applying the Tremaine-Gunn bound on phase space densities [137] to the Milky Way's dwarf spheroidal galaxies [114,115]. Other bounds can be derived from the observed matter distribution in the Universe, as the gravitational collapse of DM overdensities was the driving force for nonlinear structure formation in the matter dominated era. This

[20] A more precise analysis of this condition for $M < 140$ MeV has been performed in Ref. [29].

[21] See, e.g., Refs. [132,133] for a more detailed discussion of these bounds.

constrains the DM free-streaming length; the formation of structure smaller than the free-streaming length is strongly suppressed. In order to translate the free-streaming length into a bound on the N_1 properties, one needs to make assumptions on the N_1 momentum distribution. If it is simply proportional to a Fermi-Dirac distribution, the DM distribution in the observable Universe reconstructed from Ly_α forest observations (cf. e.g., Refs. [105,110,112,138–142]) suggests a *lower bound* on the mass $M_1 \gtrsim 8$ keV [110].[22]

The expected momentum distribution depends on the production mechanism for N_1; hence, we can only make quantitative predictions in scenario I, where this mechanism is specified. Within the νMSM, there are two different ways to produce N_1 thermally. The first one, common thermal (nonresonant) production [54], leads to a smooth distribution of momenta that is roughly proportional to a Fermi-Dirac spectrum. If this were the only mechanism, then tension between the x-ray and structure formation bounds would exclude scenario I. However, the DM production rate can be resonantly amplified by the presence of a lepton chemical potential in the plasma [19,57]. While the presence of a lepton chemical potential created by the $N_{2,3}$ freeze-out and decay at late times ($T \lesssim$ GeV) is a very generic prediction in the νMSM, it turns out to be highly nontrivial to produce the right amount of lepton asymmetry to explain Ω_{DM}. The resonant amplification of the thermal N_1 production rate occurs due to a level crossing between active and sterile neutrino dispersion relations, caused by the MSW effect. It enhances the production rate for particular momenta as they pass through the resonance, resulting in a nonthermal DM momentum distribution that is dominated by low momenta and thus "colder."[23] Effectively, this mechanism "converts" lepton asymmetries into DM abundance, as the asymmetries are erased while DM is produced. The full DM spectrum in the νMSM is a superposition of the two components. The dependence on μ_α is, however, rather complicated. In particular, the naive expectation that the largest $|\mu_\alpha|$, which maximized the efficiency of the resonant production mechanism, leads to the lowest average momentum ("coldest DM") is not true because μ_α does not only affect the efficiency of the resonance, but also the momentum distribution of the produced particles. In a realistic scenario involving both production mechanisms ($|\mu_\alpha| \gtrsim 10^{-5}$), the lower bound on M_1 from structure formation relaxes and has been estimated as $M_1 > 2$ keV [90]. In our analysis we take these results for granted, though some uncertainties remain to be clarified; see Sec. III B 1.

The N_1 abundance must correctly reproduce the observed DM density Ω_{DM}. In scenario I this requirement defines a line in the M_1-$\sum_\alpha |\theta_{\alpha 1}|^2$ plane, the production curve. All combinations of M_1 and $\sum_\alpha |\theta_{\alpha 1}|^2$ along the production curve lead to the observed DM abundance. Because of the resonant contribution, the production curve depends on μ_α. This dependence has been studied in Ref. [19], where it was assumed that $\mu_e = \mu_\mu = \mu_\tau$.

Finally, DM sterile neutrinos may have interesting effects for supernova explosions [117–121].

Figure 2 summarizes a number of bounds on the properties of N_1. The two thick black lines are the production curves for $\mu_\alpha = 0$ and $|\mu_\alpha| = 1.24 \times 10^{-4}$, the maximal asymmetry we found at $T = 100$ MeV in our analysis; see Fig. 12. The allowed region lies between these lines; above the $\mu_\alpha = 0$ line, the nonresonant production alone would already overproduce DM, and below the production curve for maximal asymmetry $N_{2,3}$ fail to produce the required asymmetry for all choices of parameters. The maximal asymmetry has been estimated as $\sim 7 \times 10^{-4}$ in Refs. [6,19], which agrees with our estimate shown in Fig. 12 up to a factor ~ 5. (The production curve corresponding to that estimate is shown as a dotted line in Fig. 2.) Our result is smaller and imposes a stronger lower bound on the N_1 mixing, which makes it easier to find this particle (or exclude it as the only constituent of the observed Ω_{DM}) in x-ray observations. However, though our calculation is considerably more precise than the previous estimate, the exclusion bound displayed in Fig. 12 still suffers from uncertainties of order 1 due to the issues discussed in Appendix A 4. It also relies on the assumption[24] $\mu_e = \mu_\mu = \mu_\tau$, made in Refs. [6,19] to find the dependence of the production curve on the asymmetry. In order to determine the precise exclusion bound, the dependence of the production curve on individual flavor asymmetries has to be determined. The shadowed (blue) region is excluded by the nonobservation of an x-ray line from N_1 decay in DM dense regions [7,13,101,103,109,122–128].

B. Future searches

1. Dark matter candidate N_1

Indirect detection.—The DM candidate N_1 can be searched for astrophysically, using high resolution x-ray

[22]See also Refs. [105,111,112]. There, it has been assumed that baryonic feedback on matter distribution (see, e.g., Refs. [143] for a discussion) has a negligible effect.

[23]The results quoted in Ref. [113] suggest that the resonantly produced sterile neutrino is "warm enough" to overcome some problems of cold DM simulations [144,145] (i.e., change the number of substructures of a Galaxy-size halo), but "cold enough" to be in agreement with Ly_α bounds on large scale structures [90].

[24]Indeed, we find that this assumption does not hold in most of the parameter space. The asymmetries in individual flavors can be very different and even have opposite signs. The reason is that asymmetries generated at $T > M$ are mainly "flavored" asymmetries (i.e., the total lepton number violation is small), but the individual flavors can carry asymmetries. In spite of this we believe that the condition $\sum_\alpha |\mu_\alpha|$ still gives the right order of magnitude, see Appendix A 4.

spectrometers to look for the emission line from its decay in DM dense regions. For details and references see the proposal submitted to European Strategy Preparatory Group by Boyarsky *et al.* [146], cf. also Refs. [65,132,147,148].

Structure formation.—Model-independent constraints on N_1 can be derived from the consideration of dynamics of dwarf galaxies [114,115,137]. The existing small scale structures in the Universe, such as galaxy subhalos, provide another probe that is sensitive to N_1 properties, because such structures would be erased if the mean free path of DM particles were too long. This can be exploited by comparing numerical simulations of structure formation to the distribution of matter in the Universe that is reconstructed from Ly_α forest observations. However, the momentum distribution of resonantly produced N_1 particles can be complicated [19,57], leading to a complicated dependence of the allowed mixing angle on the N_1 mass and lepton asymmetries μ_α in the plasma [90,110]. It is difficult to understand the implications of these spectra for the formation of small scale structures [83,90,106,107]. A reliable quantitative analysis would involve numerical simulations that use the nonthermal N_1 momentum distribution predicted in scenario I as input. While for cold dark matter extensive studies have been performed (see, e.g., Ref. [149]), simulations for other spectra have only been done for certain benchmark scenarios [113].

Direct detection.—As the solar system passes through the interstellar medium, the DM particles N_1 can interact with atomic nuclei in the laboratory via the $\theta_{\alpha 1}\theta^*_{\alpha 1}$ suppressed weak interaction. This, in principle, opens the possibility of direct detection [150]. Such detection is extremely challenging due to the small mixing angle and the background from solar and stellar active neutrinos. It has, however, been argued that this may be possible [151,152].

BBN.—The primordial abundances of light elements are sensitive to the number of relativistic particle species in the primordial plasma during BBN because these affect the energy budget, which determines the expansion rate and temperature evolution. Any deviation from the SM prediction is usually parametrized in terms of the effective number of neutrino species, N_{eff}. At temperatures around 2 MeV, most N_1 particles are relativistic. However, the occupation numbers are far below their equilibrium value, and the effect of the N_1 on N_{eff} is very small. Given the error bars in current measurements [153–155], the νMSM predicts a value for N_{eff} that is practically indistinguishable from $N_{\mathrm{eff}} = 3$.

In principle, the late-time asymmetry in active neutrinos predicted by the νMSM also affects BBN because the chemical potential modifies the momentum distribution of neutrinos in the plasma. However, the predicted asymmetry is several orders of magnitude smaller than existing bounds [42], and it is extremely unlikely that this effect can be observed in the foreseeable future. In particular, though N_1 DM particles are relativistic during BBN (while they are nonrelativistic at the time of photon decoupling), they cannot explain tentative hints for "dark radiation" in recent observations (see, e.g., Ref. [156] for a summary).

2. Seesaw partners $N_{2,3}$

The singlet fermions participate in all the reactions in which the ordinary neutrinos do, with the probability suppressed roughly by a factor U^2. However, due to their masses, the kinematic changes when an ordinary neutrino is replaced by N_I. The $N_{2,3}$ particles can be found in the laboratory [16] using the strategies outlined in Sec. III A 1, which have been applied in past searches.

One strategy, used in peak searches, is the study of kinematics of rare K, D, and B meson decays that can constrain the strength of the N_I masses and mixings. This includes two-body decays (e.g., $K^\pm \to \mu^\pm N$, $K^\pm \to e^\pm N$) or three-body decays (e.g., $K_{L,S} \to \pi^\pm + e^\mp + N_{2,3}$). The precise study of the kinematics is possible in Φ (like K long experiment), charm, and B factories, or in experiments with kaons where the initial 4-momentum is well known. For 3 MeV $< M_I <$ 414 MeV this possibility has recently been discussed in Ref. [157].

The second strategy aims at observing the decays of the N_I themselves ("nothing" $\to$ leptons and hadrons) in proton beam dump experiments. The N_I are created in the decay of K, D, or B mesons emitted by a fixed target, into which the proton beam is dumped. The detector must be placed at some distance along the beamline. Several existing or planned neutrino facilities (related, e.g., to CERN SPS, MiniBooNE, MINOS or J-PARC) could be complemented by a *dedicated* near detector for these searches. Finally, these two strategies can be unified [31], and the production and the decay could occur inside the same detector [158].

For the mass interval $M < m_K$, both strategies can be used. An upgrade of the NA62 experiment at CERN would allow us to search the mass region below the kaon mass m_K. For $m_K < M < m_D$ it is unlikely that a peak search for missing energy at beauty, charm, and τ factories will gain the necessary statistics. Thus, in this region the search for $N_{2,3}$ decays is the most promising strategy. Dedicated experiments using the SPS proton beam at CERN can completely explore the very interesting parameter range for $M < 2$ GeV. This has been outlined in detail in the European Strategy Preparatory Group by Gorbunov *et al.* [159].

An upgrade of the LHCb experiment could allow us to combine both strategies. This would allow us to constrain the cosmologically interesting region in the M-U^2 plane. With existing or planned proton beams and B-factories, the mass region between the D-mass and B-meson thresholds is, in principle, accessible, but such experiments would be extremely challenging. A search in the cosmologically interesting parameter space would require an increase in

the present intensity of the CERN SPS beam by 2 orders of magnitude or to produce and study the kinematics of more than 10^{10} B mesons [159].

IV. KINETIC EQUATIONS

Production, freeze-out and decay of the sterile neutrinos are nonequilibrium processes in the hot primordial plasma. We describe these by effective kinetic equations of the type used in Ref. [160] and further elaborated in Refs. [3,6,8,51], cf. also Refs. [161–164]. These equations are similar to those commonly used to describe the propagation of active neutrinos in a medium. They rely on a number of assumptions and may require corrections when memory effects or off-shell contributions are relevant. These assumptions are discussed in Appendix A. We postpone a more refined study to the time when such precision is required from the experimental side. In the following we briefly sketch the derivation of the kinetic equations we use. More details are given in Appendix A.

A. Short derivation of the kinetic equations

We describe the early Universe as a thermodynamical ensemble. In quantum field theory, any such ensemble—whether it be in equilibrium or not—can be described by a density matrix $\hat{\rho}$. The expectation value of any operator $\mathcal{A}$ at any time can be computed as

$$\langle \mathcal{A} \rangle = \mathrm{tr}(\hat{\rho}\mathcal{A}). \tag{28}$$

As there are infinitely many states in which the world can be, infinitely many numbers are necessary to exactly characterize $\hat{\rho}$. These can either be given by all matrix elements of $\hat{\rho}$ or, equivalently, by all n-point correlation functions for all quantum fields. Either way, any practically computable description requires truncation.

The leptonic charges can be expressed in terms of field bilinears; thus, it is sufficient to concentrate on the two-point functions. Instead of bilinears in the field operators themselves, we consider bilinears in the ladder operators a_I, $a_I^\dagger$ for sterile and a_α, $a_\alpha^\dagger$ for active neutrinos. In principle, there is a large number of bilinears, but only a few of them are relevant for our purpose.

For each momentum mode of sterile neutrinos, we consider two 2×2 matrices formed by products of ladder operators $a_I^\dagger a_J$, one for positive and one for negative helicity.[25] Since M_N is diagonal in the N_I basis, $a_I^\dagger a_I$ can be interpreted as a number operator for physical sterile neutrinos, while $a_I^\dagger a_J$ with $I \neq J$ correspond to coherences. N_I are Majorana fields, but we can define the notion of "particle" and "antiparticle" by their helicity states. In the limit $T \gg M$, i.e., for a negligibly small Majorana mass term, the total lepton number (sum over α and I) defined in this way is conserved. All other bilinears in the ladder operators for sterile neutrinos are either of higher order in F or quickly oscillating and can be neglected. Practically, we are not interested in the time evolution of individual modes, but only in the total asymmetries. We therefore describe the sterile neutrinos by momentum integrated abundance matrices ρ_N for particles and $\rho_{\bar{N}}$ for antiparticles. The precise definitions are given in Appendix A 1.

The active leptons are close to thermal equilibrium at all times under consideration. This is because kinetic equilibration is driven by fast gauge interactions, while the relaxation rates for the asymmetries are of second order in the small Yukawa couplings F. We thus describe the active sector by four numbers,[26] the temperature and three asymmetries (one for each flavor, integrated over momentum). More precisely, the asymmetry in the SM leptons of flavor α is given by the difference between lepton and antilepton abundances, which we denote by μ_α; see (14).[27] We study the time evolution of each flavor separately and find that they can differ significantly from each other. Following the steps sketched in Appendix A, one can find the effective kinetic "rate equations"

$$i\frac{d\rho_N}{dX} = [H, \rho_N] - \frac{i}{2}\{\Gamma_N, \rho_N - \rho^{\mathrm{eq}}\} + \frac{i}{2}\mu_\alpha \tilde{\Gamma}_N^\alpha, \tag{29}$$

$$i\frac{d\rho_{\bar{N}}}{dX} = [H^*, \rho_{\bar{N}}] - \frac{i}{2}\{\Gamma_N^*, \rho_{\bar{N}} - \rho^{\mathrm{eq}}\} - \frac{i}{2}\mu_\alpha \tilde{\Gamma}_N^{\alpha *}, \tag{30}$$

$$\begin{aligned} i\frac{d\mu_\alpha}{dX} = &-i\Gamma_L^\alpha \mu_\alpha + i\mathrm{tr}[\tilde{\Gamma}_L^\alpha(\rho_N - \rho^{\mathrm{eq}})] \\ &- i\mathrm{tr}[\tilde{\Gamma}_L^{\alpha *}(\rho_{\bar{N}} - \rho^{\mathrm{eq}})]. \end{aligned} \tag{31}$$

Here $X = M/T$, ρ^{eq} is the common equilibrium value of the matrices ρ_N and $\rho_{\bar{N}}$, H is the dispersive part of the effective Hamiltonian for sterile neutrinos that is responsible for oscillations, and rates Γ_N, $\tilde{\Gamma}_N^\alpha$ and Γ_L^α form the dissipative part of the effective Hamiltonian.

It is convenient to describe the sterile sector by ρ_+ and ρ_-, the CP-even and CP-odd deviations from equilibrium, rather than ρ_N and $\rho_{\bar{N}}$,

$$\rho_N - \rho^{\mathrm{eq}} = \rho_+ + \frac{\rho_-}{2}, \qquad \rho_{\bar{N}} - \rho^{\mathrm{eq}} = \rho_+ - \frac{\rho_-}{2}. \tag{32}$$

In terms of ρ_+ and ρ_-, (29)–(31) read

[25]This description is similar to the one commonly used in neutrino physics and could also be formulated in terms of "polarization vectors."

[26]It has been found in Ref. [165] that mixing amongst the different SM lepton doublets can occur due to their coupling to the right-handed neutrinos and could affect leptogenesis. However, in the νMSM the Yukawa couplings F are too tiny to lead to a sizable effect.

[27]Note that the μ_α here are abundances, not chemical potentials, which could alternatively be used to characterize the asymmetries. The relations between different characterizations of the asymmetries are given in Appendix C.

$$i\frac{d\rho_+}{dX} = [\mathrm{Re}H, \rho_+] - \frac{i}{2}\{\mathrm{Re}\Gamma_N, \rho_+\} + S_+, \tag{33}$$

$$i\frac{d\rho_-}{dX} = [\mathrm{Re}H, \rho_-] - \frac{i}{2}\{\mathrm{Re}\Gamma_N, \rho_-\} + S_-, \tag{34}$$

$$i\frac{d\mu_\alpha}{dX} = -i\Gamma^\alpha_L \mu_\alpha + S_\mu, \tag{35}$$

with

$$S_+ = -i\frac{d\rho^{eq}}{dX} + \frac{i}{2}[\mathrm{Im}H, \rho_-] + \frac{1}{4}\{\mathrm{Im}\Gamma_N, \rho_-\} - \frac{1}{2}\mu_\alpha \mathrm{Im}\tilde{\Gamma}^\alpha_N, \tag{36}$$

$$S_- = 2i[\mathrm{Im}H, \rho_+] + \{\mathrm{Im}\Gamma_N, \rho_+\} + i\mu_\alpha \mathrm{Re}\tilde{\Gamma}^\alpha_N, \tag{37}$$

$$S_\mu = i\mathrm{tr}[\mathrm{Re}(\tilde{\Gamma}^\alpha_L)\rho_-] - 2\mathrm{tr}[\mathrm{Im}(\tilde{\Gamma}^\alpha_L)\rho_+]. \tag{38}$$

Equations (33)–(38) are the basis of our numerical studies.

B. Computation of the rates

The rates appearing in (33)–(38) can be expressed as

$$\Gamma_N = \tau\sum_\alpha (\tilde{F}_{\alpha I}\tilde{F}^*_{\alpha J} R(T, M)_{\alpha\alpha} + \tilde{F}^*_{\alpha I}\tilde{F}_{\alpha J} R_M(T, M)_{\alpha\alpha}), \tag{39}$$

$$(\tilde{\Gamma}^\alpha_L)_{IJ} \simeq (\tilde{\Gamma}^\alpha_N)_{IJ} = \tau(\tilde{F}_{\alpha I}\tilde{F}^*_{\alpha J} R(T, M)_{\alpha\alpha} - \tilde{F}^*_{\alpha I}\tilde{F}_{\alpha J} R_M(T, M)_{\alpha\alpha}), \tag{40}$$

$$\Gamma^\alpha_L = \tau((FF^\dagger)_{\alpha\alpha}(R(T, M)_{\alpha\alpha} + R_M(T, M)_{\alpha\alpha})), \tag{41}$$

with no sum over α in (40) and (41). The flavor matrices R and R_M are defined in Appendix A 3; see (A42) and (A43). Here $\tilde{F} = FU_N$ and

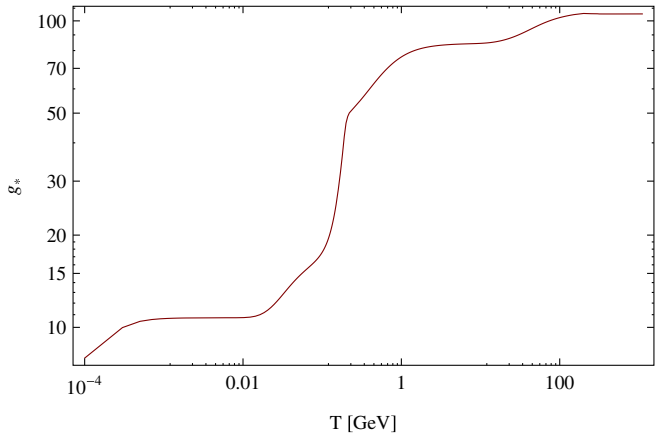

FIG. 3 (color online). Number of effective relativistic degrees of freedom g_* as a function of temperature [166].

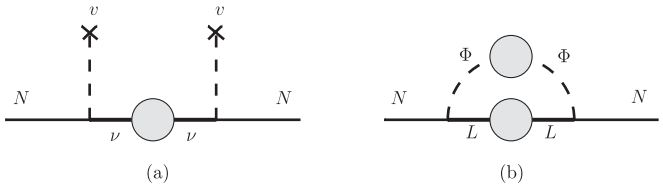

FIG. 4. Contributions to the N_I self-energies. Diagram (a) dominates for $T < v$, and diagram (b) for $T > v$. Γ_N is obtained from the discontinuity of the diagrams [205], which can be computed by cutting it in various ways [167]. The gray self-energy blobs indicate that dressed lepton and Higgs propagators have to be used. Cuts through them reveal a large number of processes, which are summarized in Refs. [8,24] and Appendix A of Ref. [6]. Recently, it has been pointed out that current estimates suffer from an error $\mathcal{O}(1)$ due to infrared and collinear enhancements at high temperatures. Systematic approaches to include these effects can be found in Refs. [176,206] for $T > M$ (relevant for baryogenesis) and [177,207,208] for $M > T$ (relevant for late-time asymmetries). We ignore this effect in our current study, as it is comparable to other uncertainties in the kinetic equations and would only slightly change the results for the relevant regions in the νMSM parameter space.

$$\tau = \frac{\partial t}{\partial X} = -\frac{T^2}{M}\frac{\partial}{\partial T}\frac{M_0}{2T^2}, \tag{42}$$

where T^2/M_0 is the Hubble rate and $M_0 = M_P(45)^{1/2}/(4\pi^3 g_*)^{1/2}$, with the effective number of relativistic degrees of freedom g_* computed in Ref. [166] and shown in Fig. 3.

The flavor matrices $R(T, M)$ and $R_M(T, M)$ are almost diagonal since off-diagonal elements of $\rho_{\alpha\beta}(p)$ include active neutrino oscillations, which are at least suppressed by m_i/T. We will always neglect the off-diagonal elements. $R(T, M)$ and $R_M(T, M)$ contain contributions from decays and scatterings. In finite temperature field theory these can be associated with different cuts [167] through the N_I self-energy shown in Fig. 4. The scatterings keep the N_I in thermal equilibrium for $T > T_-$. At $T \simeq T_-$ they become inefficient and the sterile neutrinos freeze out. Because of their small coupling they are long-lived but unstable and decay at a temperature T_d. For $T_d \ll T_-$, decay and freeze-out are two separate processes and can be treated independently. This is the case in the interesting part of the νMSM parameter space.

1. Baryogenesis

For $T > v$ the SM fields are light and M_M is negligible. We can therefore neglect $R_M(T, M)$ as well as the flavor dependence of $R(T, M)$. Dispersion relations as well as relaxation rates are dominated by contributions from scatterings between ν_R and Higgs and lepton particles. The corresponding rates can be extracted from cuts through the diagrams shown in Fig. 4(b). They have been computed in Refs. [3,22],

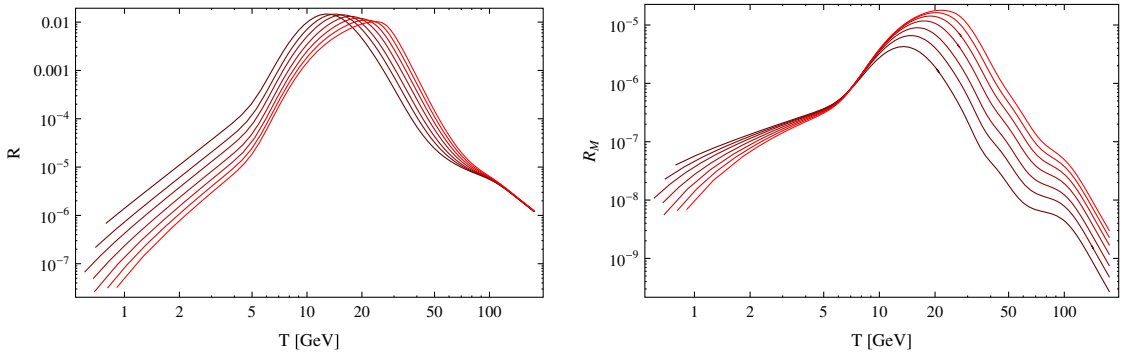

FIG. 5 (color online). The functions $R^{(S)}(T, M)$ and $R_M^{(S)}(T, M)$ for $M = 1.2$ GeV (darkest curve), $M = 1.6$ GeV, $M = 2$ GeV, $M = 2.5$ GeV, $M = 3$ GeV, $M = 3.5$ GeV, $M = 4$ GeV (lightest curve).

$$R(T, M) = 0.02\frac{T}{4}\mathbb{1}_{2\times 2},$$
$$R_M(T, M) = 0 \quad \text{for } T \gtrsim T_{\rm EW}. \tag{43}$$

2. Dark matter production

For $T_d \ll T_-$, which is the case in the interesting part of the νMSM parameter space, freeze-out and decay happen in different temperature regimes. At temperatures $T \gtrsim T_-$ the processes that keep the plasma in equilibrium are scatterings mediated by the weak interaction. Furthermore, the lepton masses are, in a first approximation, negligible.[28] Thus, $R(T, M)$ and $R_M(T, M)$ are proportional to the unit matrix and can be described by two scalar functions $R^{(S)}(T, M)$ and $R_M^{(S)}(T, M)$. Around $T_- \sim M$, $R_M^{(S)}(T, M)$ gives a small correction, which we account for in our analysis. In practice, these functions have to be computed numerically. They are displayed in Fig. 5.

To be specific, in the high temperature limit, when all lepton masses are negligible, (39) simplifies to

$$\Gamma_N \simeq \tau U_N^T((F^\dagger F)^* R^{(S)}(T, M) + F^\dagger F R_M^{(S)}(T, M))U_N^* \quad \text{at } T \sim T_-. \tag{44}$$

In the low temperature regime, where $R \simeq R_M$, one finds

$$\Gamma_N \simeq \tau \sum_\alpha \mathrm{Re}(\tilde{F}_{\alpha I}\tilde{F}^*_{\alpha J})R_\alpha^{(D)}(M) \quad \text{at } T \sim T_d. \tag{45}$$

The indices (S) and (D) indicate that the dominant contribution to the rate comes from scatterings or decays, respectively. The functions $R^{(S)}(T, M)$ and $R_M^{(S)}(T, M)$ can be obtained from the discontinuity of the N_I self-energies shown in Fig. 4 at finite temperatures. At $T < M$ the different SM lepton masses become relevant.

When the sterile neutrinos decay around $T_d \ll M$, the flavors are distinguishable. The decaying particle is nonrelativistic, and the density of the surrounding plasma is low. For $T = 0$, $R(0, M) = R_M(0, M)$ take the same values, and their elements are given by $R(0, M)_{\alpha\alpha} = R_M(0, M)_{\alpha\alpha} = R_\alpha^{(D)}(M)$, where $R_\alpha^{(D)}(M)$ are functions that can be computed from the vacuum decay rates for sterile neutrinos. The N_I can decay into various different final states; see Appendix D. There are leptonic and semileptonic channels, depending on the temperature, either with quarks (before hadronization) or mesons (after hadronization) in the final state. Let $\Gamma_{N_I\to\psi_\alpha}$ be the rate at which N_I decays into a final state ψ_α of flavor α (e.g., $\nu_\alpha q\bar{q}$ or $\nu_\alpha \bar{L}_\beta L_\beta$). Then

$$R_\alpha^{(D)}(M) = 2\sum_{\psi_\alpha}\frac{\Gamma_{N_I\to\psi_\alpha}}{|\tilde{F}_{\alpha I}|^2}, \tag{46}$$

where the sum runs over all possible final states that have flavor α. The factor 2 is due to the equal probabilities for decay into particles and antiparticles at tree level. The simple form of (46) is a result of the fact that the Yukawa couplings can be factored out of the corresponding amplitudes, and the kinematics of N_2 and N_3 is the same due to their degenerate mass. Most of the rates required for our study have been computed in Ref. [16]; the remaining ones are given in Appendix D. For $T \sim T_d \neq 0$ with $T_d \ll M$ the sterile neutrinos are nonrelativistic, and one can estimate

$$R(T \ll M, M)_{\alpha\alpha} \simeq \frac{M}{E}R_\alpha^{(D)}(M), \tag{47}$$

$$R_M(T \ll M, M)_{\alpha\alpha} \simeq \frac{E - \bar{p}}{E + \bar{p}}\frac{M}{E}R_\alpha^{(D)}(M), \tag{48}$$

with $E = (M^2 + \bar{p}^2)^{1/2}$. Here $\bar{p} \sim T$ is the average sterile neutrino momentum. We therefore do not need all elements of the matrices $R(T, M)$ and $R_M(T, M)$ at all temperatures, but only two functions $R^{(S)}(T, M)$ and $R_M^{(S)}(T, M)$ for $T \gtrsim T_-$ and three other functions $R_\alpha^{(D)}(M)$ for $T \lesssim T_d \ll M$. In practice, we can simply add these contributions at all temperatures. In principle, however, we do not know the scattering contribution outside the range plotted in Fig. 5, and

[28]For some parameter choices this assumption can be violated for the τ mass, introducing a small error.

the decay contribution is obtained from vacuum rates. This is justified because for $T \gtrsim T_-$ our expressions for the decay rates are incorrect, but $R_\alpha^{(D)}(M) \ll R^{(S)}(T, M)$. On the other hand $R_\alpha^{(D)}(M) \gg R_M^{(S)}(T, M)$ in the regime $T \ll M, T_-$, which is not covered by the data shown in Fig. 5. For $T_d < T < T_-$ our expressions for both decay and scattering rates are incorrect, but they are both smaller than the rate of Hubble expansion and have a negligible effect.

V. BARYOGENESIS FROM STERILE NEUTRINO OSCILLATIONS

The BAU in the νMSM is produced during the thermal production of sterile neutrinos N_I. This is in contrast to most other (thermal) leptogenesis scenarios, where decays and inverse decays play the central role. The violation of total fermion number by the Majorana mass term M_M is negligible at $T_{\rm EW} \gg M$, but asymmetries in the helicity states of the individual flavors can be created. The sum over these flavoured asymmetries vanishes up to terms suppressed by $M/T_{\rm EW}$, but because sphaleron processes only act on left chiral fields, the generated BAU can be much bigger. In this sense baryogenesis in the νMSM can be regarded as a version of "flavored leptogenesis."

In this section we explore the part of the νMSM parameter space where a BAU consistent with (13), i.e., $\eta \sim 10^{-10}$, can be generated. We assume two sterile neutrinos $N_{2,3}$ participate in baryogenesis, as required in scenarios I and II. This assumption is motivated by the premise that N_1 should be a valuable DM candidate, with masses and mixing consistent with astrophysical bounds. These bounds require its Yukawa interaction to be too small to be relevant for baryogenesis; see Sec. III. In this sense, we consider the νMSM as a model of both baryogenesis and DM production, but are not concerned with the DM production mechanism, which is discussed in Sec. VI. This corresponds to scenario II. The requirement to explain $\Omega_{\rm DM}$ only enters implicitly, as we demand the N_1 mass and mixing to be consistent with astrophysical observations. If one completely drops the requirement to explain the observed DM and study the νMSM as a theory of baryogenesis and neutrino oscillations only (scenario III), the resulting bounds n the parameters weaken considerably. In particular, it was found in Ref. [30] that no mass degeneracy between the sterile neutrino masses is needed.

We extend the analysis performed in Ref. [22] but take into account two additional aspects. First, we use the nonzero value for the active neutrino mixing angle θ_{13} given in Table I, which brings in a new source of CP violation through the phase δ. Second, we include the contribution from the temperature-dependent Higgs expectation value $v(T)$ to the effective Hamiltonian, coming from the real part of the diagram in Fig. 4(a). It is relevant for temperatures close to the electroweak scale.

We solve numerically the system of equations (33)–(38) to find the lepton asymmetries at $T \sim T_{\rm EW}$, assuming that there is no initial asymmetry. The effective Hamiltonian is given by (A36) and (39)–(41) with (43). We fix the active neutrino masses and mixing angles according to Table I and choose the phases δ, α_1 and α_2, as well as Reω, to maximize the asymmetry. Interestingly, for normal hierarchy of neutrino masses, the value of Reω that maximizes the asymmetry is close to $\frac{\pi}{2}$, as required in the constrained νMSM. This allows us to identify the region in the remaining three-dimensional parameter space consisting of M, ΔM and Imω, where an asymmetry $\gtrsim 10^{-10}$ can be created. Deep inside this region, the asymmetry generated for this choice of phases can be much too large, but it can always be reduced by choosing different phases. Thus, any choice of M, ΔM and Imω inside this region can reproduce the observed BAU.

In practice, it is difficult to find the phases that maximize the asymmetry in each single point, as we are dealing with a seven-dimensional parameter space. However, the analysis can be simplified. First, the choice of phases that maximize the asymmetry practically does not depend on ΔM because the dependence of the Yukawa coupling (15) on ΔM is very weak. Second, our numerical studies reveal that, in most of the parameter space, Imω is the main source of CP violation. The other phases have comparably little effect on the final asymmetry, except for the region around Im$\omega = 0$. Surprisingly, the values for δ, α_1 and α_2 that maximize it vary only very little and are always close to zero. One possible interpretation is that Imω provides the main source for the asymmetry generation, while δ, α_1 and α_2 contribute more strongly to the washout. However, due to the various different time scales involved, we cannot extract a single CP-violating parameter at this point, which is commonly used in thermal leptogenesis scenarios to study such connections analytically. The above seems to be valid everywhere except in the region Im$\omega \sim 0$, where δ, α_1 and α_2 are the only sources of CP violation.

We therefore split the parameter space into two regions. In the region $0.5 < e^{{\rm Im}\omega} < 1.5$ we choose $\alpha_2 = \pi$, $\delta = 0$, Re$\omega = \frac{7}{10}\pi$ for normal hierarchy and $\alpha_2 - \alpha_1 = \pi$, $\delta = \pi$, Re$\omega = \frac{3}{4}\pi$ for inverted hierarchy. Everywhere else we choose $\alpha_2 = \frac{7\pi}{5}$ and $\delta = \frac{3}{20}\pi$, Re$\omega = \frac{1}{2}\pi$ for normal hierarchy and $\alpha_2 - \alpha_1 = \frac{11}{10}\pi$, $\delta = \frac{11}{20}\pi$, Re$\omega = \frac{4}{5}\pi$ for inverted hierarchy. Note that for normal hierarchy F only depends on α_2 and δ, while for inverted hierarchy it depends on $\alpha_2 - \alpha_1$ and δ because one neutrino is massless. In order to determine $v(T)$ one needs to fix the Higgs mass m_H. We used the value $m_H = 126$ GeV suggested by recent LHC data [168,169], corresponding to an electroweak scale of $T_{\rm EW} \sim 140$ GeV. This is consistent with the νMSM being a valid description of nature up to the Planck scale [170].

We present our results in Fig. 6, which shows the allowed region in the ΔM-Imω plane for several masses M. The lines correspond to the exact observed asymmetry; inside, more asymmetry is generated. As pointed out

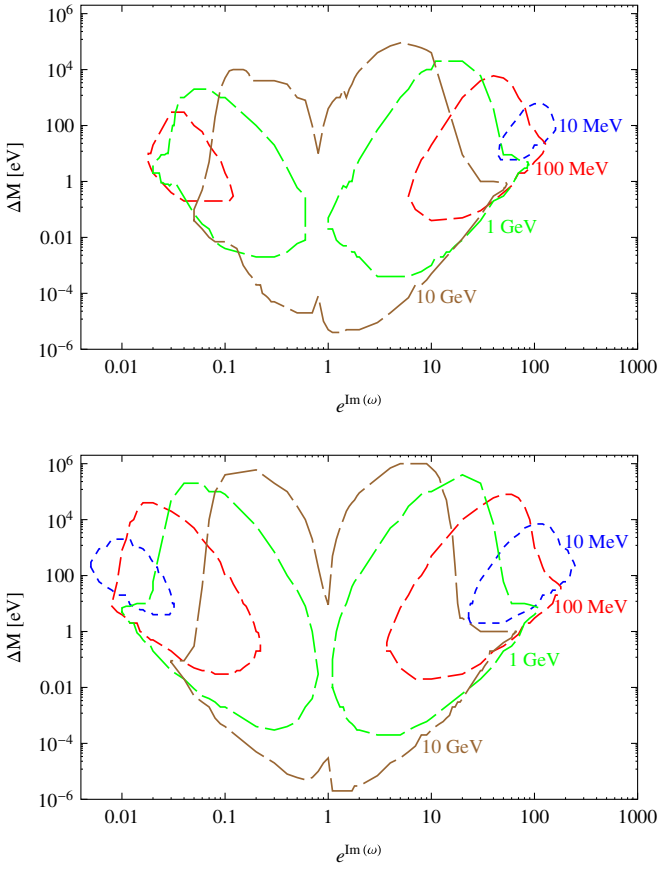

FIG. 6 (color online). Values of ΔM and $\mathrm{Im}\omega$ that lead to the observed baryon asymmetry in scenarios I and II for different sterile neutrino masses $M = 10$, 100 MeV, 1 and 10 GeV. The blue (shortest dashed) line corresponds to $M = 10$ MeV, red (short dashed) to $M = 100$ MeV, brown (long dashed) to $M = 1$ GeV and green (longest dashed) to $M = 10$ GeV. The phases that maximize the asymmetry differ significantly for $\mathrm{Im}\omega \approx 0$ and away from that region. In the region $0.5 < e^{\mathrm{Im}\omega} < 1.5$ we choose $\alpha_2 = \pi$, $\delta = 0$, $\mathrm{Re}\omega = \frac{7}{10}\pi$ for normal hierarchy and $\alpha_2 - \alpha_1 = \pi$, $\delta = \pi$, $\mathrm{Re}\omega = \frac{3}{4}\pi$ for inverted hierarchy. Everywhere else we choose $\delta = \frac{3}{20}\pi$, $\mathrm{Re}\omega = \frac{1}{2}\pi$ for normal hierarchy and $\alpha_2 - \alpha_1 = \frac{11}{10}\pi$, $\delta = \frac{11}{20}\pi$, $\mathrm{Re}\omega = \frac{4}{5}\pi$ for inverted hierarchy. The upper panel shows the results for normal hierarchy, the lower panel for inverted hierarchy.

above, any point inside the lines is consistent with observation because the asymmetry can be reduced by choosing different phases. Figure 6 shows that, even for small masses around 10 MeV, enough asymmetry can be created. However, for small masses the CP violation contained in δ, α_1 and α_2 is not sufficient, and the allowed region consists of two disjoint parts that are separated by the $\mathrm{Im}\omega \simeq 0$ region. The area of these increases with M. For masses of a few GeV, the CP violation from δ, α_1 and α_2 alone is sufficient and the regions join. Interestingly, there appear to be mass-independent diagonal lines in the ΔM-$e^{\mathrm{Im}\omega}$ plane that confine the region where enough asymmetry can be generated. We currently have not understood the origin of these lines parametrically. The inverted hierarchy generally allows one to produce more asymmetry than the normal hierarchy. There is an approximate symmetry between regions with positive and negative $\mathrm{Im}\omega$. It would be exact when simultaneously changing ξ and is related to the symmetry of the Lagrangian under the exchange of N_2 and N_3. As expected, these results are close to those obtained in Ref. [22], which provides a good consistency check. The slightly bigger asymmetry is due to the additional source of CP violation for $\theta_{13} \neq 0$.

For experimental searches, the most relevant parameters are the mass M and the mixing between active and sterile neutrinos. In Fig. 7 we translate our results into bounds on the flavor-independent mixing parameter U^2 defined in Eq. (20). Using the results displayed in Fig. 6, we choose δM to maximize the asymmetry and find the region in the

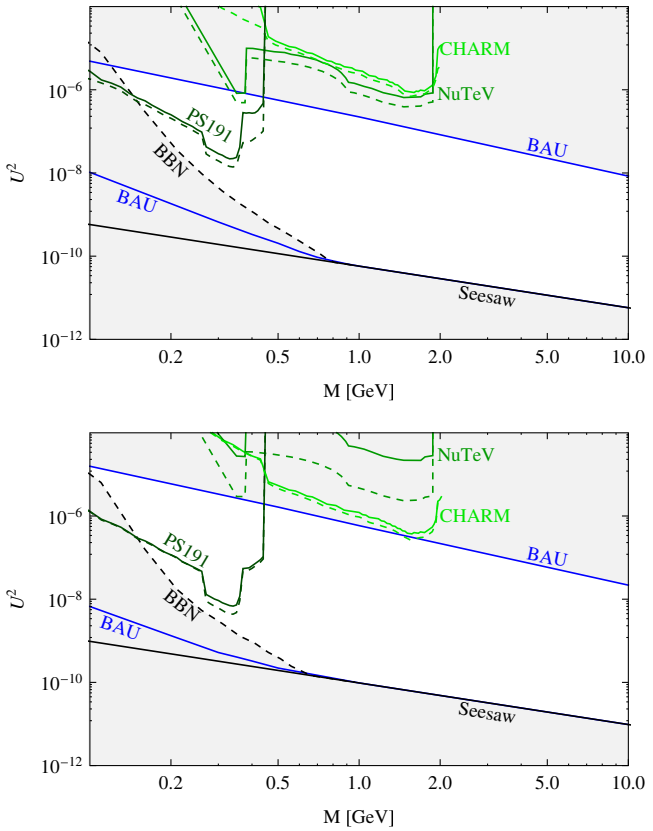

FIG. 7 (color online). Constraints on the $N_{2,3}$ masses $M_{2,3} \simeq M$ and mixing $U^2 = \mathrm{tr}(\theta^\dagger\theta)$ from baryogenesis in scenarios I and II: upper panel—normal hierarchy; lower panel—inverted hierarchy. In the region between the solid blue "BAU" lines, the observed BAU can be generated. The regions below the solid black "seesaw" line and dashed black "BBN" line are excluded by neutrino oscillation experiments and BBN, respectively. The areas above the green lines of different shades are excluded by direct search experiments, as indicated in the plot. The solid lines are *exclusion plots* for all choices of νMSM parameters; for the dashed lines the phases were chosen to maximize the BAU, consistent with the blue lines.

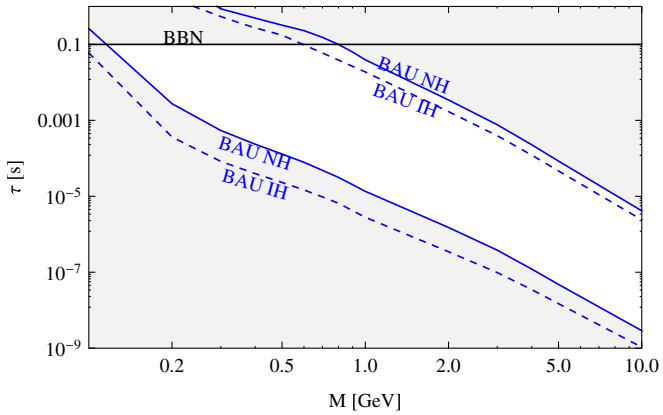

FIG. 8 (color online). Constraints on the $N_{2,3}$ masses $M_{2,3} \simeq M$ and lifetime $\tau^{-1} \simeq \frac{1}{2}\,\mathrm{tr}\Gamma_N|_{T=1\ \mathrm{MeV}}$ from baryogenesis in scenarios I and II. In the region between the blue "BAU" lines, the observed BAU can be generated (solid line—normal hierarchy; dotted line—inverted hierarchy). The region above the solid black "BBN" line is excluded by BBN.

U^2-M plane within which baryogenesis is possible. The plot has to be read as follows: For each point in the region between the blue lines, there exists at least one choice of νMSM parameter that allows for successful baryogenesis. The plots in Fig. 7 are similar to the ones of Fig. 3 in Ref. [22], but the allowed region is slightly bigger due to the effect of the new source of CP violation for $\theta_{13} \neq 0$.

The constraints on the mixing angle U^2 shown in Fig. 7 can be translated into constraints on the neutrino lifetime $\tau^{-1} \simeq \frac{1}{2}\,\mathrm{tr}\Gamma_N$ (at $T = 1$ MeV) shown in Fig. 8. The plot in Fig. 8 is similar to the ones of Fig. 4 in Ref. [22].

VI. LATE-TIME LEPTON ASYMMETRY AND DARK MATTER PRODUCTION

The lepton asymmetry at temperatures of a few hundred MeV is of crucial importance for the dark matter production in scenario I. Resonant dark matter production requires a lepton asymmetry $|\mu_\alpha| \sim 8 \times 10^{-6}$ in the plasma, much larger than the baryon asymmetry. The details of this process have been outlined in Ref. [8]. Here, we are not concerned with the dark matter production itself, but with the mechanisms that generate the required lepton asymmetry. This asymmetry must come from a source that is different from that of the baryon asymmetry because $N_{2,3}$ reach chemical equilibrium at some temperature $T_+ < T_{\mathrm{EW}}$ and the asymmetry in the leptonic sector is washed out (while the baryon asymmetry remains, as sphalerons are inefficient at $T < T_{\mathrm{EW}}$).[29] There are two distinct mechanisms that contribute to the late-time asymmetry: the freeze-out of $N_{2,3}$ at $T \sim T_-$ and their decay at $T \sim T_d$.

The requirement that these two mechanisms produce enough asymmetry puts severe constraints on the parameters of the model, described in Sec. II F. The value of $\mathrm{Re}\omega$ is fixed to values near $\pi/2$. The mass splitting ΔM is limited to a very narrow range by Eq. (25). Therefore, we will use the mass splitting in vacuum δM instead of ΔM as a free parameter in the following. All experimentally known parameters are fixed to the values given in Table I. The phases δ, α_1 and α_2 are chosen to maximize the asymmetry. As in Sec. V we observe that in most of the parameter space $\mathrm{Im}\omega$ is the main source of CP violation. We again find that it is convenient to split the parameter space into the region $0.5 < e^{\mathrm{Im}\omega} < 1.5$ and its complement. For normal hierarchy we choose the phases $\alpha_2 = \frac{\pi}{2}$, $\delta = \frac{3}{2}\pi$ in the region $0.5 < e^{\mathrm{Im}\omega} < 1.5$ and $\alpha_2 = \frac{\pi}{5}$ and $\delta = 0$ everywhere else. For inverted hierarchy we choose $\alpha_2 - \alpha_1 = \frac{7}{5}$ and $\delta = \frac{3}{5}\pi$ in the region $0.5 < e^{\mathrm{Im}\omega} < 1.5$ and $\alpha_2 - \alpha_1 = 0$, $\delta = \frac{9}{10}\pi$ everywhere else. Note that for normal hierarchy F only depends on α_2 and δ, while for inverted hierarchy it depends on $\alpha_2 - \alpha_1$ and δ because one neutrino is massless. We then study the parameter space spanned by M, δM and $\mathrm{Im}\omega$.

As in Sec. V, we use the kinetic equations (33)–(38) in order to calculate the lepton asymmetries as a function of T. The effective Hamiltonian is calculated from (A39) and (39)–(41) with (44)–(48). We impose thermal equilibrium with vanishing chemical potentials as initial conditions at a temperature $T > T_-$ and look for the parameter region where $\sum_\alpha |\mu_\alpha| > 8 \times 10^{-6}$ at $T = 100$ MeV.[30]

The results are shown in Figs. 9 and 10. The required asymmetry can be created when the sterile neutrinos have masses in the GeV range. For small masses of $M =$ 2–4 GeV the CP violation contained in α_1, α_2 and δ alone is not sufficient for normal hierarchy and barely sufficient for inverted hierarchy; a nonzero $\mathrm{Im}\omega$ is required, and the allowed region consists of two disjoint parts along the $\mathrm{Im}\omega$ axis which are separated by the $\mathrm{Im}\omega \simeq 0$ region. For larger masses ($M \gtrsim 7$ GeV for normal hierarchy, $M \gtrsim 4$ GeV for inverted hierarchy), the regions merge, but $\mathrm{Im}\omega$ continues to be the most relevant source of CP violation in most of the parameter space. In addition, one can also observe disjoint regions along the δM axis. These can be identified with the decay scenario and freeze-out scenario. In the upper part of the figures, the asymmetry is mainly created during the freeze-out of $N_{2,3}$, in the lower part during the decay. At T_-, Γ_N has considerably larger entries than at T_d. Thus, the resonance condition (21) requires a smaller mass splitting in the decay scenario. For larger masses, both regions merge. However, freeze-out and decay are always two separated processes, i.e., $T_- \gg T_d$.

[29] It has been suggested that some asymmetry may be preserved in magnetic fields down to temperatures $T < T_-$ due to the chiral anomaly [53]. Here we take the most conservative approach and do not take into account this possibility.

[30] We solve the kinetic equations down to $T = 50$ MeV in order to avoid numerical artifacts at the boundary.

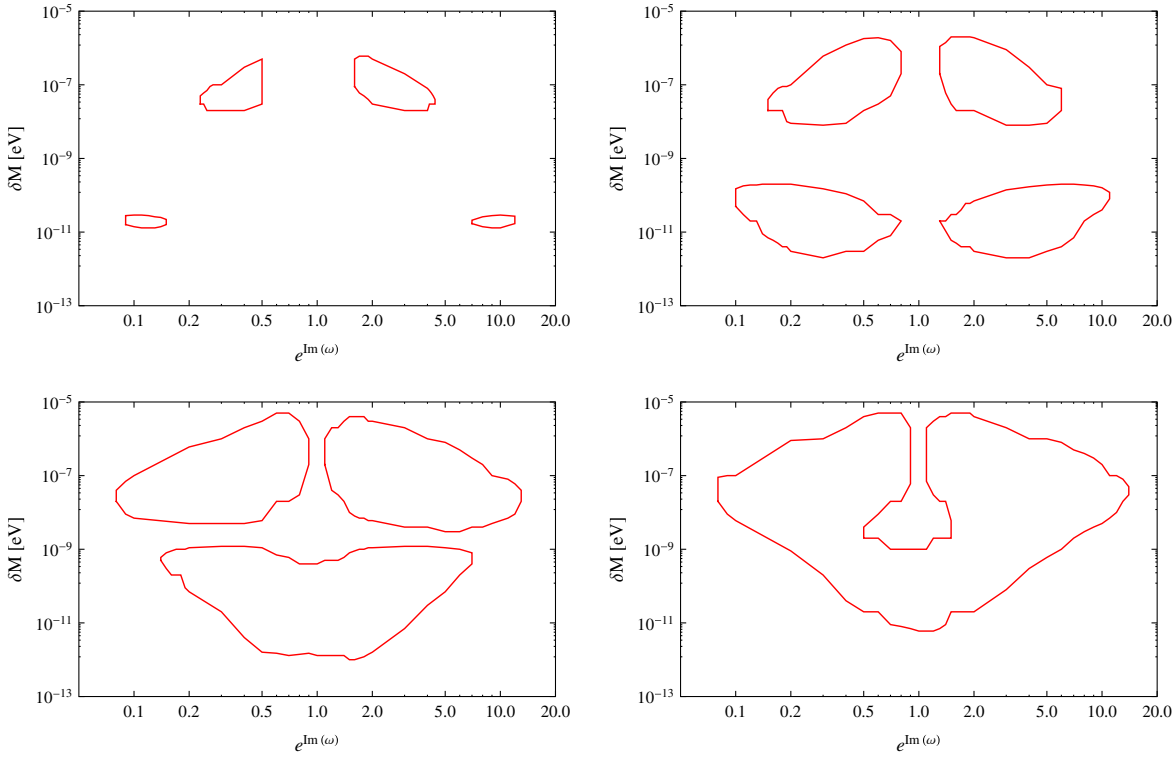

FIG. 9 (color online). Values of δM and $\mathrm{Im}\omega$ that lead to the lepton asymmetry required for dark matter production in scenario I for different singlet fermion masses, $M = 2.5$, 4, 7, and 10 GeV and for normal hierarchy. The upper left panel corresponds to $M = 2.5$ GeV, the upper right panel to $M = 4$ GeV, the lower left panel to $M = 7$ GeV and the lower right panel to $M = 10$ GeV. The phases that maximize the asymmetry differ significantly for $\mathrm{Im}\omega \approx 0$ and away from that region. We choose the phases $\alpha_2 = \frac{\pi}{2}$, $\delta = \frac{3}{2}\pi$ in the region $0.5 < e^{\mathrm{Im}\omega} < 1.5$ and $\alpha_2 = \frac{\pi}{5}$ and $\delta = 0$ everywhere else.

As in Fig. 6, there is an approximate symmetry under a change of sign for $\mathrm{Im}\omega$, which is related to the symmetry of the Lagrangian under exchange of N_2 and N_3 and becomes exact when also changing ξ.

For experimental searches for sterile neutrinos, the most relevant parameters are the mass M and the mixing between active and sterile species. As in Sec. V, we translate our results for the parameters in the Lagrangian into bounds on the mass and mixing. For each mass, we choose δM in a way that maximizes the allowed region in the U^2-M plane. The results are shown in Fig. 11.

Finally, we estimate the maximal asymmetry that can be generated at $T \sim 100$ MeV as a function of M by its largest value within the data files that we used to create Figs. 9 and 10. The maximal asymmetry allows us to impose a lower bound on the N_1 mixing; bigger lepton asymmetries make the resonant DM production more efficient and allow for smaller N_1 mixing, as displayed in Fig. 2. Furthermore, the maximal $|\mu_\alpha|$ is of interest because in Ref. [171] it was pointed out that a large lepton asymmetry may lead to a first order phase transition during hadronization. The maximal asymmetries we found are shown in Fig. 12. For both hierarchies they remains well below cosmological bounds (see Ref. [42]) at all masses under consideration and are about a factor 5 smaller than the value 7×10^{-4} estimated in Ref. [6]. However, given the uncertainties summarized in Appendix A 4, they can easily change by a factor $\mathcal{O}[1]$.

VII. DM, BAU AND NEUTRINO OSCILLATIONS IN THE νMSM

In Secs. V and VI we have studied independently the conditions for successful baryogenesis on one hand, and sufficient dark matter production on the other. The most interesting question is of course in which part of the νMSM parameter space scenario I can be realized; i.e., both can be achieved simultaneously. This region cannot be found by simply superposing the figures from the previous sections because the phases that maximize the asymmetry are different for $T \gtrsim T_{\mathrm{EW}}$ and $T \lesssim T_-$. The requirement to produce enough DM imposes the stronger constraint. We therefore fix the CP-violating phases in a way that is consistent with $\sum_\alpha |\mu_\alpha| > 8 \times 10^{-6}$ at $T = 100$ GeV in some significant region in the M-U^2 plane. We then check for which combination of M and U^2 the correct BAU is created by these phases.

We start with the phases used in Fig. 11, which were chosen to maximize the area in the M-U^2 plane where $\sum_\alpha |\mu_\alpha| > 8 \times 10^{-6}$ at $T = 100$ MeV. The result is shown

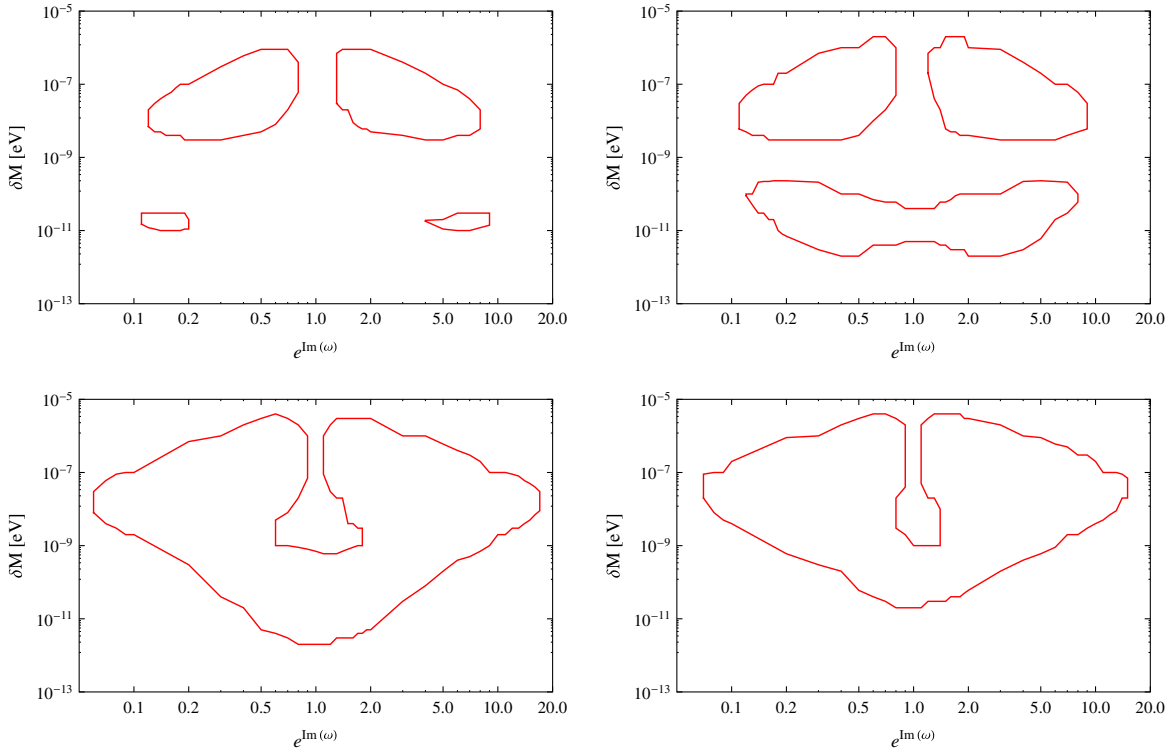

FIG. 10 (color online). Values of δM and $\mathrm{Im}\omega$ that lead to the lepton asymmetry required for dark matter production in scenario I for different singlet fermion masses, $M = 2.5, 4, 7$, and 10 GeV and inverted hierarchy. The upper left panel corresponds to $M = 2.5$ GeV, the upper right panel to $M = 4$ GeV, the lower left panel to $M = 7$ GeV and the lower right panel to $M = 10$ GeV. The phases that maximize the asymmetry differ significantly for $\mathrm{Im}\omega \approx 0$ and away from that region. We choose $\alpha_2 - \alpha_1 = \frac{7}{5}$ and $\delta = \frac{3}{5}\pi$ in the region $0.5 < e^{\mathrm{Im}\omega} < 1.5$ and $\alpha_2 - \alpha_1 = 0$, $\delta = \frac{9}{10}\pi$ everywhere else.

in Fig. 13. The blue line corresponds to the points where the asymmetry at T_{EW} corresponds to the observed BAU. While the requirement to produce enough DM only imposes a lower bound on the asymmetry at 100 MeV, the value of the BAU is known to be given by (13), i.e., has a fixed value. Thus, only the points on the blue line that lie within the region encircled by the red line (DM region) form the allowed parameter space. The shape of the blue

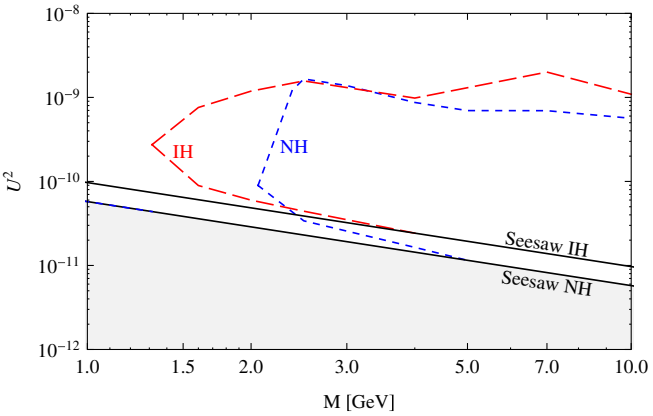

FIG. 11 (color online). Constraints on the $N_{2,3}$ masses $M_{2,3} \simeq M$ and mixing $U^2 = \mathrm{tr}(\theta^\dagger\theta)$ in scenario I. The lepton asymmetry at $T = 100$ MeV can be large enough that the resonant enhancement of N_1 production is sufficient to explain the observed Ω_{DM} inside the dashed blue and red lines for normal and inverted neutrino mass hierarchy, respectively. The regions below the "seesaw" lines are excluded by neutrino oscillation experiments for the indicated choice of hierarchy.

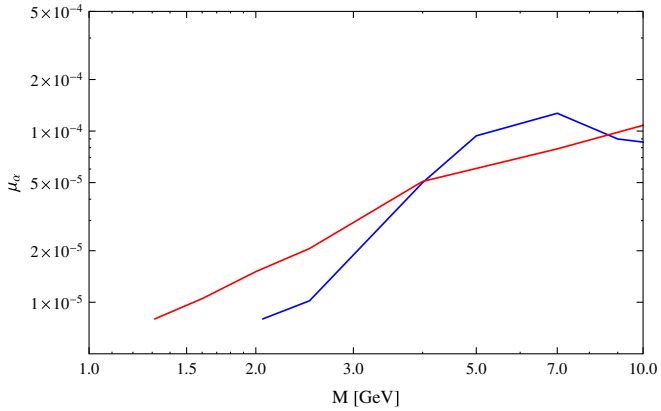

FIG. 12 (color online). Estimate of the maximal lepton asymmetry that can be created in scenario I around $T = 100$ MeV. The blue small dashed line corresponds to normal hierarchy, the red long dashed line to inverted hierarchy. This plot was generated using the maximal values found in the data files used to produce Figs. 9 and 10.

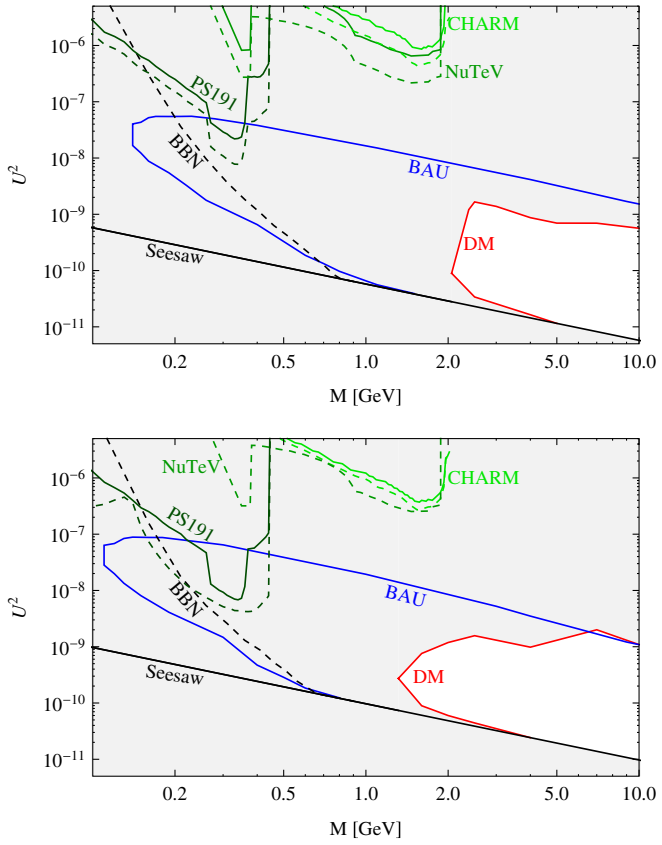

FIG. 13 (color online). Constraints on the $N_{2,3}$ masses $M_{2,3} \simeq M$ and mixing $U^2 = \mathrm{tr}(\theta^\dagger\theta)$ in the constrained νMSM (scenario I): upper panel—normal hierarchy; lower panel—inverted hierarchy. In the region between the solid blue "BAU" lines, the observed BAU can be generated. The lepton asymmetry at $T = 100$ MeV can be large enough that the resonant enhancement of N_1 production is sufficient to explain the observed Ω_{DM} inside the solid red "DM" line. The *CP*-violating phases were chosen to maximize the asymmetry at $T = 100$ MeV. The regions below the solid black "seesaw" line and dashed black "BBN" line are excluded by neutrino oscillation experiments and BBN, respectively. The areas above the green lines of different shades are excluded by direct search experiments, as indicated in the plot. The solid lines are *exclusion plots* for all choices of νMSM parameters; for the dashed lines the phases were chosen to maximize the late-time asymmetry, consistent with the red line.

BAU line can be modified by changing the phases (see Fig. 14), but this also changes the shape of the red line (DM region). Solving the kinetic equations for different phases reveals that the BAU line can be brought to most points within the DM region. This region therefore gives a good estimate of the allowed parameter space.

The constraints derived on the mixing angle U^2 are translated into constraints on the neutrino lifetime $\tau^{-1} \simeq \frac{1}{2}\,\mathrm{tr}\Gamma_N$ (at $T = 1$ MeV) in Fig. 15.

In the plots of Fig. 14, there are two regions where the BAU and DM lines are close to each other, leading to the

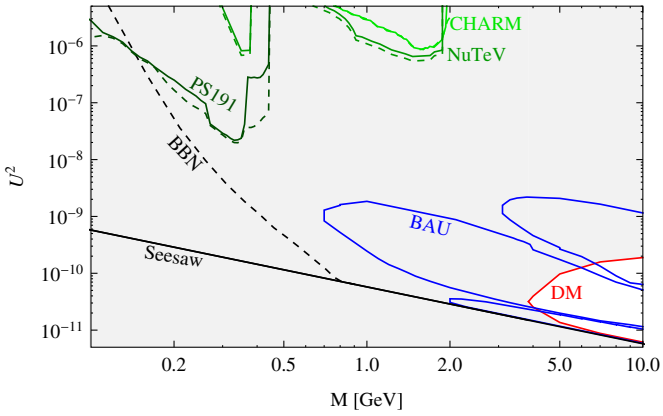

FIG. 14 (color online). Same as Fig. 13, but with a different set of *CP*-violating phases. The plot illustrates how the "BAU" line moves when the phases are changed; it can cross through points deep inside the maximal "BAU" region, while the phase still allows for DM production. The sign of the BAU is opposite in the two disjoint "BAU" regions.

successful baryogenesis and dark matter production. One is near the seesaw line and the other is for higher mixing. These regions are easier to identify in the Imω-M plane shown in Fig. 16. The baryon asymmetry almost vanishes for Imω close to 0, but this is not the case for dark matter production. Therefore, there is a region near Im$\omega = 0$ which produces the right amount of baryon asymmetry and enough dark matter. This is the region where the blue BAU line is inside the red DM line in Fig. 16. For large values of $|\mathrm{Im}\omega|$, there also are regions where the two lines are close.

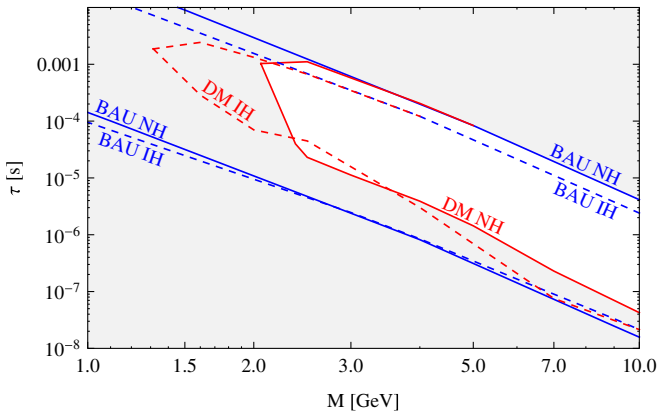

FIG. 15 (color online). Constraints on the $N_{2,3}$ masses $M_{2,3} \simeq M$ and lifetime $\tau^{-1} \simeq \frac{1}{2}\,\mathrm{tr}\Gamma_N|_{T=1\ \mathrm{MeV}}$ in the constrained νMSM (scenario I). In the region between the blue "BAU" lines, the observed BAU can be generated. The lepton asymmetry at $T = 100$ MeV can be large enough that the resonant enhancement of N_1 production is sufficient to explain the observed Ω_{DM} inside the red "DM" line. The *CP*-violating phases were chosen to maximize the asymmetry at $T = 100$ MeV. Solid lines—normal hierarchy; dotted lines—inverted hierarchy.

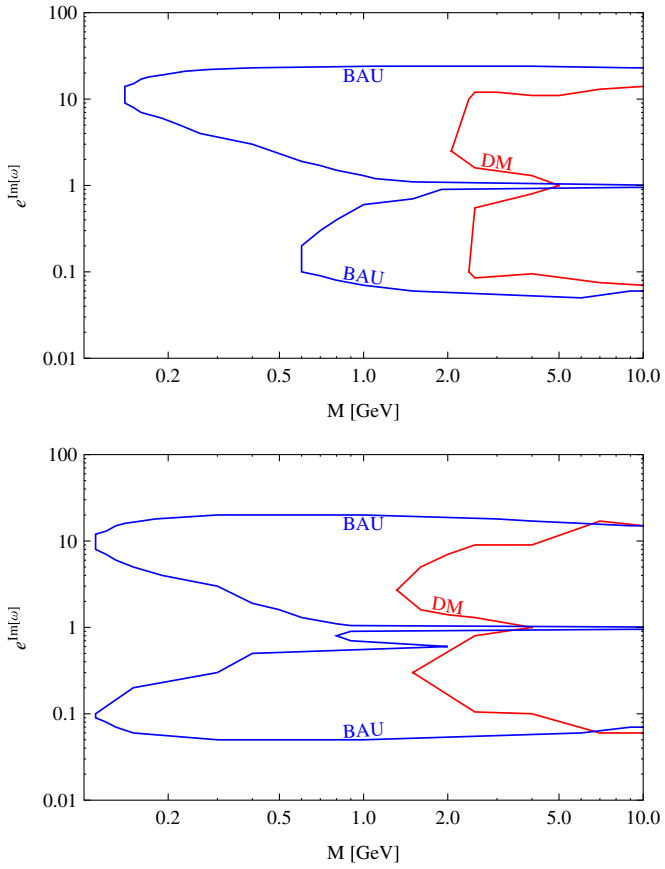

FIG. 16 (color online). Constraints on the $N_{2,3}$ masses $M_{2,3} \simeq M$ and parameter $\mathrm{Im}\omega$ in the constrained νMSM (scenario I): upper panel—normal hierarchy; lower panel—inverted hierarchy. In the region between the solid blue "BAU" lines, the observed BAU can be generated. The lepton asymmetry at $T = 100$ MeV can be large enough that the resonant enhancement of N_1 production is sufficient to explain the observed Ω_{DM} inside the solid red "DM" line. The CP-violating phases were chosen to maximize the asymmetry at $T = 100$ MeV.

VIII. CONCLUSIONS AND DISCUSSION

We tested the hypothesis that three right-handed neutrinos with masses below the electroweak scale can be the common origin of the observed dark matter, the baryon asymmetry of the Universe and neutrino flavor oscillations. This possibility can be realized in the νMSM, an extension of the SM that is based on the type-I seesaw mechanism with three right-handed neutrinos N_I. The centerpiece of our analysis is the study of sterile and active neutrino abundances in the early Universe, which allows us to determine the range of sterile neutrino parameters in which DM, baryogenesis and all known data from active neutrino experiments can be explained *simultaneously* within the νMSM. We combined our results with astrophysical constraints and reanalyzed bounds from past experiments in the face of recent data from neutrino oscillation experiments. We found that all these requirements can be fulfilled for a wide range of sterile neutrino masses and mixings; see Figs. 13 and 14 in Sec. VII.

This is the first complete quantitative study of the above scenario (scenario I), in which no physics beyond the νMSM is required. We found that the νMSM can explain all experimental data if one sterile neutrino (N_1), which composes the dark matter, has a mass in the keV range, while the other two ($N_{2,3}$) have quasidegenerate masses in the GeV range. The heavier particles $N_{2,3}$ generate neutrino masses via the seesaw mechanism and create flavored lepton asymmetries from CP-violating oscillations in the early Universe. These lepton asymmetries are crucial on two occasions in the early Universe. On one hand, they create the BAU via flavored leptogenesis. One the other hand, they affect the rate of thermal DM production via the MSW effect. The second point allows us to derive strong constraints on the $N_{2,3}$ properties from the requirement to explain the observed Ω_{DM} by thermal N_1 production; see Sec. VI. This can be achieved by resonant production, caused by the presence of lepton asymmetries in the primordial plasma at $T \sim 100$ MeV. The required asymmetries can be created when $N_{2,3}$ are heavier than 1–2 GeV and the physical mass splitting between the N_2 and N_3 masses is comparable to the active neutrino mass differences. This can be achieved in a subspace of the νMSM parameter space that is defined by fixing two of the unknown parameters (the Majorana mass splitting ΔM and a mixing angle $\mathrm{Re}\omega$ in the sterile sector). This choice, in which scenario I can be realized, is dubbed "constrained νMSM."

We also studied systematically how the parameter constraints relax if one allows N_1 DM to be produced by some unspecified mechanism beyond the νMSM (scenario II); see Sec. V. In this case the strongest constraints come from baryogenesis and the required mass degeneracy is much weaker, $\Delta M/M \lesssim 10^{-3}$. These results are based on an extension of the analysis performed in Ref. [22] that accounts for a nonzero value of the neutrino mixing angle θ_{13} and a temperature-dependent Higgs expectation value. While the low mass region is severely constrained by BBN and experiments, the allowed parameter space becomes considerably bigger for masses above $\sim$0.5 GeV. Detailed results for the allowed sterile neutrino masses and mixings are shown in Figs. 6 and 7.

If one completely drops the requirement that DM is composed of N_1 and considers the νMSM as a theory of baryogenesis and neutrino oscillations only (scenario III), no degeneracy in masses is required. Note that this also implies that no degeneracy is required in scenario II if more than three right-handed neutrinos are added to the SM.

We conclude that right-handed neutrinos can explain all confirmed detections of physics beyond the standard model, except accelerated cosmic expansion.

The testability of the model depends on the type of scenario and on the mass of sterile neutrinos. If scenario I is realized, the DM mass and mixing N_1 is bounded from all sides, allowing one to exclude (or confirm) the prediction of the νMSM by the searches of a narrow decay line in a dedicated x-ray mission (see Ref. [146] for a detailed discussion). The searches for $N_{2,3}$ at the SPS-type experiment [159], which can look for $N_{2,3}$ below the charm threshold, can only explore the case of inverted hierarchy (see Fig. 13) in a limited domain of $N_{2,3}$ masses. Going above 2 GeV is very challenging, as discussed in Ref. [16].

For scenario II the lower bound on the mixing angle of dark matter sterile neutrinos (see Fig. 2) is lost, as N_1 can be produced by some other mechanism, not related to the sterile-active neutrino mixing. In this case the x-ray searches may confirm, but will not be able to exclude, the νMSM. At the same time, the parameter space for $N_{2,3}$ opens up, allowing their search even in K-meson decays; see Fig. 7. For scenario III the constraints on $N_{2,3}$ masses and mixing angles are even more relaxed.

ACKNOWLEDGMENTS

We are grateful to Mikko Laine for providing the numerical data shown in Fig. 5. We also would like to thank Oleg Ruchayskiy, Alexey Boyarsky, and Artem Ivashko for sharing their expertise on experimental bounds. This work was supported by the Swiss National Science Foundation, the Gottfried Wilhelm Leibniz program of the Deutsche Forschungsgemeinschaft, the Project of Knowledge Innovation Program of the Chinese Academy of Sciences Grant No. KJCX2.YW.W10 and the IMPRS-PTFS.

APPENDIX A: KINETIC EQUATIONS

In the following we sketch the derivation of the kinetic equations (29)–(31). Our basic assumptions can be summarized as follows:

(1) Coherent states containing more than one N_I quantum are not relevant. Their contributions are suppressed by additional powers of the small mixing $\theta_{\alpha I}$. Processes involving one sterile neutrino include decays of N_I particles, their scatterings with SM particles, and flavor oscillations.

(2) Screened one-particle states are the only relevant propagating neutrino degrees of freedom. In particular, we do not consider any collective excitations, which are infrared effects and only give a small contribution when the typical neutrino momenta are hard, $\sim T$.

(3) The interactions that keep the SM fields in equilibrium act much faster than interactions involving N_I at all times due to the smallness of F.

(4) $T_- \gtrsim T_d$, i.e., the lifetime of the N_I is sufficiently long that freeze-out and decay are two well-separated events. This is the case in the parameter space we study.

(5) The typical momentum of N_I particles is $\bar{p} \sim T$ even when they are out of equilibrium. This is justified because they are produced from a thermal bath and freeze out from a thermal state; hence, their distribution functions are proportional to equilibrium distributions even when out of equilibrium [101].

(6) We neglect the effect of the $N_{2,3}$ on the time evolution of the entropy (or temperature). This is justified, as their contributions to the total entropy and energy densities are always small.

(7) We neglect the effect of the lepton asymmetry on hadronization. This aspect has, e.g., been discussed in Ref. [171].

1. How to characterize the asymmetries

The leptonic charges that we are interested in can be expressed in terms of field bilinears. Instead of bilinears in the field operators themselves, we consider expectation values of bilinears in the ladder operators a_I, $a_I^\dagger$ for sterile and a_α, $a_\alpha^\dagger$ for active neutrinos. To be explicit, we decompose N_I as[31]

$$N_I = \int \frac{d^3\mathbf{p}}{(2\pi)^3} \sum_s \frac{1}{\sqrt{2\omega_\mathbf{p}}} (u^s_{I,\mathbf{p}} e^{-i\mathbf{px}} a_{I,s}(\mathbf{p}, t) + v^s_{I,\mathbf{p}} e^{i\mathbf{px}} a^\dagger_{I,s}(\mathbf{p}, t)). \tag{A1}$$

Here $\mathbf{p}$ is momentum, s the spin index, and u, v the usual plane wave solutions to the Dirac equation,

$$(\not{p} - M_I) u^s_{I,\mathbf{p}} = 0 \qquad (\not{p} + M_I) v^s_{I,\mathbf{p}} = 0. \tag{A2}$$

We will, in the following, always assume that the spatial momentum is directed along the z axis, which is also the axis of angular momentum quantization. We choose the convention that $\mathfrak{h} u^s_\mathbf{p} = (-1)^{s+1} u^s_\mathbf{p}$, while $\mathfrak{h} v^s_\mathbf{p} = (-1)^s v^s_\mathbf{p}$, where $\mathfrak{h}$ is the helicity matrix

$$\mathfrak{h} = \frac{1}{2}\frac{p_i}{|\mathbf{p}|}\gamma^i\gamma^0\gamma^5 = \frac{1}{2}\frac{p_i}{|\mathbf{p}|}\Sigma_i, \quad \Sigma_i = \frac{i}{2}\epsilon_{ijk}\gamma^j\gamma^k. \tag{A3}$$

All relevant matrix elements of the density matrix $\hat{\rho}$ can be identified with expectation values of bilinears in the ladder operators. Because of this, the matrix ρ of bilinears, to be defined in (A4), is often referred to as the "density matrix" (rather than $\hat{\rho}$ itself). In principle, there is a large number of such bilinears. A complete characterization of the

[31]The sterile neutrinos may be described as Weyl, Dirac or Majorana spinors. Here we have chosen to write ν_R as a right chirality four-spinor and pulled the P_R out of the definition (6) so that the N_I are Majorana spinors.

system requires knowledge of all their expectation values at all times. However, it can be simplified dramatically, and for our purpose, it will be sufficient to follow the time evolution of two 2×2 matrices ρ_N and $\rho_{\bar{N}}$ and three chemical potentials.

The only term in (1) that violates lepton number is M_M. For $T \gg M$, it is negligible and lepton number is approximately conserved. The total lepton asymmetry is negligible at $T_{\rm EW}$ in the νMSM, but there can be asymmetries of opposite sign for fermions with different chirality. Baryogenesis occurs because sphalerons only couple to left-handed fermions. As far as the (Majorana) neutrinos are concerned, the two helicity states act as a "particle" and an "antiparticle." Terms containing two creation or two annihilation operators, such as $\langle a_I a_J \rangle$ or $\langle a_\alpha^\dagger a_\beta^\dagger \rangle$, can be related to processes that violate lepton number and are suppressed at $T > M$. For $T \lesssim M$ they could, in principle, contribute, but the leading order contribution in the Yukawa coupling F to the corresponding rates $\frac{d}{dt}\langle a_I a_J \rangle$, etc.[32] oscillates fast. We therefore only consider terms that contain exactly one creation and one annihilation operator. Since only two of the sterile neutrinos are relevant here, these form a 10×10 matrix that can be written as

$$\rho = \begin{pmatrix} \rho_{NN} & \rho_{N\bar{N}} & \rho_{NL} & \rho_{N\bar{L}} \\ \rho_{\bar{N}N} & \rho_{\bar{N}\bar{N}} & \rho_{\bar{N}L} & \rho_{\bar{N}\bar{L}} \\ \rho_{LN} & \rho_{L\bar{N}} & \rho_{LL} & \rho_{L\bar{L}} \\ \rho_{\bar{L}N} & \rho_{\bar{L}\bar{N}} & \rho_{\bar{L}L} & \rho_{\bar{L}\bar{L}} \end{pmatrix}, \tag{A4}$$

with

$$\begin{aligned}
(\rho_{NN})_{IJ} &= \langle a^\dagger_{I,1} a_{J,1} \rangle / V & (\rho_{N\bar{N}})_{IJ} &= \langle a^\dagger_{I,1} a_{J,2} \rangle / V \\
(\rho_{NL})_{I\beta} &= \langle a^\dagger_{I,1} a_{\beta,1} \rangle / V & (\rho_{N\bar{L}})_{I\beta} &= \langle a^\dagger_{I,1} a_{\beta,2} \rangle / V \\
(\rho_{\bar{N}N})_{IJ} &= \langle a^\dagger_{I,2} a_{J,1} \rangle / V & (\rho_{\bar{N}\bar{N}})_{IJ} &= \langle a^\dagger_{I,2} a_{J,2} \rangle / V \\
(\rho_{\bar{N}L})_{I\beta} &= \langle a^\dagger_{I,2} a_{\beta,1} \rangle / V & (\rho_{\bar{N}\bar{L}})_{I\beta} &= \langle a^\dagger_{I,2} a_{\beta,2} \rangle / V \\
(\rho_{LN})_{\alpha J} &= \langle a^\dagger_{\alpha,1} a_{J,1} \rangle / V & (\rho_{L\bar{N}})_{\alpha J} &= \langle a^\dagger_{\alpha,1} a_{J,2} \rangle / V \\
(\rho_{LL})_{\alpha\beta} &= \langle a^\dagger_{\alpha,1} a_{\beta,1} \rangle / V & (\rho_{L\bar{L}})_{\alpha\beta} &= \langle a^\dagger_{\alpha,1} a_{\beta,2} \rangle / V \\
(\rho_{\bar{L}N})_{\alpha J} &= \langle a^\dagger_{\alpha,1} a_{J,1} \rangle / V & (\rho_{\bar{L}\bar{N}})_{\alpha J} &= \langle a^\dagger_{\alpha,2} a_{J,1} \rangle / V \\
(\rho_{\bar{L}L})_{\alpha\beta} &= \langle a^\dagger_{\alpha,2} a_{\beta,1} \rangle / V & (\rho_{\bar{L}\bar{L}})_{\alpha\beta} &= \langle a^\dagger_{\alpha,2} a_{\beta,2} \rangle / V,
\end{aligned} \tag{A5}$$

where we have suppressed time and momentum indices (all momenta are $\mathbf{p}$ and all times t). V is the overall spatial volume, which will always drop out of the computations in the end.

[32]Whether the ladder operators or $\hat{\rho}$ or both change with time depends on whether one chooses the Heisenberg, Schrödinger or interaction picture. The expectation value, however, always has the same time dependence.

2. Effective kinetic equations

The time evolution of ρ is governed by an effective Hamiltonian. In the absence of a Hubble expansion, which we will add later, we get kinetic equation

$$i\frac{d\rho}{dt} = [\mathrm{H}, \rho] - \frac{i}{2}\{\Gamma^>, \rho\} + \frac{i}{2}\{\Gamma^<, 1 - \rho\}. \tag{A6}$$

H can be viewed as the *dispersive part* of the effective Hamiltonian. The *absorbtive part* given by the matrices $\Gamma^{\gtrless}$ arises because the system is coupled to the background plasma formed by all other degrees of freedom of the SM. Note that (A6) is valid for each momentum mode separately. The different modes are coupled by H and $\Gamma^{\gtrless}$, which, in principle, depend on ρ and the lepton chemical potentials. The smallness of the sterile neutrino couplings F allows us to simplify (A6) due to a separation of time scales: The time scale associated with the N_I dynamics and the time scale on which chemical equilibration of the lepton asymmetries occurs are much longer than the typical relaxation time to kinetic equilibrium in the SM plasma. This allows us to employ a *relaxation time approximation* and relate $\Gamma^>$ and $\Gamma^<$ by a detailed balance (or Kubo-Martin-Schwinger) relation [3,6,160],

$$i\frac{d\rho}{dt} = [\mathrm{H}, \rho] - \frac{i}{2}\{\Gamma, \rho - \rho^{eq}\}, \tag{A7}$$

with $\Gamma = \Gamma^> - \Gamma^<$. ρ^{eq} is ρ evaluated with an equilibrium density matrix, $\hat{\rho} = Z/\mathrm{tr}Z$, $Z = \exp(-\hat{H}/T)$, where $\hat{H}$ is the Hamiltonian corresponding to (1). The matrices H and Γ are Hermitian.

The effective masses of active and sterile neutrinos are very different, and fast oscillations between them play no role. We thus put ρ_{NL}, ρ_{LN}, $\rho_{\bar{N}L}$, $\rho_{\bar{L}N}$, $\rho_{N\bar{L}}$, $\rho_{L\bar{N}}$, $\rho_{\bar{N}\bar{L}}$ and $\rho_{\bar{L}\bar{N}}$ to zero. The time evolution of the asymmetries is related to the relaxation time scales of the N_I. Since interactions of the active neutrinos amongst themselves and with other SM fields are much faster, coherent effects in the active sector are negligible on this time scale. This allows us to furthermore neglect $\rho_{L\bar{L}}$ and $\rho_{\bar{L}L}$. ρ_{LL} and $\rho_{\bar{L}\bar{L}}$ are taken to be diagonal with equilibrium occupation numbers and are thus characterized by the temperature T and three slowly varying chemical potentials. Thus, we can entirely describe the active sector by four numbers. Instead of the chemical potentials, we will, in the following, use $n_\alpha = (\rho_{LL})_{\alpha\alpha} - (\rho_{\bar{L}\bar{L}})_{\alpha\alpha}$, i.e., the number of particles minus the number of antiparticles, to characterize the asymmetries.[33]

[33]We work in the $\tilde{F} = FU_N$ base in flavor space. This is the mass base of sterile neutrinos in vacuum, but the flavor base for active neutrinos. Hence, the diagonal elements of ρ_{NN} and $\rho_{\bar{N}\bar{N}}$ have a straightforward interpretation as number densities for physical particles in vacuum, while the ladder operators $a_\alpha^\dagger$ create linear combinations of physical particles, and the matrices ρ_{LL} and $\rho_{\bar{L}\bar{L}}$ are, strictly speaking, not diagonal in thermal equilibrium. This adds a subtlety to the interpretation of n_α as "particles minus antiparticles," which, however, is of no practical relevance due to the smallness of the neutrino masses.

The relation between both can be found in the Appendix C. In the sterile sector we have to keep track of coherences. The system can then be described by the following set of kinetic equations,

$$i\frac{d\rho_{NN}}{dt} = [\mathrm{H}, \rho_{NN}] - \frac{i}{2}\{\gamma_N, \rho_{NN} - \rho^{eq}_{NN}\} + \frac{i}{2} n_\alpha \tilde{\gamma}^\alpha_N, \tag{A8}$$

$$i\frac{d\rho_{\bar{N}\bar{N}}}{dt} = [\mathrm{H}^*, \rho_{\bar{N}\bar{N}}] - \frac{i}{2}\{\gamma^*_N, \rho_{\bar{N}\bar{N}} - \rho^{eq}_{\bar{N}\bar{N}}\} - \frac{i}{2} n_\alpha \tilde{\gamma}^{\alpha *}_N, \tag{A9}$$

$$\begin{aligned} i\frac{dn_\alpha}{dt} = &-i\gamma^\alpha_L n_\alpha + i\mathrm{Tr}[\tilde{\gamma}^\alpha_L(\rho_{NN} - \rho^{eq}_{NN})] \\ &- i\mathrm{Tr}[\tilde{\gamma}^{\alpha *}_L(\rho_{\bar{N}\bar{N}} - \rho^{eq}_{\bar{N}\bar{N}})]. \end{aligned} \tag{A10}$$

Here γ_N, $\gamma_{\bar{N}}$ are the appropriate block-diagonal submatrices of Γ; for the corresponding submatrix of H, we used the same symbol as for the full matrix to simplify the notations. These equations do not take into account the expansion of the Universe. As usual, it can be included by using abundances (or "yields") instead of number densities. It is also convenient to introduce the variable $X = M/T$ rather than time t.

All quantities appearing in the above equations depend on momentum. The different momentum modes are coupled by the scattering and decay processes. We have suppressed this momentum dependence. We define the abundances $\rho_N = \int d^3\mathbf{p}/(2\pi)^3 \rho_{NN}/s$, $\bar{\rho}_N = \int d^3\mathbf{p}/(2\pi)^3 \rho_{\bar{N}\bar{N}}/s$, $\rho^{eq} = \int d^3\mathbf{p}/(2\pi)^3 \rho^{eq}_{NN}/s \approx \int d^3\mathbf{p}/(2\pi)^3 \rho^{eq}_{\bar{N}\bar{N}}/s$ and $\mu_\alpha = \int d^3\mathbf{p}/(2\pi)^3 n_\alpha/s$.[34] Assumption (5) is justified if the common *kinetic equilibrium assumption*

$$\frac{(\rho_{NN})_{IJ}}{(\rho^{eq}_{NN})_{IJ}} = \frac{(\rho_N)_{IJ}}{(\rho^{eq})_{IJ}} \tag{A11}$$

holds. We can use (A11) to rewrite the anticommutator in (A8) as $\{\Gamma_N, \rho_N - \rho^{eq}\}$ with

$$\Gamma_N = \tau \int d^3\mathbf{p}\gamma_N \frac{\rho^{eq}_{NN} s}{\rho^{eq}} = \tau \int d^3\mathbf{p}\gamma_N \frac{f_F(\omega_\mathbf{p})}{n_F}, \tag{A12}$$

$$n_F = \int d^3\mathbf{q} f_F(\omega_\mathbf{q}). \tag{A13}$$

We again emphasize that ρ_{NN}, γ_N, etc., appearing in (A8)–(A10) depend on momentum, while Γ_N, ρ_N, ρ^{eq}, etc. do not.

For $T \ll M$, almost all particles have the momentum $\bar{p} \sim T$, and Γ_N is essentially obtained by evaluating γ_N at $\mathbf{p} = \bar{p}$. Practically, we compute the rates as described in Sec. IV B 2. Similarly, we can use $H = \tau \mathrm{H}|_{\mathbf{p}=\bar{p}}$ for the Hermitian part of the effective Hamiltonian. For $|\mathbf{p}| \sim T \gtrsim M$, n_F can be approximated by $n_F \approx \frac{3}{2}\zeta(3)T^3 \approx 1.8T^3$, but γ_N has to be computed numerically.

Using the above considerations, we can write down the following effective kinetic equations:

$$i\frac{d\rho_N}{dX} = [H, \rho_N] - \frac{i}{2}\{\Gamma_N, \rho_N - \rho^{eq}\} + \frac{i}{2}\mu_\alpha \tilde{\Gamma}^\alpha_N, \tag{A14}$$

$$i\frac{d\rho_{\bar{N}}}{dX} = [H^*, \rho_{\bar{N}}] - \frac{i}{2}\{\Gamma^*_N, \rho_{\bar{N}} - \rho^{eq}\} - \frac{i}{2}\mu_\alpha \tilde{\Gamma}^{\alpha *}_N, \tag{A15}$$

$$\begin{aligned} i\frac{d\mu_\alpha}{dX} = &-i\Gamma^\alpha_L \mu_\alpha + i\mathrm{Tr}[\tilde{\Gamma}^\alpha_L(\rho_N - \rho^{eq})] \\ &- i\mathrm{Tr}[\tilde{\Gamma}^{\alpha *}_L(\rho_{\bar{N}} - \rho^{eq})]. \end{aligned} \tag{A16}$$

These equations are equivalent to the ones used in Ref. [3]. Their interpretation is straightforward. In the mass base, the diagonal elements of ρ_N and $\rho_{\bar{N}}$ are the abundances of sterile neutrinos and antineutrinos, respectively. The off-diagonal elements are flavor coherences. ρ_N thus gives the abundances for particles and $\rho_{\bar{N}}$ those for antiparticles, defined as the helicity states of the Majorana fields N_I. This interpretation holds in vacuum, while at finite temperatures the effective mass matrix rotates due to the interplay between the (temperature-dependent) Higgs expectation value, the Majorana mass M_M and thermal masses in the plasma.

The first two terms in (A14) and (A15) are due to sterile neutrino oscillations and dissipative effects, respectively, either by scatterings or by decays and inverse decays of sterile neutrinos. More precisely, the Hermitian 2×2 matrix H in (A14) and (A15) is the dispersive part of the effective Hamiltonian for ρ_N and $\bar{\rho}_N$. The matrix Γ_N is the dissipative part of the effective Hamiltonian for ρ_N and $\bar{\rho}_N$ that arises because the sterile neutrinos are coupled to the SM. ρ^{eq} is the common equilibrium value of ρ_N and $\bar{\rho}_N$ in the absence of an asymmetry. All these terms appeared already in earlier studies [51]. The equations of motion (A16) for the asymmetries in the active sector follow from consistency considerations and the symmetries of the νMSM. The terms containing $\tilde{\Gamma}^\alpha_L$ in (A16) are their counterparts in the active sector. The last term is due to backreaction and has been discussed in Ref. [161].

3. The effective Hamiltonian

We follow the approach used in Ref. [8] and split the Hamiltonian in the Heisenberg picture into a free part $\hat{H}_0$ and an interaction $\hat{H}_{\mathrm{int}}$. We perform the computation in Minkowski spacetime and, for the moment, omit the factor $\partial t/\partial X$ included in the definition (A12). The same rates, multiplied by this factor, can be used in the early Universe when abundances are considered instead of number densities. The starting point of this computation is the von Neumann equation in the interaction picture,

[34] Note that the μ_α defined this way are dimensionless and basically abundances, not chemical potentials, cf. Appendix C.

$$i\frac{\mathrm{d}\hat{\rho}_{\mathrm{I}}(t)}{\mathrm{d}t} = [\hat{H}_{\mathrm{I}}(t), \hat{\rho}_{\mathrm{I}}(t)], \tag{A17}$$

where $\hat{\rho}_{\mathrm{I}} \equiv \exp(i\hat{H}_0 t)\hat{\rho}\exp(-i\hat{H}_0 t)$ is the density matrix in the interaction picture and $\hat{H}_{\mathrm{I}} = \exp(i\hat{H}_0 t)\times \hat{H}_{\mathrm{int}}\exp(-i\hat{H}_0 t)$, where $\hat{\rho}$ is the (time-independent) density matrix in the Heisenberg picture. Equation (A17) can be solved perturbatively,

$$\hat{\rho}_{\mathrm{I}}(t) = \hat{\rho}_0 - i\int_0^t \mathrm{d}t'[\hat{H}_{\mathrm{I}}(t'), \hat{\rho}_0] + (-i)^2\int_0^t \mathrm{d}t' \times \int_0^{t'} \mathrm{d}t''[\hat{H}_{\mathrm{I}}(t'), [\hat{H}_{\mathrm{I}}(t''), \hat{\rho}_0]] + \cdots, \tag{A18}$$

where $\hat{\rho}_0 \equiv \hat{\rho}(0) = \hat{\rho}_{\mathrm{I}}(0)$.

We use (A18) to compute the expectation values $\langle a^\dagger_{I,r}(\mathbf{p}, t)a_{J,s}(\mathbf{p}, t)\rangle/V$ by insertion into (28). For $\hat{\rho}_0$ we choose a product density matrix $\hat{\rho}_0 = \hat{\rho}_{\mathrm{N}} \otimes \hat{\rho}^{eq}_{\mathrm{SM}}$, where $\hat{\rho}^{eq}_{\mathrm{SM}}$ is an equilibrium density matrix for the SM fields and

$$\hat{\rho}_{\mathrm{N}} = \sum_I \mathrm{P}_{I,s} a^\dagger_{I,s}|0\rangle\langle 0|a_{I,s}. \tag{A19}$$

This is not the most general density matrix that can be built from one-particle N_I states, but it is sufficient to derive the effective Hamiltonian. The formula (A18) formally gives expressions for the bilinears at all times. These are strictly valid only at times much shorter than the sterile neutrino relaxation time because the perturbative expansion at some point breaks down due to secular terms. In the relaxation time approximation (A7) we can use a trick to deal with this problem. We differentiate $\langle a^\dagger_{I,r}(\mathbf{p}, t)a_{J,s}(\mathbf{p}, t)\rangle/V$ with respect to time to obtain a "rate." We then send t to infinity to eliminate its explicit appearance from the rate. This last step is allowed because all correlation functions of SM fields are damped on time scales much shorter than the sterile neutrino relaxation time by thermal damping rates due to the gauge interactions. Thus, the late-time part of the integrand in (A18) does not contribute significantly to $d\langle a^\dagger_{I,r}(\mathbf{p}, t)a_{J,s}(\mathbf{p}, t)\rangle/(Vdt)$. This way, we obtain the rate of change of the matrices ρ_{NN} and $\rho_{\bar{N}\bar{N}}$ at the initial time. In the relaxation time approximation, these rates can also be used at later times because backreaction is accounted for in the $\rho_N - \rho^{eq}$ term.

Repeating literally all steps in Sec. 2.2 of Ref. [8] for the two-flavor case and the initial density matrix (A19), we obtain

$$\frac{d}{dt}\frac{\langle a^\dagger_{I,r}a_{J,s}\rangle}{V} = \sum_{A=1,2}\mathrm{P}_A\Big[-i(\delta_{AI}-\delta_{AJ})\frac{M}{\omega_{\mathbf{p}}}\mathrm{Re}(\Delta\tilde{M}_M)_{IJ}\frac{1-2f_F(\omega_{\mathbf{p}})}{2\omega_{\mathbf{p}}} \times\Big[(\delta_{AI}+\delta_{AJ})\mathrm{tr}(P_R(P^{rs}_u)_{IJ}P_L\Pi^-_{IJ}(p) + P_R(P^{sr}_v)_{JI}P_L\Pi^-_{JI}(p)) + i(\delta_{AI}-\delta_{AJ})\mathcal{P}\int\frac{dq_0}{2\pi}\frac{1}{\omega_{\mathbf{p}}-q_0}\mathrm{tr}(P_R(P^{rs}_u)_{IJ}P_L\Pi^-_{IJ}(q_0,\mathbf{p}) + P_R(P^{sr}_v)_{JI}P_L\Pi^-_{JI}(q_0,\mathbf{p}))\Big]\Big], \tag{A20}$$

with

$$\Delta\tilde{M}_M = \tilde{M}_M - \mathbb{1}\bar{M}, \qquad \tilde{M}_M = U_N^T M_M U_N \tag{A21}$$

and

$$(P^{rs}_u)_{IJ} = u_{I,r}(\mathbf{p})\bar{u}_{J,s}(\mathbf{p}), \quad (P^{rs}_v)_{IJ} = v_{I,r}(\mathbf{p})\bar{v}_{J,s}(\mathbf{p}). \tag{A22}$$

In the limit $\delta M \to 0$ the projectors are independent of the sterile flavor indices and reduce to

$$(P_u)^{ss}_{IJ} = (\not{p}+\bar{M})\Big(\frac{1}{2}-(-1)^s\mathfrak{h}\Big), \qquad (P_v)^{ss}_{IJ} = (\not{p}-\bar{M})\Big(\frac{1}{2}+(-1)^s\mathfrak{h}\Big), \tag{A23}$$

where $\mathfrak{h}$ is the helicity matrix (A3). We have used $u^c = C\bar{u}^T = v$ and introduced the self-energies

$$\Pi^{\gtrless}_{IJ}(p) = \tilde{F}_{\alpha I}\tilde{F}^*_{\beta J}\int\frac{d^4k}{(2\pi)^4}(v^2\delta(p-k) + \Delta^{\gtrless}(p+k))S^{\lessgtr}_{\alpha\beta}(k), \tag{A24}$$

with $\tilde{F} = FU_N$. The thermal Wightman functions appearing therein are defined as

$$\Delta^>(x_1-x_2) = \langle\Phi(x_1)\Phi(x_2)\rangle, \tag{A25}$$

$$\Delta^<(x_1-x_2) = \langle\Phi(x_2)\Phi(x_1)\rangle, \tag{A26}$$

$$S^>_{\alpha\beta ij}(x_1-x_2) = \langle\nu_{\alpha i}(x_1)\bar{\nu}_{\beta j}(x_2)\rangle, \tag{A27}$$

$$S^<_{\alpha\beta ij}(x_1-x_2) = -\langle\bar{\nu}_{\beta j}(x_2)\nu_{\alpha i}(x_1)\rangle. \tag{A28}$$

Here i, j are spinor indices, which we suppress in the following. Transitions with $r \neq s$ do not contribute at leading order in $\theta_{\alpha I}$ due to the projectors. This justifies our description of the sterile sector by two 2×2 matrices ρ_N and $\rho_{\bar{N}}$ rather than a 4×4 matrix including elements $\propto \rho_{N\bar{N}}$, etc. Transitions with $\alpha \neq \beta$ are suppressed by the small active neutrino masses $m_i/T \ll 1$. The above expressions are written in the $\tilde{F}$ base (vacuum mass base). They can be translated into the F base used in (1) by the replacements $\tilde{F} \to F$ and $\Delta\tilde{M}_M \to \Delta M\sigma_3$. Note that $\bar{M}$ is defined at $T = 0$.

With (A19), the initial value for ρ_N can be written as $\rho_N \propto \mathrm{diag}(\mathrm{P}_1, \mathrm{P}_2)$. The right-hand side of (A20) has a real and an imaginary part. These parts allow us to extract the

dispersive and dissipative parts, H and γ_N, of the effective Hamiltonian.

a. Dispersive part H

Comparison of (A20) and (A8) in the absence of active lepton asymmetries (since we choose $\hat{\rho}^{eq}_{\rm SM}$ without chemical potentials) allows us to define the dispersive part of the effective Hamiltonian appearing in (33),

$$H_{IJ} = \tau(\bar{M}^2 + \bar{p}^2)^{\frac{1}{2}}\delta_{IJ} + \tau\int d^3\mathbf{p}\frac{f_F(\omega_\mathbf{p})}{n_F} \times\Big[-\frac{M}{\omega_\mathbf{p}}\,\mathrm{Re}(\Delta\tilde{M}_M)_{IJ} + \frac{1-2f_F(\omega_\mathbf{p})}{2\omega_\mathbf{p}} \times\Big[\mathcal{P}\int\frac{dq_0}{2\pi}\,\frac{1}{\omega_\mathbf{p}-q_0}\,\mathrm{tr}(\mathrm{P}_u\Pi^-_{IJ}(q_0,\mathbf{p}) + \mathrm{P}_v\Pi^-_{JI}(q_0,\mathbf{p}))\Big]\Big], \tag{A29}$$

where we have introduced the short notation

$$\mathrm{P}_u = P_R(P_u^{11})_{IJ}P_L = \Big(\frac{1}{2}+\mathfrak{h}\Big)P_L, \qquad \mathrm{P}_v = P_R(P_v^{11})_{JI}P_L = \Big(\frac{1}{2}-\mathfrak{h}\Big)P_L. \tag{A30}$$

The additional factor $f_F(\omega_\mathbf{p})/n_F$ and the momentum integral come from the momentum averaging, cf. (A12). One can distinguish between three contributions. The term involving $\Delta\tilde{M}_M$ comes from the splitting of the Majorana masses and remains present in vacuum. The term involving Π^-_{IJ} is due to the Yukawa interactions. It contains two contributions [see (A24)], which are related to the Feynman diagrams shown in Fig. 4. The part $\propto v(T)^2$ is due to the interaction with the Higgs condensate and produces the Dirac mass at $T < T_{\rm EW}$. The part involving $\Delta^{\gtrless}$ comes from scatterings with Higgs particles. The Higgs expectation value as a function of temperature can be calculated for a given Higgs mass. We used $m_H = 126$ GeV, as suggested by recent LHC data [168,169], to obtain the dependence shown in Fig. 17. However, we checked that varying m_H within the allowed window 115–130 GeV does not have a big effect on the results.

Evaluation of (A29) requires knowledge of the dressed active neutrino and Higgs propagators, $S^{\gtrless}_{\alpha\beta}(p)$ and $\Delta^{\gtrless}$, respectively. These are, in principle, complicated functions of p and T. However, we are mostly interested in very high or low temperatures, $T \gtrsim T_{\rm EW} \gg M$ during baryogenesis and $T \lesssim M$ in the context of DM production. This allows us to simplify the expressions. It is convenient to dissect the self-energy Π^- into the Lorentz components

$$P_L\Pi^-_{IJ}(p) = P_L(A_{IJ}(p)\not{p} + B_{IJ}(p)\not{u}), \tag{A31}$$

where $u = (1,0,0,0)$ is the four-velocity of the primordial plasma, and write

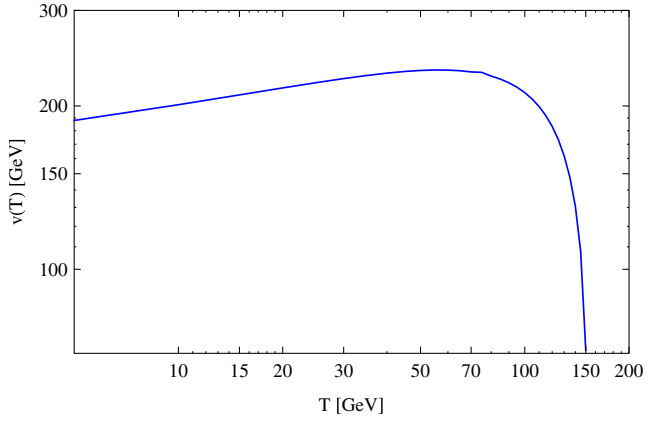

FIG. 17 (color online). The Higgs expectation value as a function of temperature for $m_H = 126$ GeV.

$$H_{IJ} = \tau(\bar{M}^2 + T^2)\delta_{IJ} + \tau\int d^3\mathbf{p}\frac{f_F(\omega_\mathbf{p})}{n_F} \times\Big[-\frac{M}{\omega_\mathbf{p}}\,\mathrm{Re}(\Delta\tilde{M}_M)_{IJ} + \frac{1-2f_F(\omega_\mathbf{p})}{2\omega_\mathbf{p}} \times\Big[\mathcal{P}\int\frac{dq_0}{2\pi}\,\frac{1}{\omega_\mathbf{p}-q_0}(\omega_\mathbf{p}(B_{IJ}+B_{JI}) + \mathbf{p}(B_{IJ}-B_{JI}) + M^2(A_{IJ}+A_{JI}))\Big]\Big]. \tag{A32}$$

Here, the momentum dependence of $B_{IJ}(q_o,\mathbf{p})$, $A_{IJ}(q_0,\mathbf{p})$ has been suppressed and $\mathbf{p}$ has to be read as $|\mathbf{p}|$. At temperatures $T \gg M$, the integral is dominated by hard momenta $\sim T$ and the term involving B_{IJ} dominates H_{IJ}. For $T \lesssim v(T)$, the interaction with the Higgs condensate dominates the N_I self-energy and B_{IJ} can be estimated as

$$B_{IJ}(p) \simeq v(T)^2\tilde{F}_{\alpha I}\tilde{F}^*_{\alpha J}\frac{\pi}{|\mathbf{p}|}b_{\alpha\beta}(p)(\delta(\omega-|\mathbf{p}|+b) - \delta(\omega+|\mathbf{p}|+b)) \quad \text{for } T \lesssim v(T). \tag{A33}$$

Here, b is the so-called "potential contribution" to the active neutrino propagator [6], obtained by decomposing the retarded active neutrino self-energy as

$$\mathrm{Re}\,\Sigma^R_{\alpha\beta}(p) = a_{\alpha\beta}(p)\not{p} + b_{\alpha\beta}(p)\not{u}. \tag{A34}$$

Since active neutrinos mainly scatter via weak gauge interactions, the coefficients are, to a good approximation, flavor independent in the primordial plasma; we can define $b\delta_{\alpha\beta} \equiv b_{\alpha\beta}(p)$, where $b_{\alpha\beta}(p)$ is to be evaluated on shell. For hard momenta, b gives [172,173]

$$b = \begin{cases} -\frac{\pi\alpha_W T^2}{8p}\Big(2+\frac{1}{\cos^2\theta_W}\Big) & T \gg M_W \\ \frac{16G_F^2}{\pi\alpha_W}(2+\cos^2\theta_W)\frac{7\pi^2T^4p}{360} & T \ll M_W. \end{cases} \tag{A35}$$

Here, θ_W is the Weinberg angle and α_W the weak gauge coupling. This leads to a contribution to H_{IJ} of the form

$$v(T)^2 \tilde{F}_{\alpha I} \tilde{F}^*_{\alpha J} \frac{\omega_{\mathbf{p}} + \mathbf{p}}{2\mathbf{p}} \frac{b\omega_{\mathbf{p}}}{M^2 + 2b\omega_{\mathbf{p}}}.$$

For $T > T_{\mathrm{EW}}$, scatterings with Higgs bosons dominate and the hard thermal loop result $H \simeq \tilde{F}^\dagger \tilde{F} T/8$ from Ref. [3] can be used. Combining the two contributions, we approximate H by

$$H \simeq -\frac{M}{T}\Delta\tilde{M} + (\tilde{F}^\dagger \tilde{F})^* \left(\frac{T}{8} + \frac{v^2(T)}{T}\right) \tag{A36}$$

during the calculations in Sec. V. In practice, it is more convenient to work in the F base, where the Hamiltonian reads $-\sigma_3 \frac{M}{T}\Delta M + F^\dagger F(\frac{T}{8} + \frac{v^2(T)}{T})$.

At temperatures $T \ll T_{\mathrm{EW}}$, there are no Higgs particles in the plasma and the Higgs expectation value is constant; thus, $B_{IJ} = v^2 \tilde{F}^*_{\alpha I} \tilde{F}_{\beta J} b_{\alpha\beta}$, $A_{IJ} = v^2 \tilde{F}^*_{\alpha I} \tilde{F}_{\beta J} a_{\alpha\beta}$. In Ref. [6] it has been estimated that thermal corrections to the active neutrino propagator are small, below a temperature

$$T_{\mathrm{pot}} = 13 \left(\frac{M}{\mathrm{GeV}}\right)^{\frac{1}{3}} \mathrm{GeV}. \tag{A37}$$

For the masses under consideration in this work, we can approximately use free active neutrino propagators in Sec. VI because $T_- < T_{\mathrm{pot}}$. Furthermore, due to the considerations in Sec. II F, we are mainly interested in the case $U_N \simeq \mathbb{1}$ for DM production; thus, $\tilde{F} \simeq F$. Then $b_{\alpha\beta}(p_0, |\mathbf{p}|) \simeq 0$ and $a_{\alpha\beta}(p_0, |\mathbf{p}|) \simeq (U_\nu)_{\alpha i} (U_\nu)^*_{\beta i} \frac{\pi}{\omega_i} \times (\delta(p_0 - \omega_i) - \delta(p_0 + \omega_i))$, with $\omega_i = (\mathbf{p}^2 + m_i^2)^{1/2}$ [174], where m_i are the active neutrino masses. This recovers the vacuum result for the mass matrix at $|\mathbf{p}| = 0$, cf. (9). H can be approximated by

$$H = \tau(\bar{p}^2 + M_N^2)^{1/2}. \tag{A38}$$

In the basis of vacuum mass eigenstates, it has the form $\mathrm{H} = \mathrm{diag}((\mathbf{p}^2 + M_2^2)^{1/2}, (\mathbf{p}^2 + M_3^2)^{1/2})$. Since $\delta M \ll T$, M we can expand in δM and obtain for $\bar{p} = T$

$$H \simeq \tau \delta M (X^{-2} + 1)^{-1/2} \sigma_3, \tag{A39}$$

with $X = M/T$ and the third Pauli matrix σ_3. The part of H that is proportional to the identity matrix has been dropped, as it always cancels out of the commutators in the kinetic equations.

b. Dissipative part Γ_N

Again comparing (A20) and (A8), we define

$$(\Gamma_N)_{IJ} = \tau \int d^3\mathbf{p} \frac{f_F(\omega_{\mathbf{p}})}{n_F} \frac{1 - 2f_F(\omega_{\mathbf{p}})}{2\omega_{\mathbf{p}}} \mathrm{tr}(\mathrm{P}_u \Pi^-_{IJ}(p) + \mathrm{P}_v \Pi^-_{JI}(p)). \tag{A40}$$

The rate for the antiparticles $\rho_{\bar{N}}$ can be found by using projectors analogous to (A30), but with helicity index 2. It is given by $(\Gamma^<_N)^*$, as expected.[35] For what follows, it is useful to pull the Yukawa matrices out of the self-energies and define

$$\bar{\Pi}^{\gtrless}_{\alpha\beta}(p) = \int \frac{d^4k}{(2\pi)^4} (v^2 \delta(p - k) + \Delta^{\gtrless}(p + k)) S^{\lessgtr}_{\alpha\beta}(k). \tag{A41}$$

Obviously, $\Pi^{\gtrless} = \tilde{F}^*_{\alpha I} \tilde{F}_{\beta J} \bar{\Pi}^{\gtrless}_{\alpha\beta}$. For the computation of Γ_N according to (39) we can now define the matrices

$$R(T, M)_{\alpha\beta} = \int d^3\mathbf{p} \frac{f_F(\omega_{\mathbf{p}})}{n_F} \frac{1 - 2f_F(\omega_{\mathbf{p}})}{2\omega_{\mathbf{p}}} \mathrm{tr}(\mathrm{P}_u \bar{\Pi}^-_{\alpha\beta}(p)), \tag{A42}$$

$$R_M(T, M)_{\alpha\beta} = \int d^3\mathbf{p} \frac{f_F(\omega_{\mathbf{p}})}{n_F} \frac{1 - 2f_F(\omega_{\mathbf{p}})}{2\omega_{\mathbf{p}}} \mathrm{tr}(\mathrm{P}_v \bar{\Pi}^-_{\alpha\beta}(p)). \tag{A43}$$

These matrices, in general, have to be computed numerically. We discuss their properties in Sec. IV B.

As usual in thermal field theory, the sterile neutrino self-energies $\Pi^<$ and $\Pi^>$ can be associated with the gain and loss rate. Their difference $\Pi^- = \Pi^> - \Pi^<$ gives the total relaxation rate Γ_N for the sterile neutrinos. This acts as the thermal production rate when their occupation numbers are below their equilibrium values and as a dissipation rate in the opposite case. In configuration space, the self-energy $\Pi^-(x)$ is related to the retarded self-energy by $\Pi^R(x) = \theta(x_0)\Pi^-(x)$. This implies $\bar{\Pi}^-(p) = 2i\mathrm{Im}\bar{\Pi}^R(p)$ in momentum space. As usual in field theory, the imaginary part of $\bar{\Pi}^R$ can be related to the total scattering cross section by the optical theorem (or its finite temperature generalization) [167], while the real part is responsible for the mass shift (or modified dispersion relation in the plasma). Both are related by the Kramers-Kronig relations. The appearance of Π^- in (A40) is in accordance with the optical theorem, and the contributions to the dispersive and dissipative parts of the effective Hamiltonian are indeed related by a Kramers-Kronig relation, cf. (A29) and (A40). This provides a good cross-check for our result.

c. The remaining rates

The remaining rates (40) and (41) appearing in (29)–(31) have to, in principle, be calculated independently. The precise computation is considerably more involved than in the case of Γ_N. Γ_N is related to the discontinuities of the N_I self-energies, which to leading order in the tiny Yukawa couplings $F_{\alpha I}$ only contain propagators of SM fields as internal lines. Due to the fast gauge interactions these are in equilibrium in the relaxation time approximation, and

[35] This can be seen by noticing that the traces are real and $P_R P^{22}_u P_L = P_R P^{11}_v P_L$, $P_R P^{22}_v P_L = P_R P^{11}_u P_L$ under the trace.

the right-hand side of (A40) can be computed by means of thermal (equilibrium) field theory. This is not possible in the computation of the damping rates for the SM-lepton asymmetries, which are related to self-energies where the out of equilibrium fields N_I appear as internal lines. For simplicity we follow the approach taken in Ref. [6] (see Sec. VI therein) and use the symmetries of the νMSM in certain limits to fix the structure of the rates.

We first consider the limit $(M_M)_{IJ} \to 0$, that is, the absence of a Majorana mass term. In this case the "total lepton number" is conserved,

$$0 = \partial_\mu \left(\sum_I J_I^\mu + \sum_\alpha J_\alpha^\mu \right)_{M_M=0}, \tag{A44}$$

$$J_I^\mu = \bar{\nu}_{R,I} \gamma^\mu \nu_{R,I}, \tag{A45}$$

$$J_\alpha^\mu = \bar{\nu}_{L,\alpha} \gamma^\mu \nu_{L,\alpha} + \bar{e}_{L,\alpha} \gamma^\mu e_{L,\alpha}. \tag{A46}$$

To leading order in the small mixing $\theta_{\alpha I}$ this implies

$$\frac{d}{dt} \left(\mathrm{tr}\rho_- + \sum_\alpha \mu_\alpha \right)_{M_M=0} \simeq 0. \tag{A47}$$

This situation is, to a good approximation, realized for $T \gg M$, when baryogenesis takes place—the total lepton number is not violated during this process and a nonzero baryon number is only realized because sphalerons couple exclusively to left-handed fields. Equation (A47) implies

$$\Gamma_N \simeq \sum_\alpha \tilde{\Gamma}_L^\alpha \qquad \mathrm{tr}\tilde{\Gamma}_N^\alpha \simeq \Gamma_L^\alpha \quad \text{for } (M_M)_{IJ} = 0. \tag{A48}$$

Other interesting limits considered in Ref. [6] include $F_{\alpha I} \to 0$ with fixed α for all I (leading to conservation of J_α^μ) and $F_{\alpha I} \to 0$ with fixed I for all α (leading to individual conservation of the combination $J_I^\mu + \sum_\alpha J_\alpha^\mu$ and the remaining current $J_{J\neq I}^\mu$). These limits allow us to fix the basic structure of Eqs. (40) and (41). For a general choice of parameters some corrections of $\mathcal{O}[1]$ to these relations may be necessary, the determination of which we postpone until the precision of experimental data on the νMSM requires it.

We also introduced an error when neglecting the N_I background in the plasma. However, at this point we are only interested in the cases $T \gtrsim T_+$ (baryogenesis), $T \approx T_-$ and $T \approx T_d$ (creation of late time asymmetry). During baryogenesis the N_I-abundances are below their equilibrium values and can be neglected in first approximation. For $T \ll M$ the effects of the N_I background are suppressed by T/M (e.g., in equilibrium $f_F(M) = (\exp(M/T) + 1)^{-1}$). This is certainly the case at $T_d \ll M$. For the decay there may be corrections $\mathcal{O}[1]$ as for some choices of parameters $T_+ > M$. We also postpone the computation of these until the precision of experimental data on the νMSM requires it.

4. Uncertainties

Our study is the most complete quantitative study of bounds on the νMSM parameter space from cosmology to date. However, the various assumptions made in the derivation of the kinetic equations lead to uncertainties that may be of order 1. These can be grouped into three categories.

(i) We only consider momentum averaged quantities. Since the sterile neutrinos can be far from thermal equilibrium, one, in principle, has to study the time evolution of each mode separately. Our treatment is a reasonable approximation as long as the kinetic equilibrium assumption (A11) holds. A study of this aspect published in Ref. [161] suggests that deviations from kinetic equilibrium are indeed only of order 1.

(ii) The rates (40) and (41) have been calculated in a rather crude way in Appendix A 3 c, leading to another source of uncertainty of order 1. In addition, a precise calculation of the BAU requires knowledge of the sphaleron rate throughout the electroweak transition. Including this is expected to yield a slightly bigger value for the BAU [175].

(iii) Though they are matrix valued and allow us to study flavor oscillations, Eqs. (A14)–(A16) are of the Boltzmann type. They assume that the system can be described as a collection of (possibly entangled) individual particles that move freely between isolated scatterings and carry essentially no knowledge about previous interactions ("molecular chaos").

The first two issues can be fixed by more precise computations. However, with the current experimental data, order 1 uncertainties are small compared to the experimental and observational bounds on the model parameters. The corrections will only slightly change the boundaries of the allowed regions in parameter space found in this work. We therefore postpone more precise calculations to the time when such precision is required from the experimental side.

In contrast, the third point is more conceptual. In a dense plasma, multiple scatterings, off-shell and memory effects may affect the dynamics. The effect of these cannot be estimated within the framework of Boltzmann-type equations; it requires a derivation from first principles that either confirms (A14)–(A16) and allows us to estimate the size of the corrections or replaces them by a modified set of equations. In the past years, much progress has been made in the derivation of effective kinetic equations from first principles [86–89,160,165,176–204]. Recent studies suggest that kinetic equations of the Boltzmann type are, in principle, applicable to study leptogenesis [88,89,188,202], but the resonant amplification may be weaker than found in the standard Boltzmann approach [88]. It remains to be seen which effects possible corrections have in the νMSM, where baryogenesis and dark matter production both crucially rely

on the resonant amplification. A first principles study is difficult in the νMSM due to the various different time-dependent scales related to production, oscillations, freeze-out and decay of the sterile neutrinos and the vast range of relevant temperatures. However, at this stage it seems likely that a first principles treatment is, if at all, only of phenomenological interest in the region around $\Gamma_N \sim \delta M$, which makes up only a small fraction of the relevant parameter space, cf. Fig. 6.

APPENDIX B: CONNECTION TO PSEUDO-DIRAC BASE

In our notation, the elements of ρ_N and $\rho_{\bar{N}}$ are bilinears in ladder operators that create quanta of the fields N_I, i.e., mass eigenstates in vacuum. This has the advantage that the diagonal elements can be interpreted as abundances of physical particles. The rates R and R_M have been introduced in Ref. [6], to which we regularly refer in this article. The basis in the field space of right-handed neutrinos there differs from the one we use in (1) and corresponds to $U\nu_R$ with

$$U = \frac{1}{\sqrt{2}}\begin{pmatrix} i & 1 \\ -i & 1 \end{pmatrix}. \tag{B1}$$

In this basis M_M is not diagonal and the Yukawa couplings should be rewritten as $hU = F$. The computation of the rates is then performed by defining a Dirac spinor

$$\Psi = U_{2I}\nu_{R,I} + (U_{3I}\nu_{R,I})^c. \tag{B2}$$

This is possible when the small mass splitting between the sterile neutrinos is neglected (or viewed as a perturbation and placed in the interacting part of $\mathcal{L}$). The fields $\nu_{R,I}$ can be recovered from this as $\nu_{R,I} = U^*_{2I}P_R\Psi + U^*_{3I}P_R\Psi^c$. In terms of Ψ, the νMSM Lagrangian reads

$$\mathcal{L} = \mathcal{L}_{\rm SM} + \mathcal{L}_0 + \mathcal{L}_{\rm int}, \tag{B3}$$

$$\begin{aligned}\mathcal{L}_0 &= \bar{\Psi}(i\partial\!\!\!/ - \bar{M})\Psi, \\ \mathcal{L}_{\rm int} &= -v(h_{\alpha 3}\bar{\nu}_{L\alpha}\Psi^c - h^*_{\alpha 3}\bar{\Psi}^c\nu_{L\alpha} - h_{\alpha 2}\bar{\nu}_{L\alpha}\Psi \\ &\quad - h^*_{\alpha 2}\bar{\psi}\nu_{L\alpha}) - \frac{1}{2}\Delta M(\bar{\Psi}^c\Psi + \bar{\Psi}\Psi^c).\end{aligned} \tag{B4}$$

The analogue of our matrix ρ_N (which is also called ρ_N in Ref. [6]) is defined as

$$\rho^\Psi_N = \int \frac{d^3\mathbf{p}}{V(2\pi)^3}\begin{pmatrix} \langle c^\dagger_1 c_1\rangle & \langle c^\dagger_1 d_1\rangle \\ \langle d^\dagger_1 c_1\rangle & \langle d^\dagger_1 d_1\rangle \end{pmatrix}, \tag{B5}$$

where c_s ($c^\dagger_s$) and d_s ($d^\dagger_s$) are the annihilation (creation) operators for Ψ particles (antiparticles) with momentum $\mathbf{p}$ and helicity s. The corresponding rate Γ^Ψ_N in the kinetic equations is given by[36]

$$\begin{aligned}\Gamma^\Psi_N = \tau \int d^3\mathbf{p}\frac{f_F(\omega_\mathbf{p})}{n_F}v^2\frac{f_F(p_0)}{2\omega_\mathbf{p}}(h_{\alpha I}h^*_{\beta J}R(T,M)_{\alpha\beta} \\ + (\sigma_1 h^\dagger)_{I\alpha}(h\sigma_1)_{\beta J}R_M(T,M)_{\alpha\beta}),\end{aligned} \tag{B6}$$

where $h = FU^\dagger$, σ_1 is the first Pauli matrix and we have neglected flavor off-diagonal elements. In the high temperature regime that was considered in Ref. [6], this simplifies to

$$\Gamma^\Psi_N\tau^{-1} = (h^\dagger h)^* R^{(S)}(T,M) + \sigma_1 h^\dagger h\sigma_1 R^{(S)}_M(T,M). \tag{B7}$$

$\sigma_1 h^\dagger h\sigma_1$ is $(h^\dagger h)^*$ with the diagonal elements swapped. Equation (A42) defines the quantities $R(T,M)$ and $R_M(T,M)$.[37] Ignoring the small mixing between active and sterile neutrinos, Γ_N is related to Γ^Ψ_N by

$$\Gamma_N \simeq (UU_N)^T\Gamma^\Psi_N(UU_N)^* \tag{B8}$$

for $T \gg m_i$.

Finally, the Yukawa matrix in Refs. [6,22] is expressed in terms of the parameters ϵ_{di}, η_{di}, ϕ_{di}, which differ from those we use here. In the limit $\epsilon_{di} \gg 1$, these can be related to our parameters by

$$\begin{aligned}\sqrt{\epsilon_{di}} &= e^{-{\rm Im}\omega}, \qquad \eta_{di} = 2\,{\rm Re}\omega, \\ \alpha_{di} &= \frac{\alpha_2}{2}, \qquad \phi_{di} = \delta.\end{aligned} \tag{B9}$$

Here, we prefer to use the parametrization fixed in Sec. II E because the expressions in terms of (B9) given in Ref. [6] are only approximate.

APPENDIX C: HOW TO CHARACTERIZE THE LEPTON ASYMMETRIES

In the νMSM neither the individual lepton numbers, related to the currents (A46), nor their sum are conserved. However, since the rates of all processes that violate them are suppressed by the small Yukawa couplings F, they evolve on a much slower time scale than other processes in the primordial plasma and are well defined. For practical purposes the magnitude of flavored lepton asymmetries in the primordial plasma can be characterized in different ways. In this article we describe them by the ratio between the number densities (particles minus antiparticles) and the entropy density $s \equiv 2\pi^2T^3g_*/45$,

$$\mu_\alpha = \frac{n_\alpha}{s}, \qquad \text{cf. (14)}.$$

This quantity is convenient because it is not affected by the expansion of the Universe, as long as the expansion is adiabatic. In the following we relate μ_α to other quantities that are commonly used in the literature, using the relations given in the Appendix of Ref. [19].

[36] Note that there were errors in the corresponding expressions (5.19), (5.20) in Refs. [6] and that, there, only the case $T \gg M$ was considered.

[37] Our definitions of R and R_M differ from those in Ref. [6] by a constant factor F_0^2 with $F_0 = 2 \times 10^{-9}$.

In quantum field theory calculations it is common to parametrize the asymmetries by chemical potentials $\boldsymbol{\mu}_\alpha$, which can be extracted from the distribution functions that appear in the free propagators at finite temperature. In the massless limit $T \gg m_i$ these are related to n_α by

$$n_\alpha = \frac{\boldsymbol{\mu}_\alpha T^2}{6} + \frac{\boldsymbol{\mu}_\alpha^3}{6\pi^2}, \tag{C1}$$

leading to

$$\mu_\alpha \approx \frac{15}{4\pi^2 g_*}\frac{\boldsymbol{\mu}_\alpha}{T}. \tag{C2}$$

Alternatively, one can normalize the lepton numbers n_α (particles minus antiparticles) by the total density of "particles plus antiparticles" in the plasma,

$$\Delta_\alpha = \frac{n_\alpha}{\mathrm{n}_\alpha^{eq}}, \tag{C3}$$

where $\mathrm{n}_\alpha^{eq} \equiv 2\int \mathrm{d}^3\mathbf{q}/(2\pi)^3/(e^{|\mathbf{q}|/T}+1) = 3\zeta(3)T^3/2\pi^2$ and

$$\mu_\alpha = \frac{135\zeta(3)}{4\pi^4 g_*}\Delta_\alpha. \tag{C4}$$

Finally, one can normalize with respect to the photon density,

$$L_\alpha \equiv \frac{n_\alpha}{n_\gamma}, \tag{C5}$$

where $n_\gamma \equiv 2\int \mathrm{d}^3\mathbf{q}/(2\pi)^3/(e^{|\mathbf{q}|/T}-1) = 2\zeta(3)T^3/\pi^2$, which yields

$$\mu_\alpha = \frac{45\zeta(3)}{\pi^4 g_*}L_\alpha. \tag{C6}$$

APPENDIX D: LOW TEMPERATURE DECAY RATES FOR STERILE NEUTRINOS

Most of the rates relevant for this work have been computed in Ref. [16], where they are listed in the Appendix. Here, we only list those rates that are needed in addition to those or that require refinement. This was necessary for the decay rates into leptons, where masses of the final state particles had been neglected in the original computation.

1. Semileptonic decay

The decay into up-type quarks through a neutral current is given by

$$\Gamma_{N_I\to\nu_\alpha u\bar{u}} = \frac{G_F^2|\Theta_{\alpha I}|^2 M^5}{192\pi^3}\left(f^{(u)}(x_q)S(x_q,x_q) + x_q^4\left(3-\frac{16}{3}C_1x_q^2+(3-8C_1)x_q^4\right)\log\left[\frac{1-4x_q^2+2x_q^4+S(x_q,x_q)(1-2x_q^2)}{2x_q^4}\right]\right), \tag{D1}$$

where $x_q = m_q/M$.

The decay into down-type quarks through a neutral current is given by

$$\Gamma_{N_I\to\nu_\alpha d\bar{d}} = \frac{G_F^2|\Theta_{\alpha I}|^2 M^5}{192\pi^3}\left(f^{(d)}(x_q)S(x_q,x_q) + x_q^4\left(3-\frac{8}{3}C_2x_q^2-(1-\frac{4}{3}C_2)x_q^4\right)\log\left[\frac{1-4x_q^2+2x_q^4+S(x_q,x_q)(1-2x_q^2)}{2x_q^4}\right]\right). \tag{D2}$$

The decay into quarks through a charged current is given by

$$\begin{aligned}\Gamma_{N_I\to e_\alpha u_n\bar{d}_m} = \frac{G_F^2|V_{nm}|^2|\Theta_{\alpha I}|^2 M^5}{192\pi^3}\Bigg(&g(x,y)S(x,y) - 12x^4\log\left[\frac{1-S(x,y)(1+x^2-y^2)-2y^2+(x^2-y^2)^2}{2x^2}\right]\\ &- 12y^4\log\left[\frac{1-S(x,y)(1-x^2+y^2)-2x^2+(x^2-y^2)^2}{2y^2}\right]\\ &+ 12x^4y^4\log\left[\frac{1-2x^2-2y^2+x^4+y^4-S(x,y)(1-x^2-y^2)}{2x^2y^2}\right]\Bigg),\end{aligned} \tag{D3}$$

where $\min(m_\alpha, m_{u_n}, m_{d_m})$ is neglected, and x and y are the two heavier masses divided by M.

2. Leptonic decay

$$\Gamma_{N_I\to e^-_{\alpha\neq\beta}e^+_\beta\nu_\beta} = \frac{G_F^2|\Theta_{\alpha I}|^2M^5}{192\pi^3}\Bigg(S(x_\alpha,x_\beta)g(x_\alpha,x_\beta) - 12x_\alpha^4\log\left[\frac{1-S(x_\alpha,x_\beta)(1+x_\alpha^2-x_\beta^2)-2x_\beta^2+(x_\alpha^2-x_\beta^2)^2}{2x_\alpha^2}\right]$$
$$- 12x_\beta^4\log\left[\frac{1-S(x_\alpha,x_\beta)(1-x_\alpha^2+x_\beta^2)-2x_\alpha^2+(x_\alpha^2-x_\beta^2)^2}{2x_\beta^2}\right]$$
$$+ 12x_\alpha^4x_\beta^4\log\left[\frac{1-2x_\alpha^2-2x_\beta^2+x_\alpha^4+x_\beta^4-S(x_\alpha,x_\beta)(1-x_\alpha^2-x_\beta^2)}{2x_\alpha^2x_\beta^2}\right]\Bigg) \tag{D4}$$

with

$$S(x,y) = \sqrt{(1-(x+y)^2)(1-(x-y)^2)}$$
$$C_1 = \sin^2\theta_W(3-4\sin^2\theta_W)$$
$$f^{(u)}(x) = \frac{1}{4}-\frac{2}{9}C_1-\left(\frac{7}{2}-\frac{20}{9}C_1\right)x^2-\left(\frac{1}{2}+4C_1\right)x^4+(-3+8C_1)x^6$$
$$C_2 = \sin^2\theta_W(3-2\sin^2\theta_W)$$
$$f^{(d)}(x) = \frac{1}{4}-\frac{1}{9}C_2+\left(\frac{10}{9}C_2-\frac{2}{7}\right)x^2-\left(\frac{1}{2}+2C_2\right)x^4-(3-4C_2)x^6$$
$$g(x,y) = 1-7x^2-7y^2-7x^4-7y^4+12x^2y^2-7x^2y^4-7x^4y^2+x^6+y^6.$$

[1] L. Canetti, M. Drewes, and M. Shaposhnikov, Phys. Rev. Lett. **110**, 061801 (2013).
[2] T. Asaka, S. Blanchet, and M. Shaposhnikov, Phys. Lett. B **631**, 151 (2005).
[3] T. Asaka and M. Shaposhnikov, Phys. Lett. B **620**, 17 (2005).
[4] W. A. Bardeen, Report No. FERMILAB-CONF-95-391-T, C95-08-27.3, Fermilab, 1995.
[5] M. Shaposhnikov, arXiv:0708.3550.
[6] M. Shaposhnikov, J. High Energy Phys. 08 (2008) 008.
[7] A. Boyarsky, A. Neronov, O. Ruchayskiy, and M. Shaposhnikov, Mon. Not. R. Astron. Soc. **370**, 213 (2006).
[8] T. Asaka, M. Laine, and M. Shaposhnikov, J. High Energy Phys. 06 (2006) 053.
[9] F. Bezrukov, Phys. Rev. D **72**, 071303 (2005).
[10] M. Shaposhnikov, Nucl. Phys. **B763**, 49 (2007).
[11] T. Asaka, M. Shaposhnikov, and A. Kusenko, Phys. Lett. B **638**, 401 (2006).
[12] A. Boyarsky, A. Neronov, O. Ruchayskiy, and M. Shaposhnikov, Phys. Rev. D **74**, 103506 (2006).
[13] A. Boyarsky, A. Neronov, O. Ruchayskiy, M. Shaposhnikov, and I. Tkachev, Phys. Rev. Lett. **97**, 261302 (2006).
[14] A. Boyarsky, A. Neronov, O. Ruchayskiy, and M. Shaposhnikov, JETP Lett. **83**, 133 (2006).
[15] M. Shaposhnikov and I. Tkachev, Phys. Lett. B **639**, 414 (2006).
[16] D. Gorbunov and M. Shaposhnikov, J. High Energy Phys. 10 (2007) 015.
[17] D. Gorbunov and M. Shaposhnikov, Proc. Sci., KAON (2008) 047.
[18] F. Bezrukov, J. Phys. Conf. Ser. **110**, 082002 (2008).
[19] M. Laine and M. Shaposhnikov, J. Cosmol. Astropart. Phys. 06 (2008) 031.
[20] A. Anisimov, Y. Bartocci, and F. L. Bezrukov, Phys. Lett. B **671**, 211 (2009).
[21] A. Boyarsky, O. Ruchayskiy, and M. Shaposhnikov, Annu. Rev. Nucl. Part. Sci. **59**, 191 (2009).
[22] L. Canetti and M. Shaposhnikov, J. Cosmol. Astropart. Phys. 09 (2010) 001.
[23] T. Asaka and H. Ishida, Phys. Lett. B **692**, 105 (2010).
[24] T. Asaka, M. Laine, and M. Shaposhnikov, J. High Energy Phys. 01 (2007) 091.
[25] V. Gorkavenko and S. Vilchynskiy, Eur. Phys. J. C **70**, 1091 (2010).
[26] T. Asaka, S. Eijima, and H. Ishida, J. High Energy Phys. 04 (2011) 011.
[27] O. Ruchayskiy and A. Ivashko, J. High Energy Phys. 06 (2012) 100.
[28] V. M. Gorkavenko, I. Rudenok, and S. I. Vilchynskiy, arXiv:1201.0003.
[29] O. Ruchayskiy and A. Ivashko, J. Cosmol. Astropart. Phys. 10 (2012) 014.
[30] M. Drewes and B. Garbrecht, J. High Energy Phys. 03 (2013) 096.
[31] T. Asaka, S. Eijima, and A. Watanabe, arXiv:1212.1062.
[32] F. L. Bezrukov and M. Shaposhnikov, Phys. Lett. B **659**, 703 (2008).
[33] F. Bezrukov, D. Gorbunov, and M. Shaposhnikov, J. Cosmol. Astropart. Phys. 06 (2009) 029.

[34] J. Garcia-Bellido, D. G. Figueroa, and J. Rubio, Phys. Rev. D **79**, 063531 (2009).
[35] M. Shaposhnikov and D. Zenhausern, Phys. Lett. B **671**, 187 (2009).
[36] M. Shaposhnikov and D. Zenhausern, Phys. Lett. B **671**, 162 (2009).
[37] J. Garcia-Bellido, J. Rubio, M. Shaposhnikov, and D. Zenhausern, Phys. Rev. D **84**, 123504 (2011).
[38] F. Bezrukov, D. Gorbunov, and M. Shaposhnikov, J. Cosmol. Astropart. Phys. 10 (2011) 001.
[39] F. Bezrukov and D. Gorbunov, J. High Energy Phys. 05 (2010) 010.
[40] A. Kusenko, Phys. Rev. Lett. **97**, 241301 (2006).
[41] K. Petraki and A. Kusenko, Phys. Rev. D **77**, 065014 (2008).
[42] L. Canetti, M. Drewes, and M. Shaposhnikov, New J. Phys. **14**, 095012 (2012).
[43] P. Minkowski, Phys. Lett. **67B**, 421 (1977).
[44] T. Yanagida, Prog. Theor. Phys. **64**, 1870 (1980).
[45] M. Gell-Mann, P. Ramond, and R. Slansky, in *Supergravity*, edited by D. Freedman *et al.* (North Holland, Amsterdam, 1979).
[46] R. N. Mohapatra and G. Senjanovic, Phys. Rev. Lett. **44**, 912 (1980).
[47] M. Fukugita and T. Yanagida, Phys. Lett. B **174**, 45 (1986).
[48] A. Roy and M. Shaposhnikov, Phys. Rev. D **82**, 056014 (2010).
[49] A. D. Sakharov, Pis'ma Zh. Eksp. Teor. Fiz. **5**, 32 (1967) [JETP Lett. **5**, 24 (1967)]; Usp. Fiz. Nauk **161**, 61 (1991) [Sov. Phys. Usp. **34**, 392 (1991)].
[50] V. A. Kuzmin, V. A. Rubakov, and M. E. Shaposhnikov, Phys. Lett. **155B**, 36 (1985).
[51] E. K. Akhmedov, V. A. Rubakov, and A. Y. Smirnov, Phys. Rev. Lett. **81**, 1359 (1998).
[52] E. Komatsu *et al.* (WMAP Collaboration), Astrophys. J. Suppl. Ser. **192**, 18 (2011).
[53] A. Boyarsky, J. Frohlich, and O. Ruchayskiy, Phys. Rev. Lett. **108**, 031301 (2012).
[54] S. Dodelson and L. M. Widrow, Phys. Rev. Lett. **72**, 17 (1994).
[55] L. Wolfenstein, Phys. Rev. D **17**, 2369 (1978).
[56] S. P. Mikheev and A. Y. Smirnov, Sov. J. Nucl. Phys. **42**, 913 (1985); Nuovo Cimento Soc. Ital. Fis. **9C**, 17 (1986).
[57] X.-D. Shi and G. M. Fuller, Phys. Rev. Lett. **82**, 2832 (1999).
[58] K. Abe *et al.* (T2K Collaboration), Phys. Rev. Lett. **107**, 041801 (2011).
[59] P. Adamson *et al.* (MINOS Collaboration), Phys. Rev. Lett. **107**, 181802 (2011).
[60] F. An *et al.* (DAYA-BAY Collaboration), Phys. Rev. Lett. **108**, 171803 (2012).
[61] J. Casas and A. Ibarra, Nucl. Phys. **B618**, 171 (2001).
[62] G. Fogli, E. Lisi, A. Marrone, A. Palazzo, and A. Rotunno, Phys. Rev. D **84**, 053007 (2011).
[63] J. Ahn *et al.* (RENO Collaboration), Phys. Rev. Lett. **108**, 191802 (2012).
[64] G. L. Fogli, E. Lisi, A. Marrone, D. Montanino, A. Palazzo, and A. M. Rotunno, Phys. Rev. D **86**, 013012 (2012).
[65] K. Abazajian, M. Acero, S. Agarwalla, A. Aguilar-Arevalo, C. Albright *et al.*, arXiv:1204.5379.
[66] A. Merle, arXiv:1302.2625.
[67] K. Harigaya, M. Ibe, and T. T. Yanagida, Phys. Rev. D **86**, 013002 (2012).
[68] M. Nemevsek, G. Senjanovic, and Y. Zhang, J. Cosmol. Astropart. Phys. 07 (2012) 006.
[69] T. Araki and Y. Li, Phys. Rev. D **85**, 065016 (2012).
[70] A. Adulpravitchai and R. Takahashi, J. High Energy Phys. 09 (2011) 127.
[71] A. Merle and V. Niro, J. Cosmol. Astropart. Phys. 07 (2011) 023.
[72] J. Barry, W. Rodejohann, and H. Zhang, J. High Energy Phys. 07 (2011) 091.
[73] M. Lindner, A. Merle, and V. Niro, J. Cosmol. Astropart. Phys. 01 (2011) 034.
[74] K. L. McDonald, Phys. Lett. B **696**, 266 (2011).
[75] A. Kusenko, F. Takahashi, and T. T. Yanagida, Phys. Lett. B **693**, 144 (2010).
[76] F. Bezrukov, H. Hettmansperger, and M. Lindner, Phys. Rev. D **81**, 085032 (2010).
[77] K. Kadota, Phys. Rev. D **77**, 063509 (2008).
[78] M.-C. Chen, A. de Gouvea, and B. A. Dobrescu, Phys. Rev. D **75**, 055009 (2007).
[79] K. Allison, arXiv:1210.6852.
[80] S. Iso and Y. Orikasa, arXiv:1210.2848.
[81] A. Merle, J. Phys. Conf. Ser. **375**, 012047 (2012).
[82] F. Bezrukov, A. Kartavtsev, and M. Lindner, arXiv:1204.5477.
[83] D. Boyanovsky, Phys. Rev. D **78**, 103505 (2008).
[84] X.-G. He and W. Liao, Phys. Lett. B **681**, 253 (2009).
[85] A. Mazumdar and S. Morisi, Phys. Rev. D **86**, 045031 (2012).
[86] M. Drewes, arXiv:1012.5380.
[87] M. Beneke, B. Garbrecht, M. Herranen, and P. Schwaller, Nucl. Phys. **B838**, 1 (2010).
[88] M. Garny, A. Kartavtsev, and A. Hohenegger, Ann. Phys. (Amsterdam) **328**, 26 (2013).
[89] M. Drewes, S. Mendizabal, and C. Weniger, Phys. Lett. B **718**, 1119 (2013).
[90] A. Boyarsky, J. Lesgourgues, O. Ruchayskiy, and M. Viel, Phys. Rev. Lett. **102**, 201304 (2009).
[91] J. Kersten and A. Y. Smirnov, Phys. Rev. D **76**, 073005 (2007).
[92] T. Yamazaki *et al.*, *Proceedings of 22nd International Conference on High-Energy Physics, Leipzig, Germany, 1984*, edited by A. Meyer and E. Wieczorek (Academy of Sciences of the German Democratic Republic, Berlin, 1984), p. 262.
[93] M. Daum, M. Janousch, P.-R. Kettle, J. Koglin, D. Poc anić, J. Schottmüller, C. Wigger, and Z. G. Zhao, Phys. Rev. Lett. **85**, 1815 (2000).
[94] G. Bernardi *et al.*, Phys. Lett. **166B**, 479 (1986).
[95] G. Bernardi *et al.*, Phys. Lett. B **203**, 332 (1988).
[96] A. Vaitaitis *et al.* (NuTeV Collaboration), Phys. Rev. Lett. **83**, 4943 (1999).
[97] F. Bergsma *et al.* (CHARM Collaboration), Phys. Lett. **166B**, 473 (1986).
[98] P. Astier *et al.* (NOMAD Collaboration), Phys. Lett. B **506**, 27 (2001).

[99] A. M. Cooper-Sarkar *et al.* (WA66 Collaboration), Phys. Lett. **160B**, 207 (1985).
[100] A. Atre, T. Han, S. Pascoli, and B. Zhang, J. High Energy Phys. 05 (2009) 030.
[101] A. D. Dolgov and S. H. Hansen, Astropart. Phys. **16**, 339 (2002).
[102] K. Abazajian, G. M. Fuller, and M. Patel, Phys. Rev. D **64**, 023501 (2001).
[103] K. Abazajian, G. M. Fuller, and W. H. Tucker, Astrophys. J. **562**, 593 (2001).
[104] A. Merle, Phys. Rev. D **86**, 121701 (2012).
[105] U. Seljak, A. Makarov, P. McDonald, and H. Trac, Phys. Rev. Lett. **97**, 191303 (2006).
[106] D. Boyanovsky and J. Wu, Phys. Rev. D **83**, 043524 (2011).
[107] D. Boyanovsky, Phys. Rev. D **83**, 103504 (2011).
[108] J. Wu, C.-M. Ho, and D. Boyanovsky, Phys. Rev. D **80**, 103511 (2009).
[109] A. Boyarsky, D. Iakubovskyi, O. Ruchayskiy, and V. Savchenko, Mon. Not. R. Astron. Soc. **387**, 1361 (2008).
[110] A. Boyarsky, J. Lesgourgues, O. Ruchayskiy, and M. Viel, J. Cosmol. Astropart. Phys. 05 (2009) 012.
[111] M. Viel and M. G. Haehnelt, Mon. Not. R. Astron. Soc. **365**, 231 (2006).
[112] M. Viel, J. Lesgourgues, M. G. Haehnelt, S. Matarrese, and A. Riotto, Phys. Rev. Lett. **97**, 071301 (2006).
[113] M. R. Lovell, V. Eke, C. S. Frenk, L. Gao, A. Jenkins, T. Theuns, J. Wang, S. D. M. White, A. Boyarsky, and O. Ruchayskiy, Mon. Not. R. Astron. Soc. **420**, 2318 (2012).
[114] A. Boyarsky, O. Ruchayskiy, and D. Iakubovskyi, J. Cosmol. Astropart. Phys. 03 (2009) 005.
[115] D. Gorbunov, A. Khmelnitsky, and V. Rubakov, J. Cosmol. Astropart. Phys. 10 (2008) 041.
[116] A. Kusenko, Phys. Rep. **481**, 1 (2009).
[117] G. M. Fuller, A. Kusenko, and K. Petraki, Phys. Lett. B **670**, 281 (2009).
[118] G. M. Fuller, A. Kusenko, I. Mocioiu, and S. Pascoli, Phys. Rev. D **68**, 103002 (2003).
[119] A. Kusenko and G. Segre, Phys. Rev. D **59**, 061302 (1999).
[120] J. Hidaka and G. M. Fuller, Phys. Rev. D **76**, 083516 (2007).
[121] J. Hidaka and G. M. Fuller, Phys. Rev. D **74**, 125015 (2006).
[122] A. Boyarsky, J. Nevalainen, and O. Ruchayskiy, Astron. Astrophys. **471**, 51 (2007).
[123] C. R. Watson, J. F. Beacom, H. Yuksel, and T. P. Walker, Phys. Rev. D **74**, 033009 (2006).
[124] K. Abazajian and S. M. Koushiappas, Phys. Rev. D **74**, 023527 (2006).
[125] K. N. Abazajian, M. Markevitch, S. M. Koushiappas, and R. C. Hickox, Phys. Rev. D **75**, 063511 (2007).
[126] S. Riemer-Sorensen, S. H. Hansen, and K. Pedersen, Astrophys. J. **644**, L33 (2006).
[127] A. Boyarsky, D. Malyshev, A. Neronov, and O. Ruchayskiy, Mon. Not. R. Astron. Soc. **387**, 1345 (2008).
[128] M. Loewenstein, A. Kusenko, and P. L. Biermann, Astrophys. J. **700**, 426 (2009).
[129] H. de Vega and N. Sanchez, Mon. Not. R. Astron. Soc. **404**, 885 (2010) 885.
[130] H. de Vega and N. Sanchez, Int. J. Mod. Phys. A **26**, 1057 (2011).
[131] C. Destri, H. J. de Vega, and N. G. Sanchez, New Astron. **22**, 39 (2013).
[132] A. Boyarsky, D. Iakubovskyi, and O. Ruchayskiy, Phys. Dark Univ. **1**, 136 (2012).
[133] M. Drewes, J. Mod. Phys. E (to be published).
[134] S. Riemer-Sorensen, S. H. Hansen, and K. Pedersen, Astrophys. J. **644**, L33 (2006).
[135] A. Boyarsky, O. Ruchayskiy, and M. Markevitch, Astrophys. J. **673**, 752 (2008).
[136] S. Riemer-Sorensen and S. H. Hansen, arXiv:0901.2569.
[137] S. Tremaine and J. E. Gunn, Phys. Rev. Lett. **42**, 407 (1979).
[138] S. H. Hansen, J. Lesgourgues, S. Pastor, and J. Silk, Mon. Not. R. Astron. Soc. **333**, 544 (2002).
[139] M. Viel, J. Lesgourgues, M. G. Haehnelt, S. Matarrese, and A. Riotto, Phys. Rev. D **71**, 063534 (2005).
[140] P. Colin, O. Valenzuela, and V. Avila-Reese, Astrophys. J. **673**, 203 (2008).
[141] M. Viel, G. D. Becker, J. S. Bolton, M. G. Haehnelt, M. Rauch, and W. Sargent, Phys. Rev. Lett. **100**, 041304 (2008).
[142] R. K. de Naray, G. D. Martinez, J. S. Bullock, and M. Kaplinghat, arXiv:0912.3518 [Astrophys. J. (to be published)].
[143] E. Semboloni, H. Hoekstra, J. Schaye, M. P. van Daalen, and I. J. McCarthy, arXiv:1105.1075.
[144] A. A. Klypin, A. V. Kravtsov, O. Valenzuela, and F. Prada, Astrophys. J. **522**, 82 (1999).
[145] B. Moore, S. Ghigna, F. Governato, G. Lake, T. R. Quinn, J. Stadel, and P. Tozzi, Astrophys. J. **524**, L19 (1999).
[146] O. R. A. Boyarsky and M. Shaposhnikov, Searching for Dark Matter, Contribution to Open Symposium—European Strategy Preparatory Group, Krakow, Poland, 2012, https://indico.cern.ch/contributionDisplay.py?contribId=127&confId=175067.
[147] A. Boyarsky, A. Neronov, O. Ruchayskiy, and I. Tkachev, Phys. Rev. Lett. **104**, 191301 (2010).
[148] J. den Herder, A. Boyarsky, O. Ruchayskiy, K. Abazajian, C. Frenk *et al.*, arXiv:0906.1788.
[149] V. Springel, J. Wang, M. Vogelsberger, A. Ludlow, A. Jenkins, A. Helmi, J. F. Navarro, C. S. Frenk, and S. D. M. White, Mon. Not. R. Astron. Soc. **391**, 1685 (2008).
[150] S. Ando and A. Kusenko, Phys. Rev. D **81**, 113006 (2010).
[151] Y. Li and Z.-z. Xing, Phys. Lett. B **695**, 205 (2011).
[152] W. Liao, Phys. Rev. D **82**, 073001 (2010).
[153] J. Hamann, S. Hannestad, G. G. Raffelt, I. Tamborra, and Y. Y. Wong, Phys. Rev. Lett. **105**, 181301 (2010).
[154] G. Steigman, arXiv:1008.4765.
[155] G. Steigman, Adv. High Energy Phys. **2012**, 268321 (2012).
[156] S. Riemer-Sørensen, D. Parkinson, and T. M. Davis, arXiv:1301.7102 [Pub. Astron. Soc. Aust. (to be published)].
[157] L. Lello and D. Boyanovsky, arXiv:1208.5559.
[158] P. Achard *et al.* (L3 Collaboration), Phys. Lett. B **517**, 75 (2001).

[159] D. Gorbunov and M. Shaposhnikov, Search for GeV-scale Sterile Neutrinos Responsible for Active Neutrino Masses and Baryon Asymmetry of the Universe, Contribution to Open Symposium—European Strategy Preparatory Group, Krakow, Poland, 2012, https://indico.cern.ch/contributionDisplay.py?contribId=17&confId=175067.

[160] G. Sigl and G. Raffelt, Nucl. Phys. **B406**, 423 (1993).

[161] T. Asaka, S. Eijima, and H. Ishida, J. Cosmol. Astropart. Phys. 02 (2012) 021.

[162] D. Boyanovsky, Phys. Rev. D **76**, 103514 (2007).

[163] D. Boyanovsky and C. Ho, Phys. Rev. D **76**, 085011 (2007).

[164] D. Boyanovsky and C. Ho, J. High Energy Phys. 07 (2007) 030.

[165] B. Garbrecht, Nucl. Phys. **B868**, 557 (2013).

[166] M. Laine and Y. Schroder, Phys. Rev. D **73**, 085009 (2006).

[167] P. F. Bedaque, A. K. Das, and S. Naik, Mod. Phys. Lett. A **12**, 2481 (1997).

[168] G. Aad *et al.* (ATLAS Collaboration), Phys. Lett. B **716**, 1 (2012).

[169] S. Chatrchyan *et al.* (CMS Collaboration), Phys. Lett. B **716**, 30 (2012).

[170] F. Bezrukov and M. Y. Kalmykov, J. High Energy Phys. 10 (2012) 140.

[171] D. J. Schwarz and M. Stuke, J. Cosmol. Astropart. Phys. 11 (2009) 025.

[172] H. A. Weldon, Phys. Rev. D **26**, 2789 (1982).

[173] D. Notzold and G. Raffelt, Nucl. Phys. **B307**, 924 (1988).

[174] M. L. Bellac, *Thermal Field Theory*, Cambridge Monographs on Mathematical Physics (Cambridge University Press, Cambridge, England, 2000).

[175] M. D'Onofrio, K. Rummukainen, and A. Tranberg, J. High Energy Phys. 08 (2012) 123.

[176] A. Anisimov, D. Besak, and D. Bodeker, J. Cosmol. Astropart. Phys. 03 (2011) 042.

[177] M. Laine and Y. Schroder, J. High Energy Phys. 02 (2012) 068.

[178] T. Konstandin, T. Prokopec, and M. G. Schmidt, Nucl. Phys. **B716**, 373 (2005).

[179] T. Konstandin, T. Prokopec, M. G. Schmidt, and M. Seco, Nucl. Phys. **B738**, 1 (2006).

[180] W. Buchmuller and S. Fredenhagen, Phys. Lett. B **483**, 217 (2000).

[181] T. Prokopec, M. G. Schmidt, and S. Weinstock, Ann. Phys. (Amsterdam) **314**, 208 (2004).

[182] T. Prokopec, M. G. Schmidt, and S. Weinstock, Ann. Phys. (Amsterdam) **314**, 267 (2004).

[183] F. Fillion-Gourdeau, J.-S. Gagnon, and S. Jeon, Phys. Rev. D **74**, 025010 (2006).

[184] M. Lindner and M. M. Muller, Phys. Rev. D **73**, 125002 (2006).

[185] M. Lindner and M. M. Muller, Phys. Rev. D **77**, 025027 (2008).

[186] A. De Simone and A. Riotto, J. Cosmol. Astropart. Phys. 08 (2007) 002.

[187] A. Anisimov, W. Buchmuller, M. Drewes, and S. Mendizabal, Ann. Phys. (Amsterdam) **324**, 1234 (2009).

[188] A. Anisimov, W. Buchmuller, M. Drewes, and S. Mendizabal, Phys. Rev. Lett. **104**, 121102 (2010).

[189] J.-S. Gagnon and M. Shaposhnikov, Phys. Rev. D **83**, 065021 (2011).

[190] B. Garbrecht, Nucl. Phys. **B847**, 350 (2011).

[191] M. Beneke, B. Garbrecht, C. Fidler, M. Herranen, and P. Schwaller, Nucl. Phys. **B843**, 177 (2011).

[192] M. Garny, A. Hohenegger, A. Kartavtsev, and M. Lindner, Phys. Rev. D **81**, 085027 (2010).

[193] A. Anisimov, W. Buchmuller, M. Drewes, and S. Mendizabal, Ann. Phys. (Amsterdam) **326**, 1998 (2011).

[194] C. P. Kiessig, M. Plumacher, and M. H. Thoma, Phys. Rev. D **82**, 036007 (2010).

[195] C. Kiessig and M. Plumacher, J. Cosmol. Astropart. Phys. 07 (2012) 014.

[196] C. Kiessig and M. Plumacher, J. Cosmol. Astropart. Phys. 09 (2012) 012.

[197] M. Garny, A. Hohenegger, A. Kartavtsev, and M. Lindner, Phys. Rev. D **80**, 125027 (2009).

[198] V. Cirigliano, C. Lee, M. J. Ramsey-Musolf, and S. Tulin, Phys. Rev. D **81**, 103503 (2010).

[199] M. Garny, A. Hohenegger, and A. Kartavtsev, arXiv:1005.5385.

[200] M. Herranen, K. Kainulainen, and P. M. Rahkila, J. High Energy Phys. 02 (2012) 080.

[201] M. Herranen, K. Kainulainen, and P. M. Rahkila, J. High Energy Phys. 12 (2010) 072.

[202] B. Garbrecht and M. Herranen, Nucl. Phys. **B861**, 17 (2012).

[203] C. Fidler, M. Herranen, K. Kainulainen, and P. M. Rahkila, J. High Energy Phys. 02 (2012) 065.

[204] T. Frossard, M. Garny, A. Hohenegger, A. Kartavtsev, and D. Mitrouskas, arXiv:1211.2140 [Phys. Rev. D (to be published)].

[205] H. A. Weldon, Phys. Rev. D **28**, 2007 (1983).

[206] D. Besak and D. Bodeker, J. Cosmol. Astropart. Phys. 03 (2012) 029.

[207] M. Laine, A. Vuorinen, and Y. Zhu, J. High Energy Phys. 09 (2011) 084.

[208] A. Salvio, P. Lodone, and A. Strumia, J. High Energy Phys. 08 (2011) 116.